GROUND MOTION PREDICTION EQUATIONS BASED ON SIMULATED GROUND MOTIONS

A THESIS SUBMITTED TO
THE GRADUATE SCHOOL OF NATURAL AND APPLIED SCIENCES
OF
MIDDLE EAST TECHNICAL UNIVERSITY

BY

KADER GÜR

IN PARTIAL FULFILLMENT OF THE REQUIREMENTS
FOR
THE DEGREE OF MASTER OF SCIENCE
IN
EARTHQUAKE STUDIES

OCTOBER 2018

Approval of the thesis:

GROUND MOTION PREDICTION EQUATIONS BASED ON SIMULATED GROUND MOTIONS

submitted by **KADER GÜR** in partial fulfillment of the requirements for the degree of **Master of Science in Earthquake Studies Department, Middle East Technical University** by,

Prof. Dr. Halil Kalıpçılar
Dean, Graduate School of **Natural and Applied Sciences** ________________

Prof. Dr. Ayşegül Askan Gündoğan
Head of Department, **Earthquake Studies** ________________

Prof. Dr. Ayşegül Askan Gündoğan
Supervisor, **Earthquake Studies, METU** ________________

Assist. Prof. Dr. Özkan Kale
Co-Supervisor, **Civil Engineering, TED University** ________________

Examining Committee Members:

Prof. Dr. Ahmet Yakut
Earthquake Studies, METU ________________

Prof. Dr. Ayşegül Askan Gündoğan
Earthquake Studies, METU ________________

Prof. Dr. Murat Altuğ Erberik
Earthquake Studies, METU ________________

Assist. Prof. Dr. Özkan Kale
Civil Engineering, TED University ________________

Assist. Prof. Dr. Abdullah Sandıkkaya
Civil Engineering, Hacettepe University ________________

Date: 24.10.2018

I hereby declare that all information in this document has been obtained and presented in accordance with academic rules and ethical conduct. I also declare that, as required by these rules and conduct, I have fully cited and referenced all material and results that are not original to this work.

Name, Surname: Kader Gür

Signature:

ABSTRACT

GROUND MOTION PREDICTION EQUATIONS BASED ON SIMULATED GROUND MOTIONS

Gür, Kader
Master of Science, Earthquake Studies
Supervisor: Prof. Dr. Ayşegül Askan Gündoğan
Co-Supervisor: Assist. Prof. Dr. Özkan Kale

October 2018, 154 pages

Ground Motion Prediction Equations (GMPEs) are one of the key elements in seismic hazard assessment to estimate ground motion intensity measures by basically taking into account source, path and site effects. Most of the existing predictive models are derived from databases compiled from real (or observed) ground motion data. However, in data-poor regions, a novel practice to develop new GMPEs is to use simulated or hybrid ground motion datasets for performing reliable seismic hazard analysis. Simulations obtained from stochastic, deterministic or hybrid methods can provide reliable ground motion estimates and assist to understand the mechanisms of the earthquakes. This study starts with a discussion on the theory of stochastic finite-fault technique and the simulation process including source mechanisms, site and path effect parameters from the 1992 Erzincan (M_w 6.6) and the 1999 Duzce (M_w 7.1) earthquakes. Then the development of the regional GMPEs based on the synthetic database compiled from the Erzincan and Duzce earthquake simulations is presented. The proposed predictive model is evaluated by residual analysis under the synthetic model development database and the recorded Turkish ground motion database. The trends of the proposed ground motion model are also compared to the existing regional, local and global GMPEs. These comparisons indicate a good agreement

which is promising in the sense that the simulated ground motions can be contributed to the future development of GMPEs.

Keywords: Earthquake, Ground motion simulation, Stochastic finite-fault method, Ground motion prediction equation, Seismic hazard assessment

ÖZ

BENZEŞTİRİLMİŞ YER HAREKETLERİNE DAYANAN YER HAREKETİ TAHMİN DENKLEMLERİ

Gür, Kader
Yüksek Lisans, Deprem Çalışmaları
Tez Danışmanı: Prof. Dr. Ayşegül Askan Gündoğan
Ortak Tez Danışmanı: Dr. Öğr. Üyesi Özkan Kale

Ekim 2018, 154 sayfa

Yer Hareketi Tahmin Denklemleri (YHTD), temel olarak depremlerin kaynak, yayılım ve saha etkilerini dikkate alarak yer hareketi yoğunluk ölçümlerini tahmin etmek için kullanılan sismik tehlike analizlerinin başlıca unsurlarından biridir. Mevcut tahmin modellerinin çoğu, gerçek (veya gözlemsel) yer hareketi verilerinden derlenen veritabanlarından üretilmiştir. Bununla birlikte, veri eksikliği olan bölgelerde, YHTD geliştirmeye yönelik yeni bir uygulama, güvenilir sismik tehlike analizileri için benzeştirilmiş veya karma yer hareketi verisetlerini kullanmaktır. Stokastik, deterministik veya karma yöntemlerden elde edilen simülasyonlar, güvenilir yer hareketi tahminleri sağlar ve depremlerin mekanizmalarını anlamaya yardımcı olur. Bu çalışmada ilk olarak, stokastik sonlu-fay tekniğinin teorisi ve 1992 Erzincan (M_w 6.6) ve 1999 Düzce (M_w 7.1) depremlerinin kaynak mekanizmaları, yayılım ve saha parametreleri dahil simülasyon süreci ele alınmıştır. Çalışmada daha sonra, Erzincan ve Düzce deprem simülasyonlarından derlenen sentetik veritabanı altında bölgesel YHTD gelişimi sunulmaktadır. Önerilen tahmin modeli, model geliştirme sentetik veritabanı ve kaydedilmiş Türk yer hareketi veritabanı altında residüel analizi ile değerlendirilmiştir. Önerilen yer hareketi tahmin modelinin eğilimleri, ayrıca mevcut bölgesel, yerel ve küresel YHTD ile karşılaştırılmıştır. Bu karşılaştırmalar, benzeştirilmiş yer hareketlerinin gelecekteki YHTD gelişimine katkıda bulunabileceğini belirten iyi bir uyum olduğunu göstermektedir.

Anahtar Kelimeler: Deprem, Yer hareketi simülasyonu, Stokastik sonlu-fay yöntemi, Yer hareketi tahmin denklemi, Sismik tehlike analizi

To Mavi, Gözen, Mom and

To my supervisor Prof. Dr. Ayşegül Askan Gündoğan

ACKNOWLEDGMENTS

I would like to express my deepest gratitude to my supervisor Prof. Dr. Ayşegül Askan Gündoğan, whose encouragement, knowledge and support from the initial to the final level enabled me to develop an understanding of the subject. It was a great honor to study my thesis with her guidance, foresight and optimism. It was a great chance to study with a strong, versatile and intelligent advisor who always inspired me and improved my vision.

I would thank my co-supervisor Assist. Prof. Dr. Özkan Kale for his guidance, patience and support. With his participation and leadership, this study is enhanced and became a multi-disciplinary work. I am also heartily thankful to Dr. Shaghayegh Karimzadeh Naghshineh for all the knowledge about simulations she shared with me and for her valuable suggestions. I also thank Prof. Dr. Ahmet Yakut, Prof. Dr. Murat Altuğ Erberik and Assist. Prof. Dr. Abdullah Sandıkkaya for participating in the defense jury and their contribution to the thesis.

I would like to express my deepest appreciation to my mom Lütfiye, my dad Ali, and my sisters Pınar and Nurdan for their endless patience, faith, support, and motivation in every stage of my life. I am thankful to them for the feeling of safety they offer. I am also grateful to my beauties Zeynep, Aylin, Ada and Mehmet for the joy and hope they bring to my life. I also would like to thank to my friends for their friendship, understanding and love.

Finally, I am specifically grateful to my beloved Gözen Gözener for his love, greatest support, motivation and encouragement in all parts of this study and my life and to my baby Mavi for her unconditional love.

TABLE OF CONTENTS

LIST OF TABLES

TABLES

LIST OF FIGURES

FIGURES

LIST OF SYMBOLS AND ABBREVIATIONS

1D	One-dimensional
2D	Two-dimensional
3D	Three-dimensional
EAF	East Anatolian Fault
EMME	Earthquake Model of the Middle East Region
ERD	Earthquake Research Department
EW	East-West
f	Frequency
f_c	Corner Frequency
F-K	Frequency-Wavenumber
FAS	Fourier Amplitude Spectrum
GMPEs	Ground Motion Prediction Equations
GMRotI50	Rotation-Independent Average Horizontal Component
H/V	Horizontal-to-Vertical
M_0	Seismic moment
MASW	Multi-Channel Array Surface Waves
M_w	Moment magnitude
NAF	North Anatolian Fault
NAFZ	North Anatolian Fault Zone
NEAF	North East Anatolian Fault
NEHRP	National Earthquake Hazards Reduction Program
NGA	Next Generation of Ground Motion Attenuation Models
NS	North-South
PEER	Pacific Earthquake Engineering Research Center
PGA	Peak Ground Acceleration
PGA_{REF}	Peak Ground Acceleration for Reference Rock Site
PGV	Peak Ground Velocity
PSA	Pseudo Acceleration Response Spectra with 5% damping

PSV	Pseudo-Spectral Velocity
R	Source-to-site-distance
ReMi	Refraction Microtremor
$\mathbf{R_{EPI}}$	Epicentral distance
$\mathbf{R_{HYP}}$	Hypocentral distance
$\mathbf{R_{JB}}$	Joyner-Boore distance
$\mathbf{R_{RUP}}$	Rupture distance
RMS	Root Mean Square
RotD50	50th-percentile of the Rotated Orientation-independent, Period-Dependent Combined Horizontal Components
RS	Response Spectra
Q	Quality Factor
SASW	Spectral Analysis of Surface Waves
SFF	Stochastic Finite-Fault
SPAC	Spatially Averaged Coherency
T	Period
$\mathbf{T_0}$	Source Duration
$\mathbf{V_{S30}}$	The 30m-average shear wave velocity in units of m/s
$\boldsymbol{\beta}$	Crustal shear wave velocity
$\boldsymbol{\rho}$	Crustal Density
$\boldsymbol{\mu}$	Shear Modulus
$\boldsymbol{\tau}$	Between-event (inter-event) Standard Deviation
$\boldsymbol{\phi}$	Within-event (intra-event) Standard Deviation
$\boldsymbol{\eta_i}$	Between-event (inter-event) Residual
$\boldsymbol{\varepsilon_{ij}}$	Within-event (intra-event) Residual
$\boldsymbol{\sigma}$	Effective Stress
$\boldsymbol{\Delta\sigma}$	Stress drop
$\boldsymbol{\kappa_0}$	Zero-distance Kappa

CHAPTER 1

INTRODUCTION

1.1. General

Ground Motion Prediction Equations (GMPEs) provide peak ground motion intensity parameters such as peak ground acceleration and spectral acceleration depending on earthquake magnitude, faulting mechanism, source to station distance and soil condition etc. GMPEs are mathematical forms that fit parametric models to previous ground motion data to predict future ground motion estimates. For most of the applications, ground motion models are derived from the datasets that include real (i.e., observed or recorded) ground motion data. GMPEs could be specifically developed for a study region with enough data and parameter content, however, in spite of efforts to increase the number of seismic networks around the world, there are still seismically active areas with rare or no local observation points. For such regions, the formulation of GMPEs based on real regional records is significantly limited, despite an option to use real records from different parts of the world that have similar tectonics as well as soil conditions. But, it is not easy to find regions with the same or very similar physical characteristics on Earth.

Regional GMPEs may contain greater uncertainties since their databases are poorly represented for large magnitude earthquakes at close distances. In addition, global predictive models are based on extensive databases whose local properties may not be accurately expressed which can lead to uncertainty due to the small number of large earthquakes, even on a global extent. As another option, physics-based simulated ground motions with sufficient magnitude and distance ranges can be used in GMPEs to fill the gaps in real ground motion databases by constraining the GMPEs beyond data limits. The principal approach of ground motion simulations for reliable estimates, is to model the source mechanisms as well as regional wave propagation characteristics. Besides, for the site-specific assessment of future earthquakes, simulated records combined with real past ground motions can be used instead of pure empirical data which are fitted to time series generally by interpolation, extrapolation and scaling. Consequently, one of the common practices for developing reliable regional GMPEs with limited data is to use simulated or hybrid strong ground motion datasets.

Three general types of simulation methods are deterministic, stochastic, and hybrid methods. The deterministic method is based on numerical or analytical solution of full wave propagation. This method gives the most accurate ground motion simulations with well-defined source properties and regional velocity model. Besides, this method requires significant computational resource and intensive knowledge of near surface soil materials. Deterministic method provides solutions to low frequency (long period) ground motion simulations. High frequency part of seismic waves is naturally random and qualified by the incoherency in their phase spectrum. Hence, high frequency ground motions are not mostly modeled by deterministic techniques. Stochastic method generates the acceleration time histories by combining the deterministic theoretical far field shear wave spectrum and random phase angels. High frequencies are efficiently modeled by this method although complete wave propagation and complex source effects are insufficient since the stochastic technique does not accurately model some effects of earthquake properties such as surface waves and directivity. The frequency range of the simulation methods is limited both in deterministic and stochastic techniques. Hybrid methods can accurately model the whole frequency range of time histories. In this method, the low frequencies are simulated with deterministic techniques and high frequencies are simulated by stochastic techniques. (e.g.: Kamae et al., 1998; Hartzell et al., 1999; Martin Mai and Beroza 2003; Hartzell et al., 2005; Hisada, 2008; Frankel, 2009; Graves and Pitarka, 2010; Mai et al., 2010).

The following section summarizes former studies on ground motion simulations followed by the past and current studies on ground motion prediction models.

1.2. Literature Review on Stochastic Ground Motion Simulations

Ground motion simulations have always received the attention of the earthquake community. Earth scientists usually take advantage of simulated ground motions to find out fault effects, path and site conditions, while earthquake engineers utilize the simulations to obtain ground motion intensity measures and earthquake time history characteristics (frequency content, amplitude and duration) of a previous or future earthquake.

Stochastic approach is introduced to simulate moderate and high frequencies since deterministic simulations are restricted to low frequencies. Stochastic method was initially formed by combining impulses which have randomness in amplitudes and durations (Housner, 1947, 1955; Thomson, 1959). Aki (1967) modeled a ω-square source spectrum where displacement is a ramp function of time. In comparison to similar studies (e.g.: Brune, 1970; Hanks, 1979), high frequency ground motion characteristics are best represented by Aki (1967). Brune (1971) determined the frequency characteristics of the fault rupture by including the effective stress near the fault plane into the previously proposed source-time function. Hanks and McGuire (1981) used finite duration, band-limited, white Gaussian noise to represent the random nature of the high frequency motions. Stochastic approach models an accelerogram which is random in time, with a Fourier amplitude spectrum based on geological and seismological information to describe the earthquake source, path effect, and the site parameters (Hanks and McGuire, 1981; Boore, 1983).

The stochastic point-source simulation proposed by Boore (1983) combined the source spectrum models of aforementioned authors with the works of Hanks and McGuire (1981) to generate high frequency time histories. Stochastic point-sources are used to generate earthquake sources in this technique. However, for large earthquakes point-source modeling does not include finite-fault features (rupture dimensions, spatial slip variation, rupture directivity) that significantly affect the basic characteristics of ground motions (frequency content, amplitude and duration). As a result, stochastic finite-fault methods have been advanced to model near field acceleration time histories of large events (Beresnev and Atkinson, 1997, 1998a, b). The finite-fault technique simulates accelerograms by summing the contributions from discretized sub-faults with each sub-fault modeled as a point-source with a ω-square spectrum. Rupture propagation initiates radially from the hypocenter which is on a sub-fault. Motazedian and Atkinson (2005) revised the stochastic finite-source model by introducing dynamic corner frequency to be time-dependent instead of static corner frequency that depends on the sub-faults size.

The use of ground motion simulation methods has recently draw the attention of earthquake engineering. The stochastic simulation approaches (either point-source or finite-fault) are widely used globally to generate accelerograms of moderate and larger earthquakes (e.g.: Hanks and Boore, 1984; Atkinson, 1984; Toro and McGuire, 1987; Beresnev and Atkinson, 1997; Atkinson and Silva, 2000; Erdik and Durukal, 2001; Durukal, 2002; Roumelioti et al., 2004; Motazedian and Atkinson, 2005; Yalcinkaya 2005; Motazedian and Moinfar, 2006; Shoja-Taheri and Ghofrani, 2007; Castro et al., 2008; Atkinson et al., 2009; Boore, 2009; Raghukanth and Somala, 2009, Ugurhan and Askan, 2010; Ugurhan et al., 2012; Ghofrani et al., 2013; Askan et al., 2013; Akinci and Antonioli, 2012; Zengin and Cakti, 2014; Askan et al., 2015; Askan et al., 2016; Ozlu et al., 2018; Karimzadeh and Askan, 2018). In the recent past, simulated ground motions have also been employed in engineering applications such as seismic demand evaluations, seismic loss and damage estimations and nonlinear dynamic structural analysis (e.g.: Sucuoglu et al., 2003; Bazzurro et al., 2004; Pacor et al., 2005; Krishnan et al., 2006a,b; Zhao et al., 2007; Ansal et al., 2009; Graves and Pitarka, 2010; Ugurhan et al., 2011; Atkinson and Goda, 2010; Atkinson et al., 2011; Galasso et al., 2013; Galasso and Zareian, 2014; Goda et al., 2015; Sørensen and Lang, 2015, Karimzadeh et al., 2017a; Karimzadeh et al., 2017b; Karimzadeh, et al., 2017c; Ozsarac et al., 2017; Ozlu et al., 2018; Karimzadeh et al., 2018).

In this study, simulated ground motions obtained by the stochastic finite-fault technique (Motazedian and Atkinson, 2005) are employed in regional GMPEs.

1.3. Literature Survey on Ground Motion Prediction Equations

Practice of GMPEs started in the western United States following the first attenuation relationships introduced by Esteva and Rosenblueth (1964). This first model is followed by several ground motion prediction relations developed for United States, which considered only peak ground motions or both peak ground motions and spectral ordinates (e.g.: Trifunac and Brady, 1975, 1976; McGuire, 1976, 1977; Idriss, 1978, 1991; Hays, 1980; Campbell, 1981, 1989; Boore and Joyner, 1982; Joyner and Boore, 1981, 1988; 1996, Boore et. al., 1994; Boore et. al., 1997; Abrahamson and Silva, 1993, 1997). The evolution of GMPEs in United States is continued with improvements in the functional forms of prediction equations and compilation of the data from shallow crustal earthquakes of other seismic zones with attenuation characteristics similar to the western USA (e.g.: Campbell and Bozorgnia, 2000, 2003; Atkinson and Boore, 2003; Atkinson, 2006). Thereafter, a multidisciplinary research program named as the "Next Generation of Ground Motion Attenuation Models" (NGA) project (Power et al., 2008) is coordinated using an updated and expanded Pacific Earthquake Engineering Research Center (PEER) ground motion dataset. New models inside of this project named as NGA-West1 are improved for extensive ranges of magnitude, distance, soil classification, as well as spectral periods of than those used in the previous ground motion relations (e.g.: Abrahamson and Silva, 2008; Boore and Atkinson, 2008; Campbell and Bozorgnia, 2008; Chiou and Youngs, 2008). Lastly, the NGA-West2 project is constituted to improve the NGA-West1 models with respect to additional ground motion records, predictor variables, enlarged magnitude and distance boundaries (e.g.: Abrahamson et al., 2014; Boore et al., 2014; Campbell and Bozorgnia, 2014; Chiou and Youngs, 2014).

On the other hand, Ambraseys (1975) started GMPE studies in Europe, about 10 years after the first attenuation relationships presented in USA. Predictive models continued by a number of revisions and advancements to finally provide an extensive study on GMPEs for seismic regions of Europe and the Middle East (e.g.: Ambraseys, 1978, 1990, 1995; Ambraseys et al., 1996; Ambraseys et al., 2005). As a result of growing size and quality of the ground motion datasets, the number of new predictive models exclusive to a zone or country as well as models using combined data from different countries are increased (e.g.: Bommer et al., 2007; Akkar and Bommer, 2007, 2010, Akkar et al., 2014). The complexity level to express the physical formation of earthquakes increased with extended data of earthquake catalogs within global or national programs. Correspondingly, GMPEs regarding country-based datasets are generated for several European countries (e.g.: Danciu and Tselentis, 2007; Akkar and Cagnan, 2010; Bindi et al., 2010; Ameri et al., 2017). Recently, Kale et al. (2015) provided a ground motion predictive model for Turkey using data from both Turkey and Iran which is compiled from the Earthquake Model of the Middle East Region (EMME) project to explore the regional characteristics that affect amplitudes of recorded time histories in shallow crustal earthquakes.

In the meantime, the attenuation relationships in Turkey are developed by Inan et al. (1996), Aydan et al. (1996), Aydan (2001), Gulkan and Kalkan (2002), Kalkan and Gulkan (2004), Ozbey et al. (2004), Ulusay et al. (2004), Akyol and Karagoz (2009) and Ulutas and Ozer (2010). The estimator parameters of Turkish GMPEs generally have different measures for magnitude scale, type of distance and the soil effect categorization. Inan et al. (1996), Aydan et al. (1996) and Aydan (2001) estimates the peak ground acceleration (PGA) for Turkish earthquakes with very limited dataset by simple functional forms that contains only surface magnitude and epicentral distance. However, the rest of above-mentioned GMPEs predict the PGA and 5% damped pseudo acceleration (PSA) response spectra (Ulusay et al. (2004) estimates only the PGA) and employ moment magnitude, different distance measures (closest horizontal distance, epicentral distance, rupture distance, hypocentral distance) and different site effect considerations from datasets with record numbers ranging between 90 and 210. Site characterization based on the averaged shear-wave velocity in the upper 30 m (V_{S30}) is employed in the studies of Gulkan and Kalkan (2002), Kalkan and Gulkan (2004), while Ozbey et al. (2004), Ulusay et al. (2004) and Akyol and Karagoz (2009) use the rock, stiff soil, soil, and soft soil groups for soil conditions. Ulutas and Ozer (2010) do not include the site effects. The minimum magnitude used in aforementioned Turkish GMPEs are generally varies from 5 down to 4, while the upper limits are 7.4 and 7.6. Recently, the more sophisticated GMPEs based on larger and more comprehensive national databases are developed by Akkar and Cagnan (2010) and Kale et al. (2015). Peak ground velocity (PGV) is also estimated by these GMPEs in addition to PGA and spectral accelerations. As a significant difference from previous GMPEs, faulting mechanism for strike-slip, normal and reverse earthquakes is included in the functional forms by these two ground motion model, in addition to other predictor variables that are moment magnitude and Joyner-Boore distance (R_{JB}: distance closest to the surface projection of fault rupture) and site effects based on V_{S30}. Datasets used by these recent GMPEs are extended and improved. Akkar and Cagnan (2010) have 433 records from 137 earthquakes in their dataset while Kale et al. (2015) has a database with 670 accelerograms from 175 Turkish earthquakes. However, due to limited datasets as a result of sparsely installed strong motion stations in the country, there is still a need of better developed local ground motion predictive models with extended magnitude and distance range to estimate peak ground motions (Kale et al., 2015). Although global GMPEs consist of comparatively larger datasets, they may not mimic the regional characteristics properly.

Physics-based ground motion simulations significantly contribute in developing synthetic datasets to fill the gaps in real strong motion datasets with as many earthquake-site pairs as needed under controlled parameter selection. Broadband simulations are necessary in characterizing the engineering viewpoint of seismic ground motions particularly for poorly represented conditions in ground motion databases, e.g., in the NGA-West1 project, the data from higher magnitudes ($M_w > 7$) at moderate to close distances (< 45 km) are relatively sparse (Chiou et al., 2008). Therefore, simulations derive solutions to two important issues of ground motion prediction as follows: constraining the GMPEs beyond data limits; and response history analysis using waveforms for conditions not represented in empirical databases. In the recent times, several studies have been proposed to develop regional GMPEs with simulated strong ground motion datasets (e.g.: Campbell, 2003; Atkinson and Boore, 2006; Atkinson and Macias, 2009; Allen, 2012; Edwards and Fah, 2013; Bauman and Dalguer, 2014; Yenier and Atkinson, 2015; Shahjouei and Pezeshk, 2016; Bora et al., 2017) and with hybrid strong ground motion databases (e.g.: Anbazhagan et al., 2013; Sharma and Harbindu, 2014; Bydlon et al., 2017; D'Amico et al., 2018).

1.4. Objective and Outline

In this dissertation, the use of regional GMPEs developed from a simulated ground motion database is assessed by comparing the proposed model with the up-to-date local Turkish ground motion model (Kale et al., 2015) and other previous local and global GMPEs.

Accelerograms are simulated from the Erzincan and Duzce regions which are on the Eastern and Western territories of seismically active North Anatolian Fault zone (NAFZ), respectively. The approach is employed for the most hazardous fault zone in Turkey, both considering a well-investigated and densely monitored area (Western part, Duzce) and a relatively less studied but seismically very active region with sparse seismic stations (Eastern part, Erzincan). In this thesis, the synthetic ground motion dataset is implemented from the past studies (Ugurhan and Askan, 2010; Askan et al., 2013; Askan et al., 2015; Karimzadeh et al., 2017b; Karimzadeh et al., 2018).

Simulated ground motion records of Erzincan and Duzce regions are generated by investigating source mechanisms, path, and site parameters from the March 13, 1992 Erzincan (M_w 6.6) and the November 12, 1999 Duzce (M_w 7.1) events with stochastic finite-source technique based on dynamic corner frequency. For this purpose, in these studies first the underlying physical source mechanism, path effect and site properties are analyzed. Then, these earthquakes are simulated with seismological and geological parameters obtained from the regions to confirm the simulated accelerograms. Validated models are used to produce a large number of ground motion data from potential scenario earthquakes. Thus, the simulated database employed in this study is well constrained.

Simulated ground motion database is used herein for the development of regional GMPEs. The functional form is structured by the limitations of the simulated database with the number of estimator parameters (i.e., magnitude, distance, faulting mechanism, soil classification, etc.). Regression analysis is applied and the simulated database is regressed to obtain model coefficients and standard deviations. Predictive model results are obtained as median estimations and standard deviation values. Residual analysis is also employed. Finally, the proposed regional GMPEs is compared to previous regional models as well as NGA-West2 GMPEs.

Chapter 2 presents the fundamentals of finite-fault stochastic method. Details of the stochastic approaches (both point-source and finite-fault) are introduced. Model parameters are also described in detail.

In Chapter 3, Erzincan and Duzce regions are presented with the history of regional seismic characteristics. Strong ground motion records of the near-source recording stations are studied. Next, the simulation parameters are explained. Simulation results at the stations and simulated ground motion datasets for each region are presented.

In Chapter 4, definitions of response variables (dependent variables or ground motion intensity parameters) and estimator parameters (independent variables in the regression analysis) are given. Simulated ground motion database used in development of GMPE with main features is provided. Functional form that is structured by the limitations of the simulated dataset is provided with the number of estimator parameters (i.e., magnitude, distance, faulting mechanism, soil classification, etc.). Regression analysis approach is explained. Then, the stochastic data is regressed to obtain model coefficients and sigma values. Predictive model results are provided. In addition, residual analysis is presented. Finally, an evaluation of proposed ground motion model is performed against previous global and regional ground motion predictive models.

Chapter 5 presents the important findings and conclusions of this dissertation. In addition, suggestions for future studies are discussed at the end of the thesis.

CHAPTER 2

STOCHASTIC GROUND MOTION SIMULATION METHODOLOGY

2.1. General

The basic principles of the stochastic simulation method are presented in this chapter. Deterministic and stochastic simulation methods are used to generate the amplitudes and frequency content of acceleration time histories of earthquakes. Deterministic approach needs precise source characteristics and material models to generate the lower frequencies of time histories (< 1 Hz) that are usually coherent. However, high frequency band of ground motions (>1 Hz) has a random characteristic which constituted of random phases (Hanks and McGuire, 1981). Stochastic method is principally proposed to model this incoherency in phase angles. Two fundamental stochastic approaches exist: point-source and finite-fault techniques. The scope of this thesis includes the stochastic finite-fault method only. Thus, deterministic approach is not presented herein.

Section 2.2 presents the stochastic point-source methodology. This technique combines the earthquake source characteristics, rupture propagation pattern and site model as a windowed Gaussian noise in frequency space to generate synthetic ground motions. It is a practical method to simulate far-field accelerograms of small to moderate magnitude events. In subsections 2.2.1 to 2.2.3, earthquake source, propagation and site effects are described in depth, respectively. The finite-fault approach in detail is presented in Section 2.3. The differences between the alternative methods are also expressed.

2.2. Stochastic Point-Source Modeling

High frequencies of accelerograms (especially S-waves) are responsible for structural damage. Besides, S-waves constitute the major content of ground motions, specifically of the horizontal components. Stochastic approach depends on the stochastic nature in the energy propagation of the earthquake source, thus past events can be simulated effectively. Using random phases and frequency domain highly reduces the computational works in stochastic method. In this technique, ground motion intensity measures (peak acceleration and velocity) in time-domain, the short period P- and S- wave amplitudes, and also Fourier Amplitude Spectrum (FAS) in frequency domain can be estimated accurately (e.g.: Hanks and McGuire, 1981; Boore, 1983; Boore and Atkinson, 1987; Silva and Lee, 1987; Toro and McGuire, 1987).

The essence of the stochastic method is to filter a set of windowed, random acceleration time series to reach a deterministic target spectrum. The ω-square source spectrum, which represents the high frequency ground motion characteristics, suggested by Aki (1967) started the accurate prediction of peak ground acceleration. Later, Brune (1971) determined the frequency characteristics of the fault rupture by including the effective stress close the fault plane into the previously proposed source-time function.

Boore (1983) proposed stochastic point-source approach to create S-wave part of the seismic waves, and followed the studies of Hanks and McGuire (1981) to model the random nature of the high frequency ground motion of shear-waves. The point-source model is proportional to earthquake magnitude that depends on only the seismic moment. This approach is applied with one source parameter: stress drop (the difference of stress before and after the rupture occurs). This basic idea provides an accurate representation of high frequency band of strong ground motion recordings.

In stochastic simulation methodology, the following process is employed to generate the time histories. A band-limited Gaussian white noise for a specified finite duration of motion is generated. This noise is windowed to get a physical appearance of an accelerogram, and then converted to the frequency domain. Mostly, boxcar and Saragoni-Hart windows (Saragoni and Hart, 1973) are used. Spectrum of the windowed noise is normalized by the square root of its mean square amplitude spectrum and is multiplied by the deterministic theoretical S-wave amplitude spectrum. The spectrum is transformed back to the time domain to yield the ground motion acceleration time series. Simulation of ground motion in this manner manage two main subjects: generation of time series with a finite duration, and a specified amplitude spectrum finalized with physical representation of the earthquake source, rupture propagation and site characteristics (Boore, 1983). The algorithm is described given in Figure 2.1.

The Fourier amplitude spectrum of a ground motion in stochastic point-source method as proposed by Boore (1983) is presented in Equation 2.1. This is the result of the source spectrum E, path effect filter P, site effect filter G and the type of motion parameter I:

$$Y\,(M_0, R, f) = E(M_0, f) * P(R, f) * G(f) * I(f) \tag{2.1}$$

where M_0 is the seismic moment, R is the source-to-site-distance, f is the frequency, and $I(f) = (2\pi f i)^{\,n}$ states the type of time series, for ground displacement; (n = 0), ground velocity; (n = 1), or ground acceleration; (n = 2).

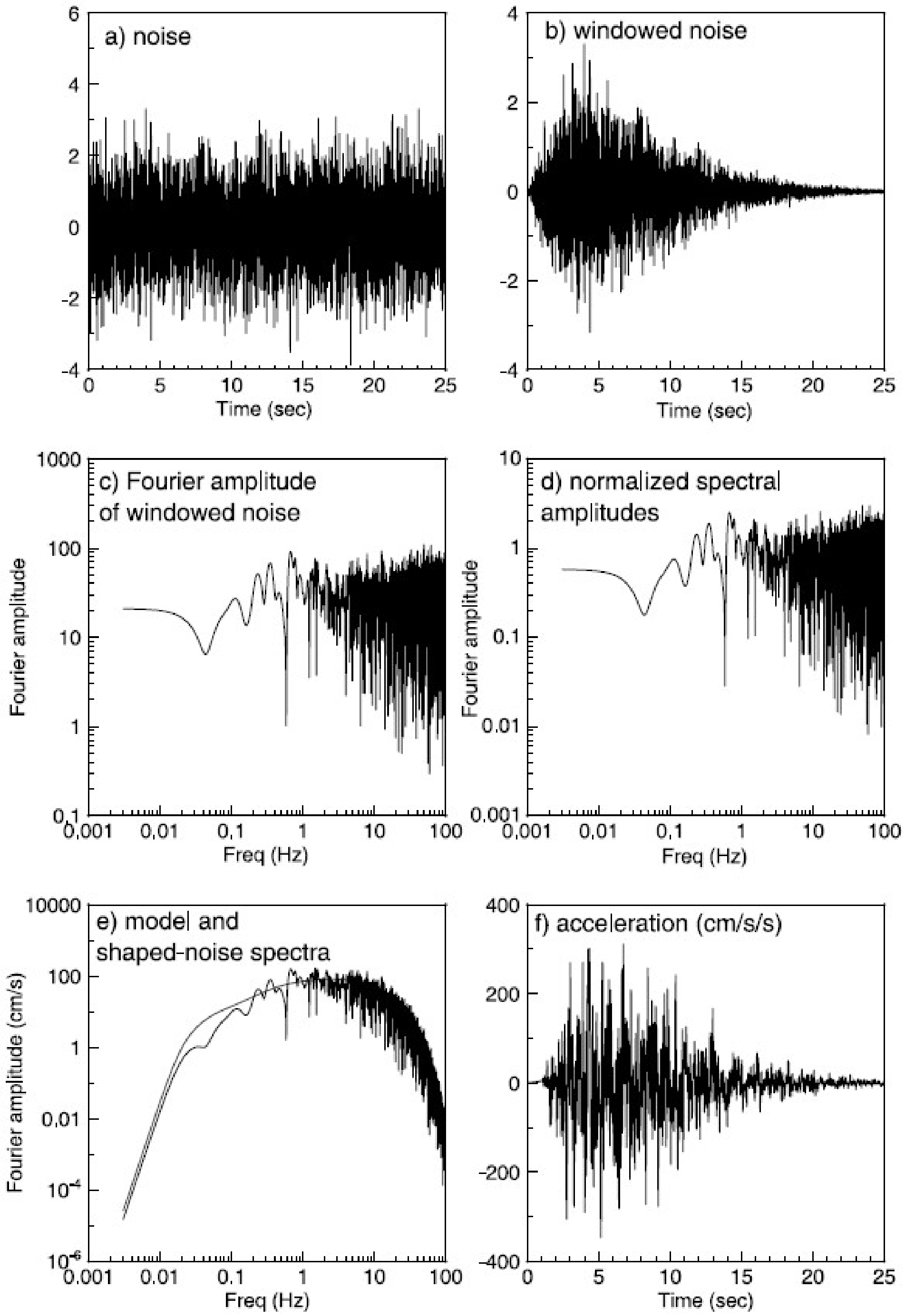

Figure 2.1. Algorithm of the stochastic point-source modeling (Adapted from Boore, 2003)

2.2.1. Source Spectrum

Source models contain parameters of a kinematic rupture process like fault plane geometry, depth of the fault, rupture velocity, slip distribution, stress drop and earthquake magnitude. Source spectrum describes displacements of physical process occured at the source because of the shear wave propagation. Source-time function is the most uncertain part of the representation of seismic displacements.

To characterize the source spectrum, theoretical solution for the far-field shear wave displacement in a homogeneous, isotropic, unbounded medium due to a point shear dislocation is presented as follows:

$$u(x,t) = \frac{\Re_{\theta\emptyset}}{4\pi\rho\beta^3 R} M'(t)\left(t - \frac{R}{\beta}\right) \quad (2.2)$$

where u (x, t) is the dynamic displacement field at point x, $R_{\theta\emptyset}$ indicates the radiation pattern reflecting the variation of the displacement field for different directions due to a shear dislocation, β is the shear-wave velocity which is assumed to be constant at the crustal level, R is the source to receiver distance and M'(t) is the moment rate function which is the time derivative of the seismic moment M(t) as defined in Aki and Richards (1980).

In general, seismic moment is described as follows:

$$M(t) = \mu\bar{u}(t)A \quad (2.3)$$

where μ is the shear modulus or rigidity which is assumed to be constant at the crustal level, $\bar{u}$(t) is the source time function and A is the dislocation area.

In stochastic technique, the source-time function which is a smoothed ramp function and its time derivative are defined as follows:

$$\bar{u}(t) = \frac{\sigma}{\mu}\beta t\left[1 - \left(1 + \frac{t}{\tau}\right)e^{-\frac{t}{\tau}}\right]$$

$$\bar{u}'(t) = \frac{\sigma}{\mu}\beta\left(\frac{t}{\tau}\right)e^{-\frac{t}{\tau}} \tag{2.4}$$

where σ is the effective stress that is effective on the dislocation area, and time parameter τ, manages the rate of displacements.

The total seismic moment can be expressed as:

$$M_0 = \mu\bar{u}(\infty)A \tag{2.5}$$

where we obtain ū(∞) from Equation 2.4 as $\bar{u}(\infty) = \frac{\sigma}{\mu}\beta\tau$.

Combining Equations 2.2, 2.3 and 2.4, the corresponding displacement can be obtained as follows:

$$u(x,t) = \frac{\Re_{\theta\emptyset} M_0}{4\pi\rho\beta^3 R\tau}\left(\frac{t-\frac{R}{\beta}}{\tau}\right)e^{-\frac{\left[t-\frac{R}{\beta}\right]}{\tau}} \tag{2.6}$$

The Fourier transform of Equation 2.6 yields:

$$u(x,\omega) = \frac{\Re_{\theta\emptyset} M_0}{4\pi\rho\beta^3 R}\left[\frac{1}{1+\left(\frac{\omega}{\omega_c}\right)^2}\right] \tag{2.7}$$

The corner frequency ($f_c = \omega_c/2\pi$) is expressed by Brune (1970, 1971) as:

$$f_c = 4.9 \times 10^6 \beta_s \left(\frac{\Delta\sigma}{M_0}\right)^{1/3} \tag{2.8}$$

where f_c is in Hz, β_s is shear wave velocity in km/s, $\Delta\sigma$ is stress drop in bars, and M_0 is in dyne-cm. Equations 2.7 and 2.8 form the source function.

The theoretical source spectrum used in the stochastic simulations is in the functional form generally given as:

$$E(M_0, f) = C.\, M_0.\, S(f) \tag{2.9}$$

where $C = (R_{\theta\phi}.\ FS.\ PRTITN)/(4\pi\rho_s\beta_s^3\ R_0)$ indicates a scaling constant, $R_{\theta\phi}$ is the radiation pattern constant and generally taken as 0.55 for shear waves. FS denotes the amplification on the free surface and is taken as 2. $PRTITN$ is a reduction term with value of $1/\sqrt{2}$, that indicates the separation of the total energy into two horizontal components. ρ_s is the density and β_s is the shear wave velocity. M_0 is the seismic moment usually formulated by $\mu\bar{u}A$ where μ is the shear modulus or rigidity, $\bar{u}$ states for the average slip and A is the fault area.

Hanks and Kanamori (1979) developed the Equation 2.10 to express a relationship between seismic moment (M_0) and moment magnitude (M) as follows:

$$M = \frac{2}{3}\log(M_0) - 10.73 \tag{2.10}$$

$S(f)$ in Equation 2.9, is the principal factor for building the source spectrum which accounts for the displacement source function. Brune (1970) spectrum model is one of the most well-known functions for source spectrum. In this model, propagation of shear waves starts from the focus at the center of a fault plane. The seismic moment, M_0 and constant stress drop, $\Delta\sigma$ that controls the high frequency amplitudes of earthquakes are the main factors controlling this model. The source spectrum by Brune (1970) is expressed as follows:

$$S(f, f_c) = \frac{1}{1+\left(\frac{f}{f_c}\right)^2} \tag{2.11}$$

For most stochastic simulations Brune spectrum predicts the higher frequency ground motion amplitudes effectively. However, this spectrum assumes a circular fault rupture and cannot give adequate results specifically at low frequencies for large magnitude events in which fault geometry is substantial. Alternatively, as provided in Section 2.3, finite-fault techniques are improved for large magnitude events.

In stochastic finite-fault technique, Brune source spectrum with only one corner frequency is utilized. This method is enhanced with a dynamic corner frequency theory where corner frequency is considered as time-dependent. Eventually, source effects are quite complicated and uncertain when compared to all other seismic properties since complex source behavior cannot be fully included. Because of this reason, stochastic simulations are limited at low frequencies that are highly influenced by the source mechanism of large magnitude earthquakes (Askan et al., 2013).

2.2.2. Path Effects

The path effect is the second significant factor in Equation 2.1 that affect the characteristics of ground motion records. Seismic waves are subjected to several processes as they travel within the earth. This causes modification in their frequency content, amplitudes, durations and velocities. Path propagation can be grouped as elastic and anelastic effects. Geometric spreading and scattering are elastic processes which express the decrease of ground motion amplitudes since seismic waves radiate over a continually growing area. Besides, the anelastic attenuation represents the energy loss in the form of heat energy, mostly due to particle interactivity (Romero and Rix, 2001). Consequently, in geometric spreading seismic energy is preserved, however in anelastic attenuation seismic energy is lost.

Geometric spreading indicates the decrease of amplitudes, inversely proportional to distance from source to site in the region of interest. As a result, geometric spreading parameter is generally used in accordance with the available regional datasets. Also geometric spreading models derived from global data can be utilized for similar seismological and geological regions.

Seismic waves are subjected to damping while travelling through the Earth which is not perfectly elastic. Hence, the spectral amplitudes of the waves decrease as they propagate along the mediums with different properties. This sort of damping is called "anelastic attenuation" and identified with the quality factor, Q (Lay and Wallace, 1995). Q value varies depends on the seismological and geological features of the regions (Aki, 1980).

Q value is frequency-dependent specifically at higher frequencies and is generally given as $Q = Q_0 f^n$. The constant Q_0 defines heterogeneities in soil and n is a regional constant (Raghukanth and Somala, 2009). If the Q value is small for a region, this expresses that the waves are subjected to higher attenuation and their amplitudes decreases rapidly.

The total path effect is a combination of geometrical spreading and anelastic attenuation and given as follows:

$$P(R,f) = Z(R)e^{\left(-\frac{\pi.f.R}{Q(f).\beta}\right)} \qquad (2.12)$$

where $Z(R)$ is geometrical spreading function, R indicates distance of the recorder from the focus, $Q(f)$ is the quality factor. The anelastic attenuation term in Equation 2.12, gives the exponential decay of ground motion amplitudes. Spectral ratio and Coda wave methods based on weak motion data analyses are mostly used to obtain Q factors (Atkinson and Mereu, 1992).

Z(R) is mostly given in terms of distance-dependent piecewise continuous functions as follow (Boore, 2003):

$$Z(R) = \begin{cases} \frac{R_0}{R} & R \leq R_1 \\ Z(R_1)\left(\frac{R_1}{R}\right)^{p_1} & R_1 \leq R \leq R_2 \\ \quad\quad . & \\ \quad\quad . & \\ Z(R_n)\left(\frac{R_n}{R}\right)^{p_n} & R \leq R_n \end{cases} \tag{2.13}$$

In stochastic modeling, another significant path parameter is the ground motion duration that is directly related with the rupture kinematics and source-to-site distance. It is an important factor to simulate signal accurately since amplitudes attenuate with duration. In general, the duration model is given as:

$$T = T_0 + bR \tag{2.14}$$

T_0 is the source duration, b is a region-dependent parameter (can be constant or distance-dependent) and R is distance of the receiver from the focus. T_0 increases with the magnitude, and it is related with the corner frequency ($T_0 = 1/(2f_c)$ Beresnev and Atkinson, 1997).

Eventually, specifying regional models for quality factor, geometric spreading and duration are not an effortless process. Extensive and reliable local databases are required. Comparison of simulated and observed time histories give an accurate understanding of earthquake source and propagation characteristics; but, it is an iterative process with trade-off property. Ideal parameters are usually obtained by comparing the FAS of the observed and generated ground motions.

2.2.3. Site Effects

The amplification and diminution of the seismic waves are directly affected by the soil profile of a site. The local site characteristics are related with the reflection, refraction, and diffraction of waves through the heterogeneous medium under the sites. For easiness the structure of earth is generally modeled with one-dimensional medium. Hence, soil material, thicknesses, and wave velocity properties are significant for an adequate site effect modeling.

The amplitude, duration, and frequency content of the seismic waves are influenced by the site properties. The soil velocity and density usually decreases from bedrock levels up to the ground. As the seismic waves travel the seismic impedance reduces, so wave amplitudes increase to preserve the elastic energy (Kramer, 1996). In the meantime, wave amplitudes counteracting decrease due to the damping impact in soft soil strata. As a result, site effects contain both amplification and diminution of the waves.

In stochastic method, the complete site effects filter is given as:

$$G(f) = A(f)\, D(f) \tag{2.15}$$

where $A(f)$ is the amplification and $D(f)$ is the energy loss at high frequencies independent of path. Site and path effects have different characteristics. Path effects are principally related with the wave propagation from source within the deep layers of earth but site response contains the shallow soil strata below the surface.

Next, the theory of amplification and diminution factors are presented.

i: Calculation of A(f):

Identifying soil properties and site amplification is a main part of simulations process. Among numerous techniques for modeling site effects, theoretical transfer functions method that uses the complete soil velocity profiles gives the most adequate results. Boreholes, seismic reflection and refraction are the well-known procedures to obtain the velocity profiles. But these techniques are expensive and complicated, especially for deep sites. Theoretical transfer functions can be calculated by analyses from the one-, two- and three-dimensional velocity models (Haskell, 1960; Kennett, 1983; Sanchez-Sesma, 1987; Pitarka et al., 1998).

An alternative technique to get the shallow or deep velocity profiles is surface wave measuring by "active sources" (i.e., hammers, vibrators, shakers, etc.). Two well-known active-source methodologies to obtain velocity profiles are Spectral Analysis of Surface Waves (SASW) (Stokoe et al., 1994) and Multi-Channel Array Surface Waves (MASW) (Park et al., 1999). Theoretical dispersion curves of the generated and measured velocity profiles are matched as a result of iteration steps (Rosenblad and Li, 2009).

Shallow wave models can be also determined by "passive seismic" methods that employ microtremors. These small vibrations within earth are recorded and studied with one of the existing passive techniques which are Refraction Microtremor (ReMi) (Louie, 2001), Frequency-Wavenumber (F-K) (Schmidt, 1986) and Spatially averaged coherency (SPAC) (Asten et al., 2003).

The quarter wavelength approach is another option to compute the site amplification factors (Joyner and Fumal, 1985; Boore and Joyner, 1997). The equation is expressed as:

$$A(f(z)) = \sqrt{\frac{\rho_s \beta_s}{\bar{\rho}(z)\bar{\beta}(z)}} \tag{2.16}$$

where $f(z) = \frac{1}{4S_{tt}(z)}$ is the frequency corresponding to depth z where $S_{tt}\,(z)$ defines S-wave travel time from depth z to the ground; ρ_s and β_s indicates the density and S-wave velocity around the source, respectively; $\bar{\rho}(z)$ and $\bar{\beta}(z)$ is travel-time-weighted average of density and S-wave velocity to depth z, respectively. (ρ_s β_s : seismic impedance at source level, $\bar{\rho}(z)\,\bar{\beta}(z)$: average seismic impedance calculated over depth z corresponding to a quarter of wavelength).

The close estimations of the quarter wavelength method are checked against the exact theoretical amplifications and their accuracy is verified (e.g.: Boore and Joyner, 1991; Silva and Darragh, 1995; Boore and Joyner, 1997). This approach applied on representative soil profiles by Boore and Joyner (1997) and they attained generic site amplification functions in accordance with National Earthquake Hazards Reduction Program (NEHRP 2009) site classes. When detailed soil profile is not available at a certain site, generic amplification functions can be used considering their uncertainty.

Another popular technique to determine site amplification factors is empirical Horizontal-to-Vertical ratio (H/V) approach for sites that velocity profile does not exist (Nakamura, 1989). This technique uses the assumption that the horizontal components of ground motions are more exposed to local soil effects. The ratio of the components measured at the surface (horizontal to vertical) eliminates the complex source and path propagation effects. The result of this division is the site amplification which is experienced by horizontal component. Weak ground motions and aftershocks are used to predict the fundamental frequencies and the related amplifications, as an advantage of this method. The strong motions, however, fail to find amplifications although they can effectively find the fundamental frequencies of soils (Sisman et al., 2018). The H/V method has been utilized in many research studies to obtain local site amplifications and its success has been verified (e.g.: Lermo and Cháves-García, 1994; Suzuki et al., 1995; Huang and Teng, 1999; Raghukanth and Somala, 2009; Sisman et al., 2018).

Among the aforementioned methods to model local soil effects in stochastic simulations, Boore and Joyner (1997) approach is used in Erzincan region; while, both H/V and Boore and Joyner (1997) methods are applied in Duzce (Ugurhan and Askan, 2010; Askan et al., 2013; Askan et al., 2015; Karimzadeh et al., 2017b; Karimzadeh et al., 2018).

ii: Calculation of D(f):

Diminution factor, $D(f)$ defines the energy loss at high frequencies that is not dependent on path. At near-field sites, spectral values at high frequencies rapidly decay and this decreasing is not related with the wave propagation attenuation (Boore, 1983). There are some opinions regarding the reason of this energy loss. According to Papageorgiou and Aki (1983) the reason of this decay is the earthquake source mechanism, while Hanks (1982) and Atkinson (2004) relates this behavior to the near-surface site conditions. Two basic filters are used to model the reduction of amplitudes at higher frequencies. The f_{max} filter (Hanks, 1982) is the first one, that the diminution function given as:

$$D(f) = \left[1 + \left(\frac{f}{f_{max}}\right)^8\right]^{-0.5} \tag{2.17}$$

where f_{max} is the high-cut filter frequency.

Second method to represent the high frequency spectral attenuation is the "kappa operator" proposed by Anderson and Hough (1984) which characterizes the decay with an exponential function. Horizontal and vertical kappa values can be calculated with this approach. Kappa factor determination process starts with generating the Fourier acceleration spectrum of each ground motion component in semi-logarithmic scale. Linear fit to the decaying part is determined. Then, the slope of the best-fit line is divided to $-\pi$, and the kappa factors of each component are determined. The computed kappa values versus the epicentral distances of the stations is plotted and the line that determines the model is obtained. The estimated kappa value at the zero epicentral distance gives the κ_0 (zero-distance kappa) of the related site. In stochastic method κ_0 values are utilized as the near-surface attenuation parameter to remove distance effects, since the path attenuation between the source and station is already included in the path effects (Margaris and Boore, 1998). The corresponding kappa filter function is given as:

$$D(f) = e^{-\pi \kappa_0 f} \tag{2.18}$$

2.3. Stochastic Finite-Fault Modeling

Stochastic point-source technique is useful to generate ground motions for far distances and small to moderate magnitude earthquakes. Besides, stochastic finite-fault simulations can successfully model ground motions for near-source stations or large magnitude events, since finite-fault features (rupture geometry, spatial slip variation, rupture directivity) have a remarkable effect on ground motion characteristics. Beresnev and Atkinson (1997) introduced the initial stochastic finite-fault technique to generate ground motions of close-source stations. In this approach, the fault plane is divided into smaller rectangular sub-faults of specified dimensions to reflect the finite-fault effects (Hartzell, 1978). A sub-fault is modeled as a point-source with a ω-square spectrum. Rupture propagation initiates radially with a constant shear wave velocity from the hypocenter which is assumed on the center of a sub-fault. The final ground motion is obtained by summing the contributions from all sub-faults in time domain by including time delay of each sub-fault (Atkinson et al., 2009). The total response of the fault plane is given as:

$$a(t) = \sum_{i=1}^{nl} \sum_{j=1}^{nw} a_{ij} \left(t - \Delta t_{ij} - T_{ij}\right) \quad (2.19)$$

where $a(t)$ is the ground acceleration at time t, nl and nw is the number of sub-faults along the length and width of the main fault, respectively; Δt_{ij} is the delayed time of the radiated wave from ij^{th} sub-fault to the station; $a_{ij}(t)$ is the ground acceleration of ij^{th} sub-fault modeled as a point-source as defined by Boore (1983). Figure 2.2 represents the rupture propagation on the fault plane.

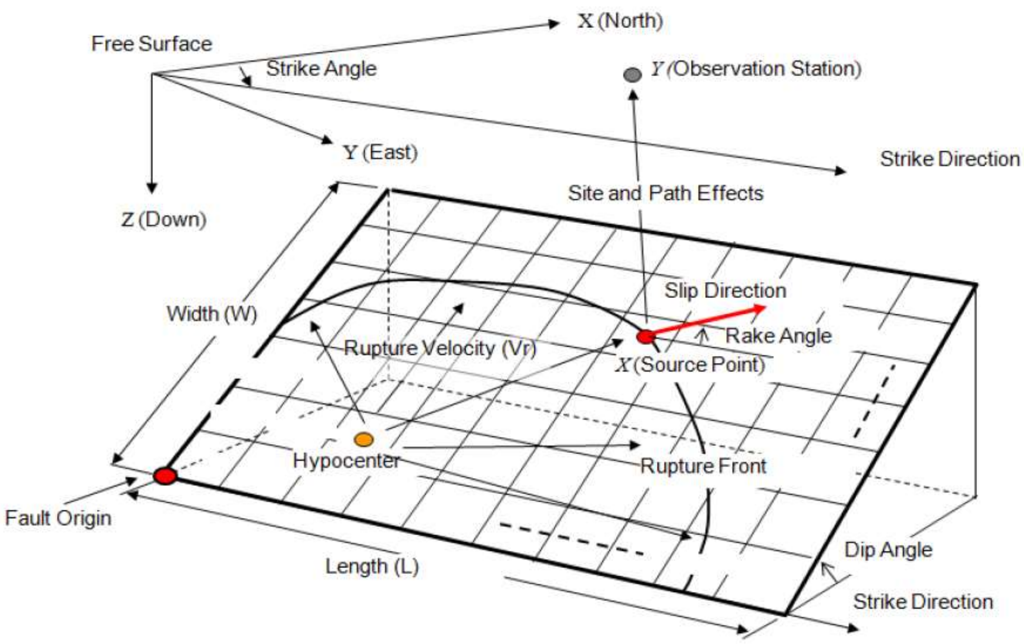

Figure 2.2. Wave propagation on a rectangular finite-fault model (Adapted from Hisada, 2008)

The original model for the acceleration Fourier amplitude spectrum of a sub-fault was as follows (Aki, 1967; Brune, 1970; Boore, 1983; Beresnev and Atkinson 1997):

$$A_{ij}(f) = CM_{0ij}\frac{(2\pi f)^2}{\left[1+\left(\frac{f}{f_{cij}}\right)^2\right]}\frac{1}{R_{ij}}\, exp\left(-\frac{\pi f R_{ij}}{Q(f)\beta}\right)\exp(-\pi\kappa f)\, A(f) \qquad (2.20)$$

where M_{0ij}, f_{cij}, and R_{ij} is the seismic moment, corner frequency, and distance from the observation point of the ijth sub-fault, respectively. C is a constant defined as $C = \Re_{\theta\varphi}FV/(4\pi\rho\beta^3)$, where $\Re_{\theta\varphi}$ is radiation pattern constant and usually is equal to 0.55 for shear waves, F is free surface amplification as 2, V is partition into two horizontal components equal to 0.71. $f_{cij} = 4.9E^{+6}\beta(\Delta\sigma/M_{0ij})^{1/3}$, where $\Delta\sigma$ is stress drop in bars, M_{0ij} is ijth sub-fault seismic moment in dyne-cm, and β is shear wave velocity in km/s. The term $1/R$ indicates geometric attenuation. The term $exp\left(-\frac{\pi f R_{ij}}{Q(f)\beta}\right)$ indicates the anelastic attenuation as Q is the quality factor. The term $exp(-\pi f\kappa)$ expresses the kappa effects. $A(f)$ indicates the amplification filter.

The FINSIM software is improved for stochastic finite-fault technique (Beresnev and Atkinson, 1998a and 1998b). This approach considers the seismic moment of each sub-fault as the ratio of its area to the total fault area, given as:

$$M_{0ij} = \frac{M_0}{N} \qquad (2.21)$$

where N is the total number of the sub-faults, M_0 is the total seismic moment of the fault plane, and M_{0ij} is the seismic moment of the ij^{th} sub-fault.

The seismic moment for each sub-fault with different sizes is given as:

$$M_{0ij} = \frac{M_0 S_{ij}}{\sum_{l=1}^{nl}\sum_{k=1}^{nw} S_{kl}} \qquad (2.22)$$

where S_{ij} is the relative slip weight of the ij^{th} sub-fault.

Motazedian and Atkinson (2005) revised the stochastic finite-source model to include a dynamic corner frequency which is time-dependent instead of static corner frequency. Motazedian and Atkinson (2005) developed the software EXSIM by including the theory of dynamic corner frequency. The several researchers have studied that in stochastic point-source technique the corner frequency is inversely proportional to the total duration or entire ruptured area, directly or indirectly (e.g.: Hirasawa and Stauder, 1965; Boore, 1983; Boatwright and Choy 1992; Hough and Dreger, 1995). In the finite-fault approach, the entire rupture area is a function of time, and consequently the corner frequency. The followed formula is improved by Motazedian and Atkinson (2005) to include the dependency of corner frequency on rupture time:

$$f_{cij}(t) = N_R(t)^{-1/3}\, 4.9 \times 10^6 \beta \left(\frac{\Delta\sigma}{M_{0ave}}\right)^{1/3} \tag{2.23}$$

where $N_R\ (t)$ is the cumulative number of ruptured sub-faults at time t, M_{0ave} is the average seismic moment of sub-faults equal to M_0/N.

Motazedian and Atkinson (2005) has introduced a second substantial change to original form of the finite-fault methodology by defining pulsing area percentage. This concept separates the sub-faults as passive and active rupture areas, and formulated as the ratio of the ruptured (active) area to the total fault area. Rupture propagates till the pulsing area percentage is reached by sub-faults. Hence, until specified pulsing area percentage is achieved, the corner frequency and the radiated energy of high frequencies reduces due to its relation with the ruptured sub-faults. Hereafter, the dynamic corner frequency becomes constant. Because of the decreasing radiated energy problem, a scaling factor H_{ij} is described to balance the high frequency spectral level of sub-faults (Motazedian and Atkinson, 2005).

$$H_{ij} = \left\{ N \frac{\Sigma\left[\frac{f^2}{1+\left(\frac{f}{f_c}\right)^2}\right]}{\Sigma\left[\frac{f^2}{1+\left(\frac{f}{f_{cij}}\right)^2}\right]} \right\}^{1/2} \tag{2.24}$$

Pulsing area percentage and stress drop have substantial influences on the final amplitudes of the generated ground motions. The first parameter controls the amplitudes of low- frequency band of simulated accelerograms. Stress drop affects the amplitudes at high frequencies. Low stress drop values result in small amplitudes of response spectra at high frequencies. Consequently, various amplitudes of time histories at high and low frequencies can be generated through modifying the stress drop and pulsing area percentage. But this should not be a random fitting and selected simulation parameters are need to be suitable to the physical characteristics of the observed earthquake.

The final form of stochastic finite-fault technique used to compute the acceleration Fourier amplitude spectrum proposed by Motazedian and Atkinson (2005) given as follows:

$$A_{ij}(f) = CM_{0ij}H_{ij}\frac{(2\pi f)^2}{\left[1+\left(\frac{f}{f_{cij}(t)}\right)^2\right]}\frac{1}{R_{ij}}\ exp\left(-\frac{\pi f\ \ _{ij}}{Q(f)\beta}\right)\exp(-\pi\kappa f)\,A(f) \tag{2.25}$$

where the terms are as described earlier.

The basics of finite-fault simulation technique is same as stochastic point-source approach as provided in Section 2.2, but it is modified with additional major revisions related with source mechanism.

In this thesis, the synthetic ground motion dataset is implemented from the past simulation studies (Ugurhan and Askan, 2010; Askan et al., 2013; Askan et al., 2015;

Karimzadeh et al., 2017b Karimzadeh et al., 2018). In those studies, finite-fault method as introduced in Motazedian and Atkinson (2005) is utilized to generate acceleration time histories. The free software EXSIM is employed, which is globally used for simulation purposes and validated by numerous researchers (e.g.: Motazedian and Atkinson, 2005; Atkinson et al., 2009; Boore, 2009). Stochastic finite-fault technique is chosen since high frequencies are efficiently modeled by this method, although complete wave propagation and complex source effects are insufficient. Besides, it has been employed in many regions with lack of recorded ground motions. Eventually, this method is globally used to generate synthetic accelerograms in engineering and seismological studies (e.g.: Motazedian and Moinfar, 2006; Raghukanth and Somala, 2009; Ugurhan and Askan, 2010; Chopra et al., 2012; Ghofrani et al., 2013; Askan et al., 2013; Mahood et al., 2014; Askan et al., 2015; Goda et al., 2017; Zhang et al., 2018; Karimzadeh and Askan, 2018).

CHAPTER 3

GROUND MOTION SIMULATIONS IN ERZINCAN AND DUZCE REGIONS

3.1. Introduction

In this section, the simulated ground motions used in developing a GMPE are presented. The synthetic ground motion dataset used to derive the GMPEs is implemented from the past studies of Ugurhan and Askan (2010), Askan et al. (2013); Askan et al. (2015), Karimzadeh et al. (2017b) and Karimzadeh et al. (2018). In those studies, stochastic finite-fault simulation technique as provided in Chapter 2 is applied. Stochastic methods practically yield ground motion amplitudes for larger events, for observation points located close to the fault ruptures and for sparsely monitored seismically active regions.

This section presents the applications of the stochastic finite-fault technique to generate simulated accelerograms. The organization of this chapter is given in following paragraphs. In Section 3.2, the seismological and geological information of Erzincan and Duzce regions are presented. Section 3.3 introduces the first case: Development of the synthetic ground motion database in Erzincan region. Subsection 3.3.1 provides the real ground motions of the March 13, 1992 Erzincan (Eastern Turkey) mainshock (M_w 6.6), while the Subsection 3.3.2 presents the ground motion simulations of this event with the stochastic model parameters used in simulations. Comparison of the real and simulated records of the 1992 Erzincan event and the simulated ground motion database for Erzincan region are presented in Subsection 3.3.3 and 3.3.4, respectively. The second case which is development of the synthetic ground motion database in Duzce region is presented in Section 3.4. Subsection 3.4.1 indicates the real ground motion records of the November 12, 1999 Duzce (Western Turkey) event (M_w 7.1) obtained at the near fault stations. Subsection 3.4.2 provides the ground motion simulations of this earthquake with the selected model parameters. Subsection 3.4.3 compares the observed and simulated accelerograms of the 1999 Duzce earthquake while Subsection 3.4.4 provides the simulated ground motion database for Duzce region.

3.2. Study Regions

North Anatolian Fault (NAF) is an energetic right-lateral strike-slip fault zone located in Northern Turkey and is among the most hazardous seismic regions of the world. The main reason for selecting Duzce and Erzincan as study area is that they both contain strike slip mechanisms and are located upon NAFZ. While the former is on western part of NAFZ with a high population and seismically well investigated due to adequate number of seismic networks, the latter is on eastern part of NAFZ which is relatively less studied and sparsely instrumented. In the past century, NAFZ has caused highly devastating earthquakes in Turkey. The east of NAFZ is shaken by the 1939 Erzincan (M_s~8.0) and 1992 Erzincan (M_w 6.6) events while the western part is affected by the 1999 Kocaeli (M_w 7.6) and 1999 Duzce (M_w 7.1) earthquakes. The tectonic map of Turkey is displayed in part (a) of Figure 3.1. Parts (b) and (c) of Figure 3.1 provide regional maps of Duzce and Erzincan showing the focal mechanisms, fault planes, epicenters of the November 12, 1999 Duzce and March 13, 1992 Erzincan earthquakes as well as strong ground motion stations that recorded the aforementioned events, respectively.

Erzincan is situated on a very thick alluvial basin inside of a seismically complex zone, at the intersection of the following active faults: Right lateral NAF, the left lateral North East Anatolian Fault (NEAF) and East Anatolian Fault (EAF) zones. However, Erzincan area in Eastern Turkey is not investigated efficiently due to lack of seismic observation points in contrast with the critical seismic activity. The destructive sequence of earthquakes on NAFZ in the past century began with the earthquake in 1939 in Erzincan and resulted in more than 30.000 deaths, causing the city to be resettled in the north. In the recent past, Erzincan was affected by a devastating earthquake at the intersection of the NAFZ and Ovacik faults on March 13, 1992 (M_w 6.6), causing significant structural damage, suffering 500 casualties and US \$ 3-5 million (Akinci et al., 2001).

Duzce is a city located on a shallow alluvial pull-apart basin in the western of NAFZ and surrounded by major industrial facilities and dense residential building stock. A major right-lateral strike slip earthquake occurred on Duzce fault on November 12, 1999 with M_w 7.1, and caused almost 900 deaths and 3000 injuries with significant structural damage (Akyuz et al., 2002). The city has survived two major earthquakes, named as 1999 Kocaeli (M_w 7.6) and 1999 Duzce (M_w 7.1), 3 months apart in 1999. These earthquakes are important because of the wide-scale damage they caused to the industrial heartland and the most intensely populated regions in Turkey. Furthermore, seismological community places a particular importance to these events because of the arguments on whether Duzce earthquake is a mainshock. The supershear rupture issue (when rupture velocity is faster than the S-wave velocity of the source material) is the other major characteristic of the Duzce event. Thus, this area deserves detailed studies involving simulations.

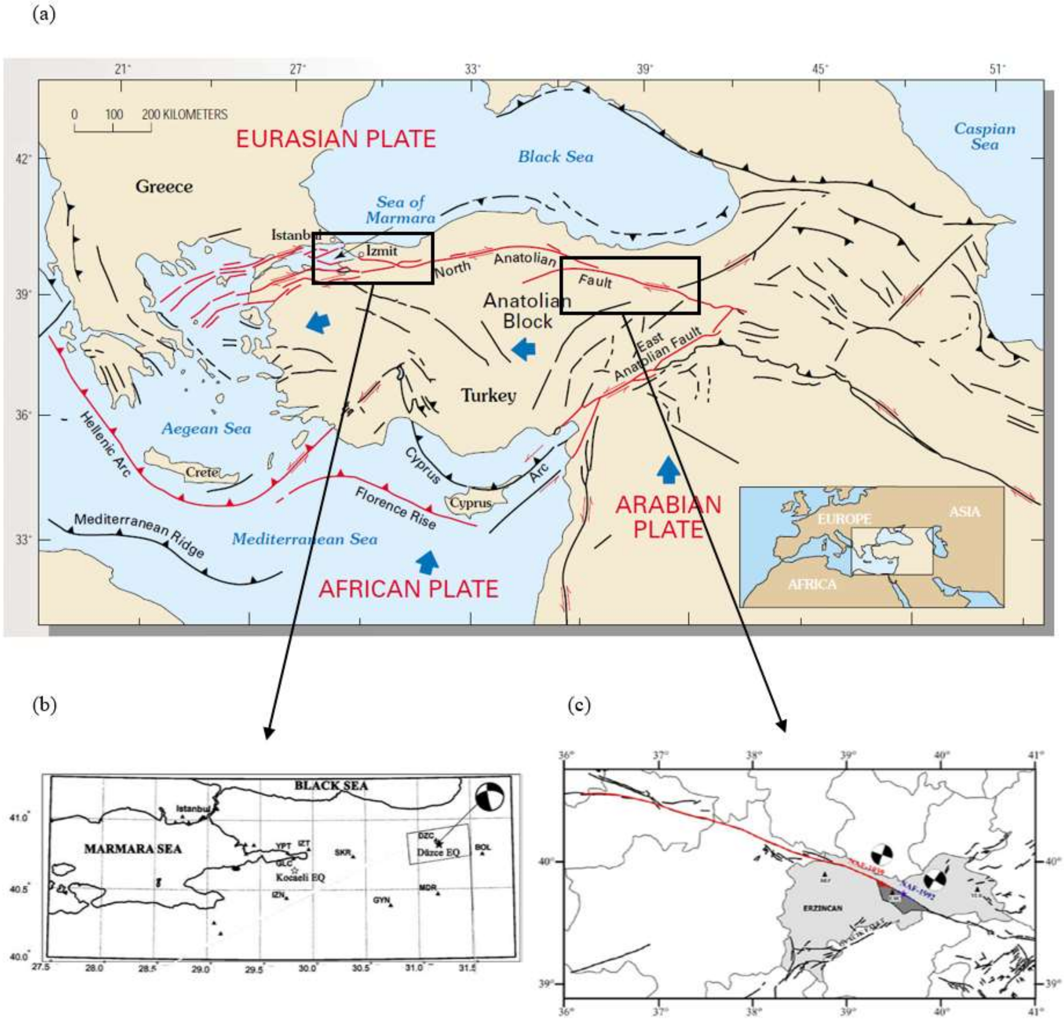

Figure 3.1. (a) Tectonic map of Anatolian Block (Adapted from Holzer, 2000). (b) Regional figure indicates the focal mechanism of the November 12, 1999 Duzce event. The triangles show the stations. The epicenters of the 1999 Duzce and Kocaeli earthquakes are shown with a solid and an empty star, respectively (Adapted from Ugurhan and Askan, 2010). (c) Regional plot displays the fault planes, the focal mechanisms and epicenters of the 1939 and 1992 mainshocks (epicenters are shown in order of with red and blue stars). The points shown with black triangles are the observation stations which recorded March 13, 1992 Erzincan event. Additionally, Erzincan basin is represented by a shady part parallel to the 1992 fault (Adapted from Askan et. al., 2013). (For explanations of the color references in this figure, please refer to the online version of this thesis.)

3.3. Development of the Synthetic Ground Motion Database in Erzincan Region

3.3.1. Recorded Ground Motion Data of the 1992 Erzincan Earthquake

Erzincan basin has dimensions of 50 x 15 km and it is a pull-apart basin due to the tectonic effects between NAFZ and Ovacik Faults. It is the biggest basin on the NAFZ that is close to the Firat River. The center of the basin is composed of deep alluvial layers and the thickness diminishes close to the mountains (Lav et al., 1993). As a result, seismic risk in Erzincan fundamentally increases due to the basin effects which amplifies ground motion amplitudes.

Up to now, Erzincan has been monitored by a small number of observation stations. The strong ground motions of March 13, 1992 earthquake was recorded by only three stations. Figure 3.2 shows the area with the fault plane, epicenter and the positions of the seismic observers. Table 3.1 lists the names and codes of the stations, station coordinates, site classes, epicentral distances (R_{EPI}: the distance between the epicenter and the station), Joyner-Boore distances (R_{JB}), two horizontal (East-West, EW and North-South, NS) PGA and PGV values. Soil classifications are provided in accordance with the NEHRP (2009) site classifications. The raw acceleration time histories of the records are obtained from strong ground motion database of Turkey (http://kyhdata.deprem.gov.tr/2K/kyhdata_v4.php). Baseline correction and filtering in the frequency band of 0.1-10 Hz using a 4th order Butterworth filter is applied to all time histories.

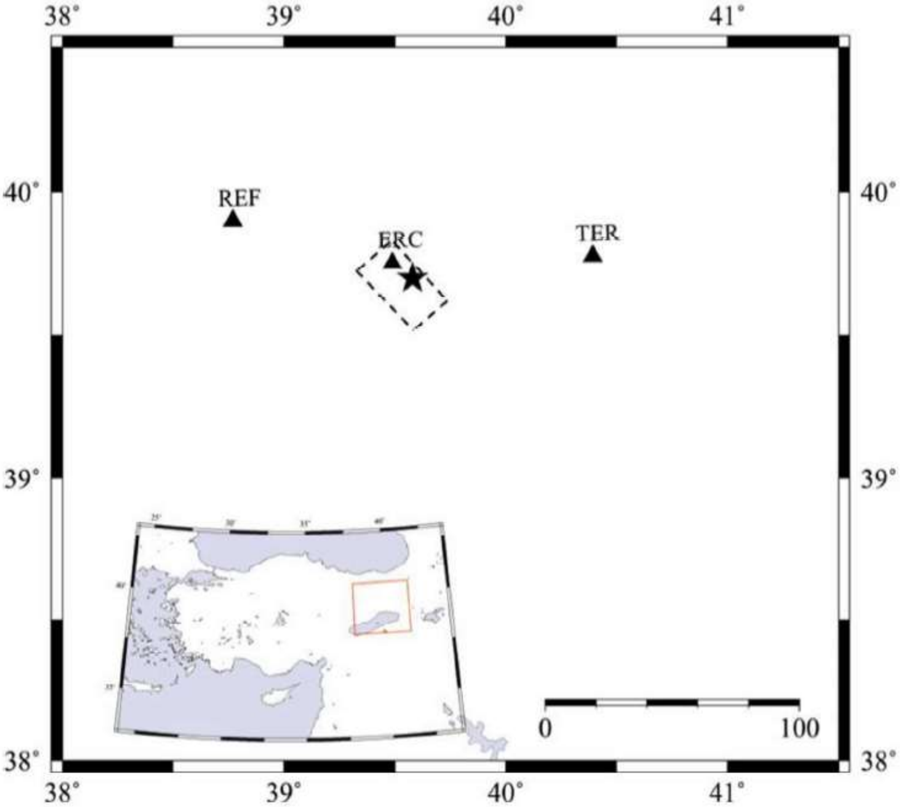

Figure 3.2. Map presents the epicenter, fault plane and observation points of the 1992 Erzincan mainshock (Adapted from Karimzadeh, 2016)

Table 3.1. *Data of the seismic stations that recorded the 1992 Erzincan mainshock*

Station Name	Station Code	Latitude (°)	Longitude (°)	Site Class (NEHRP)	R_{EPI} (km)	R_{JB} (km)	PGA (EW) (cm/s^2)	PGA (NS) (cm/s^2)	PGV (EW) (cm/s)	PGV (NS) (cm/s)
Erzincan-Merkez	ERC	39.752	39.487	D	12.83	5.04	430.66	509.20	56.80	79.84
Refahiye	REF	39.899	38.768	C	76.45	63.50	75.26	66.78	3.67	3.93
Tercan	TER	39.777	40.391	D	65.62	40.39	25.56	37.90	4.30	2.86

3.3.2. Ground Motion Simulation of the 1992 Erzincan Earthquake

Determining the input parameters is the basic step to obtain simulated free-field motions. For reliable estimations, seismic parameters should be derived from regional data. If the regional data and surveys are not satisfactory, generic model parameters of similar seismotectonics or soil conditions can be employed in simulations.

Earthquake source, propagation, and site model parameters of the Erzincan mainshock are validated by Askan et al. (2013), and these verified input parameters are used in EXSIM program. Askan et al. (2013) has employed the verified models of the prior studies related with the region for faulting and path input effects, but has obtained the local site parameters for each real record of three stations.

3.3.2.1. Source Model

As recommended in Askan et al. (2013), source model given by Bernard et al. (1997) is utilized among numerous models. This model gives the smallest error from Fourier Amplitude Spectra (FAS) of observed versus simulated time histories, particularly in low frequency portion of accelerograms which is principally influenced by source effects. Table 3.2 lists the source input parameters explained in Chapter 2. Furthermore, uniform slip distribution is used according to observations made in Legrand and Delouis (1999). Askan et al. (2013) has determined stress drop to be 80 bars and the pulsing area percentage to be 50%. These values give the smallest mismatch between the observed versus generated records both in time and frequency domain.

3.3.2.2. Path Model

To define seismic wave propagation from the earthquake source, three main parameters exist: geometric spreading, quality factor and duration effects. The quality factor model provided by Grosser et al. (1998) as $Q = 122f^{0.68}$ is used in Erzincan, since it matches the spectral amplitudes closely. The following geometrical spreading function of Akinci et al. (2001) for Erzincan region is employed:

$$\begin{array}{ll} R^{-1.1}, & R \leq 25\ km \\ R^{-0.5}, & R > 25\ km \end{array} \tag{3.1}$$

The duration model of Herrmann (1985) is used which depends on source duration (T_0) and hypocentral distance (R):

$$T = T_0 + 0.05R \tag{3.2}$$

Table 3.2. *Simulation parameters of the 1992 Erzincan event*

Parameter	**Value**
Moment Magnitude	6.6
Hypocenter Location	39.716°N, 39.629°E
Hypocenter Depth	9 km
Depth to the Top of the Fault Plane	2 km
Fault Orientation	Strike: 125°, Dip: 90°
Fault Dimensions	25 km x 9 km (Wells and Coppersmith, 1994)
Subfault Dimensions	5 km x 3 km
Crustal Shear Wave Velocity, β	3700 m/s
Rupture Velocity (0.8β)	3000 m/s
Crustal Density, ρ	2800 kg/m^3
Stress Drop, Δσ	80 bars (Mohammadioun and Serva, 2001)
Pulsing Percentage Area	50
Geometrical Spreading	$R^{-1.1}$, $R \leq 25$ km $R^{-0.5}$, $R > 25$ km
Quality Factor, Q	$Q = 122 f^{0.68}$
Duration Model, T	$T = T_0 + 0.05R$
Windowing Function	Saragoni-Hart
Kappa Factor, (κ_0)	Regional Kappa Model (κ_0 = 0.066) (Askan et al., 2013)
Site Amplification Factors	Local soil model at each station (Askan et.al., 2015)

3.3.2.3. Site Model

In stochastic method, the true modelling of the site conditions is very critical due to the direct impact of frequency-dependent amplification factors on the ground motion amplitudes. Site response is the sum of local site amplification and high frequency decay (kappa) activity at the observation points. As provided in Askan et al. (2013), both amplification and kappa functions are evaluated according to previous ground motions observed at ERC, REF and TER stations. Accelerograms employed for amplification and kappa investigations are mostly obtained from earthquakes with M_w 3-5. Site amplification factors are calculated by theoretical 1D site response analysis at all stations. Since the high quality real ground motions at REF, and TER stations were limited, empirical H/V ratio technique could not be used. The theoretical transfer function, that is the spectral ratio between the input acceleration time history at the bed rock plane and the surface motion get from 1D wave propagation in the soil strata, is given as the output of site-response studies. In Askan et al. (2013), a weak time history (0.001g in PGA) observed at ERC from a M_w 3.4 event is used as the input ground motion. The theoretical site amplification factors are used at all selected stations (Figure 3 in Askan et al., 2013).

Askan et al. (2013) has noticed that the accelerograms of all stations show very similar decrease in high frequency band of FAS. Because of this, a local kappa model has estimated by combining the time histories of all recording sites. In stochastic method, the zero-distance kappa is utilized to isolate the regional attenuation characteristics that are already presented in the frequency-dependent quality term. The zero-distance kappa (κ_0) value was calculated to be 0.066 by analyzing of available records in Erzincan territory (Figure 4 of Askan et al., 2013).

3.3.3. Comparisons of the Simulated and Recorded Ground Motions of the 1992 Erzincan Earthquake

For comparisons, 2 observed and 1 generated horizontal components are available at each station. Simulated and real time series have not been scaled or modified: Only baseline corrections and filtering within the frequency band of 0.1-10 Hz with a 4th order Butterworth filter is applied. Figure 3.3 displays the acceleration time histories and the FAS for both recorded and simulated ground motions of each station.

Comparison results shown in Figure 3.3 for station ERC indicate a satisfactory agreement between the recorded and simulated FAS for high frequencies, while the simulated record underestimates the low frequency motions due to the source effects. At ERC station, observed acceleration time series display high acceleration and short duration, probably due to the forward directivity effects. In stochastic finite-fault method, directivity effect cannot be modelled accurately (Assatourians and Atkinson, 2007). This is the probable reason of the mismatch at low frequencies of time histories at ERC station. Figure 3.3 demonstrates that at station REF, the EW component of the real ground motion matches closely with the synthetic spectra, while the NS component displays small amplitudes compared to both the EW component and the simulated accelerogram. Finally, the recorded and simulated spectra at TER station are consistent with each other; probably because of the use of local site factors at this station. However, the generic duration model (Herrmann, 1985) can not sufficiently mimic the duration of real acceleration time history at TER, as seen clearly in Figure 3.3. Since Erzincan is positioned on an alluvial basin, possible basin effects can be seen with long durations and large surface wave amplitudes, as it is in TER record. It should be noted that, much better results can be obtained with well-defined physical models and wave velocity models.

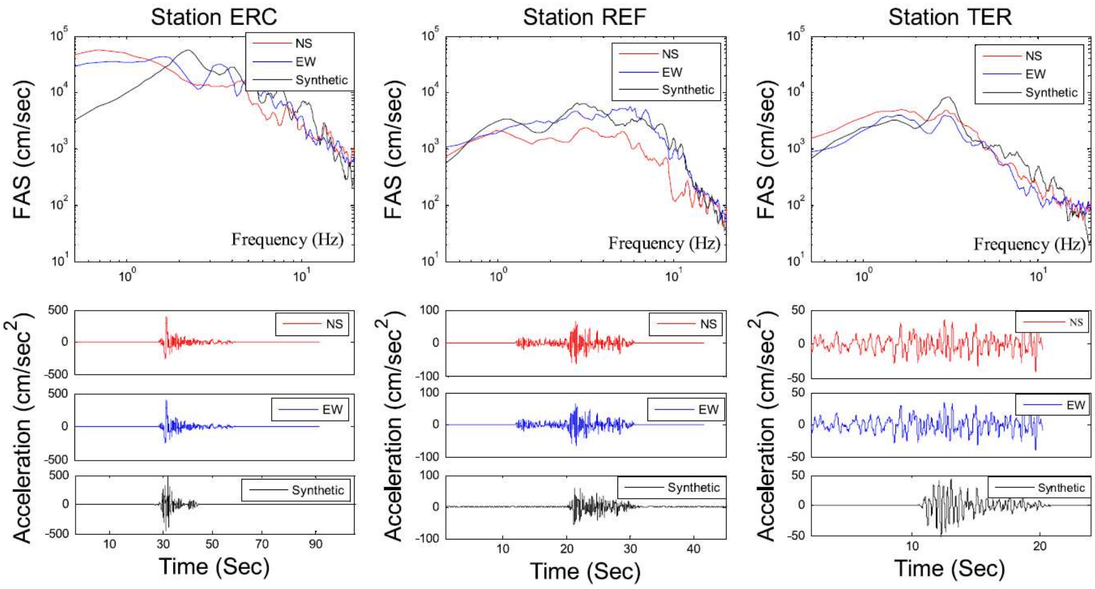

Figure 3.3. Comparison of Fourier amplitude spectra and acceleration time series of the real and simulated ground motions of 1992 Erzincan event (Adapted from Askan et al.,2013)

3.3.4. Simulated Ground Motion Database for Erzincan Region

Accelerograms were simulated for scenario earthquakes of several sites (M_w 5.0, 5.5, 6.0, 6.5, 6.6 (1992 event) 7.0, and 7.5) within the previous studies by Askan et al. (2015) and Karimzadeh et al. (2018). The epicenter of all scenario events was taken the same as the epicenter of the 1992 event, which is critically in the vicinity of city center. The source, site and path models were also taken from Askan et al. (2013) and Askan et al. (2015). The predicted parameters are verified by comparison of the simulated seismograms with the observed ones of 1992 Erzincan mainshock. Random slip distribution models were considered for all shaking scenarios, since the finite-fault slip distribution model of the simulated events is not available. Table 3.2 displays the simulation parameters. Between all kinematic source modeling parameters, only stress drop and fault plane geometry take different values for each moment magnitude.

In the simulated database, Erzincan area lies within a rectangular box localized by 39°-40° Northern latitudes, 39°-40° Eastern longitudes. A total of 244 points are chosen in this area to generate full waveforms of scenario events. Figure 3.4 presents the distribution of 123 of points in the region. A total of 90 of the points symbolized with red circle signs and are about 1 km away from each other. 24 of the nodes indicated with black triangular show the coordinates of all districts in Erzincan city center. The final 9 points shown with green rectangular are the stations which have comprehensive S-wave velocity soil profiles (Askan et al, 2016; Karimzadeh et al., 2018). Besides, additional 121 nodes are 10 km away from each other, and defined at the outside of Erzincan, and cannot be shown on the figure due to scaling problems. As expressed in Askan et al. (2015), the velocity profiles at 9 stations were constructed with a microtremor array technique. Since site velocity profiles are not available for the rest of the points, the V_{S30} value of the nearest station is considered at each node. This perspective produced uncertainty in the simulations, but due to the proximity of the nodes, the ultimate error can be ignored. Finally, 1587 simulated ground motion records are obtained in Erzincan region to use in the development of GMPEs.

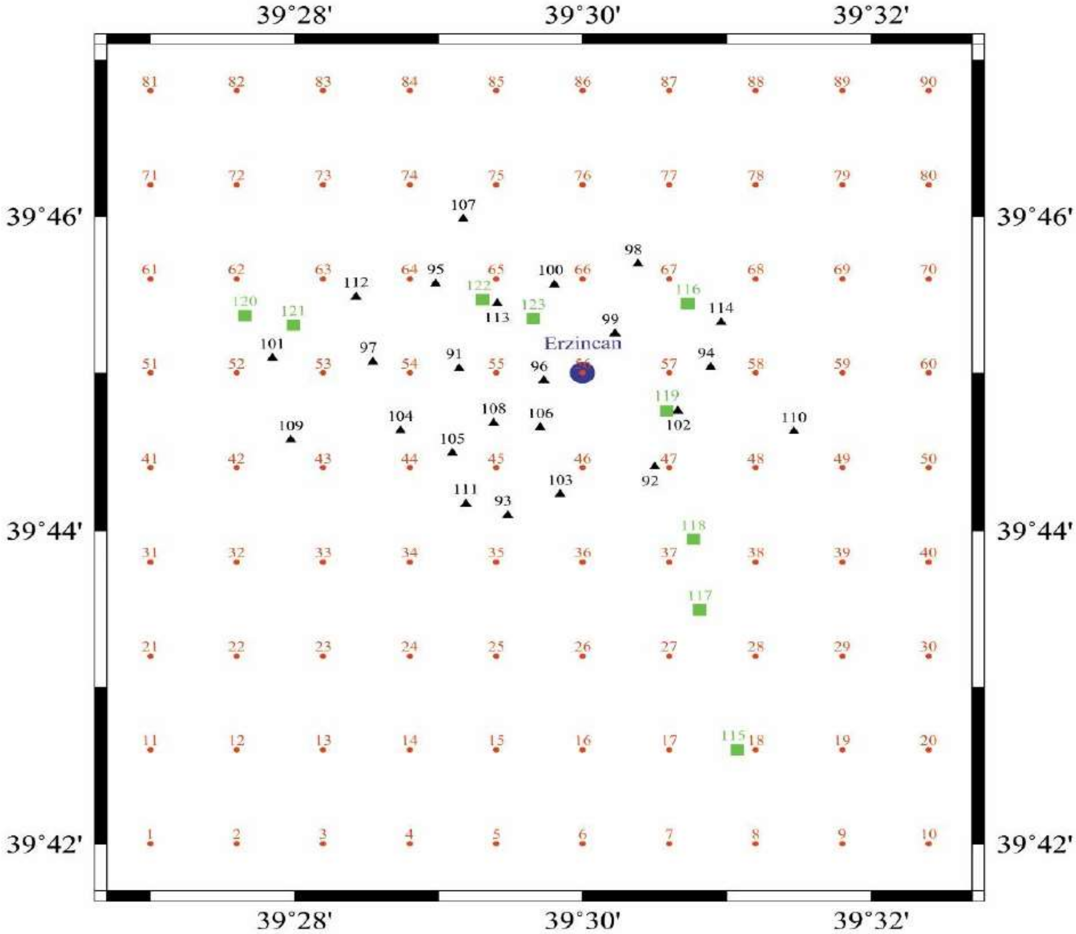

Figure 3.4. Distribution of the nodes in Erzincan region (Adapted from Karimzadeh et al., 2018)

3.4. Development of the Synthetic Ground Motion Database in Duzce Region

3.4.1. Recorded Ground Motion Data of the 1999 Duzce Earthquake

The 1999 Duzce earthquake is recorded by a regional network which consists of 32 seismic stations. Among these, 5 stations whose epicentral distances smaller than 125 km were considered for simulations in Karimzadeh et al. (2017b), due to high damage potential of the near-source accelerograms. Figure 3.5 represents the fault plane, epicenter and the selected stations. Table 3.3 presents the names and codes of the stations, hypocentral coordinates, site classes, epicentral and Joyner-Boore distances, PGA and PGV values for each direction. The raw motions at the five stations are taken from strong ground motion database of Turkey (http://kyhdata.deprem.gov.tr/2K/kyhdata_v4.php). Baseline correction and filtering in the frequency band of 0.1-10 Hz using a 4th order Butterworth filter has been applied to all time histories.

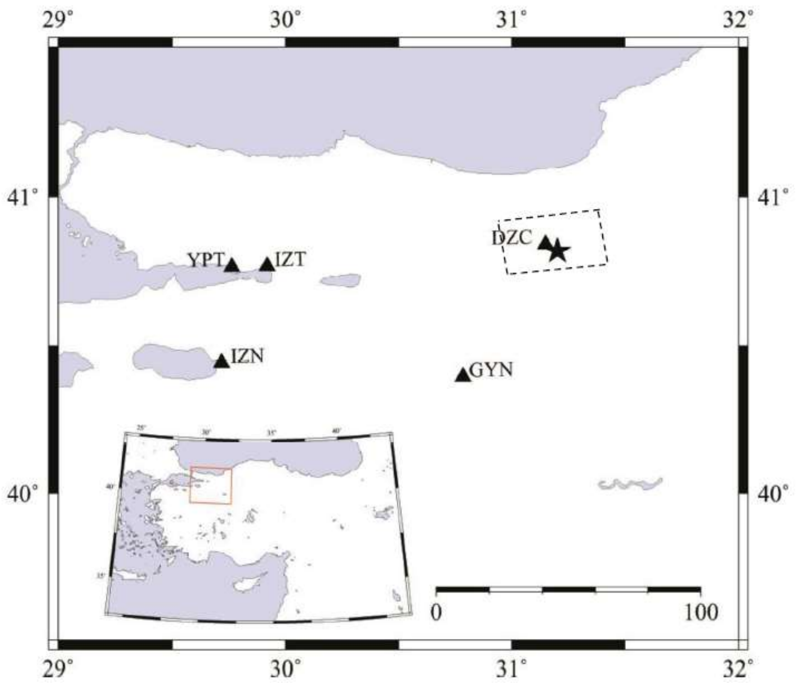

Figure 3.5. Map plots the epicenter, fault area and seismic stations of the 1999 Duzce event (Adapted from Karimzadeh et al., 2017b)

Table 3.3. *Data of the seismic stations which recorded the 1999 Duzce event*

Station Name	Station Code	Latitude (°)	Longitude (°)	Site Class (NEHRP)	R_{EPI} (km)	R_{JB} (km)	PGA (EW) (cm/s^2)	PGA (NS) (cm/s^2)	PGV (EW) (cm/s)	PGV (NS) (cm/s)
Duzce	DZC	40.8436	31.1488	D	9.31	0.14	520.41	328.03	86.54	54.53
Goynuk	GYN	40.3965	30.7830	D	55.16	38.46	22.17	25.79	5.84	4.49
Iznik	IZN	40.4416	29.7168	D	123.67	91.67	20.06	21.25	1.97	2.27
Izmit	IZT	40.7665	29.9172	C	100.70	67.86	16.41	18.73	2.27	1.73
Yarimca Petkim	YPT	40.7639	29.7620	D	116.85	80.92	16.15	23.47	4.08	8.38

3.4.2. Ground Motion Simulation of the 1999 Duzce Earthquake

In this section, simulated records of Duzce earthquake previously studied by Karimzadeh et al. (2017b) is presented. The simulated records in Karimzadeh et al. (2017b) employed the site-specific parameters confirmed by Ugurhan and Askan (2010) with a minor change in site functions.

3.4.2.1. Source Model

The epicenter coordinates are stated as 40.82º N, 31.20º E by Earthquake Research Department of General Directorate of Disaster Affairs at that time (ERD). The hypocentral depth is taken equal to 12.5 km (Milkereit et al., 1999). The fault area is 65 x 25 km in length and width (Umutlu et al., 2004) while the sub-fault dimensions are taken 5 km in both directions. Fault orientation is described with strike and dip angles of 264º and 64º, respectively. There are different slip distribution models available in the literature. However, a bilateral fault distribution model proposed by Umutlu et al. (2004) is verified using the FAS misfit calculations of observed and generated data (Ugurhan and Askan, 2010). The stress drop and pulsing area percentage values which are the most uncertain source terms are decided after all path attenuation and soil parameters are defined to reduce the misfit between real and synthetic accelerograms. Stress drop is chosen to minimize the prediction error and to control higher frequencies of the spectra, by incorporation of all observers. All prior parameters and the high frequency band of FAS are stabilized, then the low frequency portion is monitored by assigning varied pulsing area percentage values iteratively (Motazedian and Atkinson, 2005). Predicted stress drop value for the Duzce event is taken as 100 bars, while the pulsing area percentage is 30%. The assumed earthquake mechanism parameters are presented in Table 3.4 along with the path and site factors.

Table 3.4. *Simulation parameters of the 1999 Duzce earthquake*

Parameter	**Value**
Moment Magnitude	7.1
Hypocenter Location	40.82°N, 31.20°E
Hypocenter Depth	12.5 km
Depth to the Top of the Fault Plane	2 km
Fault Orientation	Strike: 264°, Dip: 64°
Fault Dimensions	65 km x 25 km
Subfault Dimensions	5 km x 5 km
Crustal Shear Wave Velocity, β	3700 m/s
Rupture Velocity (0.8β)	3000 m/s
Crustal Density, ρ	2800 kg/m^3
Stress Drop, Δσ	100 bars
Pulsing Percentage Area	30
Geometrical Spreading	R^{-1}, $R \leq 30$ km $R^{-0.4}$, $30 \text{ km} < R \leq 60$ km $R^{-0.6}$, $60 \text{ km} < R \leq 90$ km $R^{-0.8}$, $90 \text{ km} < R \leq 100$ km $R^{-0.5}$, $R > 100$ km
Quality Factor, Q	$Q = 88 f^{0.9}$
Duration Model, T	$T = T_0 + 0.05R$
Windowing Function	Saragoni-Hart
Kappa Factor, (κ_0)	Regional Kappa Model ($\kappa_0 = 0.047$) (Ugurhan and Askan, 2010)
Site Amplification Factors	H/V ratios and NEHRP D Amp. Factor (Ugurhan and Askan, 2010, Karimzadeh et al., 2018)

3.4.2.2. Path Model

For geometrical spreading in Duzce region, the model proposed by Ansal et al. (2009) is employed, as follows:

$$\begin{array}{ll} R^{-1}, & R \leq 30\ km \\ R^{-0.4}, & 30 < R \leq 60\ km \\ R^{-0.6}, & 60 < R \leq 90\ km \\ R^{-0.8}, & 90 < R \leq 100\ km \\ R^{-0.5}, & R > 100\ km \end{array} \tag{3.3}$$

Between numerous frequency-dependent quality factor equations, $Q = 88f^{0.9}$ suggested by Boore (1984) is used. The analyses in Ugurhan and Askan (2010) show that this Q factor gives the most accurate spectral amplitudes at high frequencies. The global duration formula proposed by Herrmann (1985) provided in Equation 3.2 is used in Duzce as well.

3.4.2.3. Site Model

The site amplification values suggested by Ugurhan and Askan (2010) based on the empirical H/V approach and generic amplifications by Boore and Joyner (1997) are used at stations in Duzce. For validation, PGA, PGV, and FAS values obtained from the real seismograms are compared with the simulated time histories generated with two alternative types of site amplification factors. The empirical H/V factors provided by Ugurhan and Askan (2010) show better consistency between generated and real accelerograms at DZC, GYN, IZT, and YPT stations. Yet, at IZN, generic amplification factors by Boore and Joyner (1997) for soil category D produces synthetic ground motions more consistent with the real ones.

The vertical ground motion component is the one subjected to least amplification in the soil strata, as expressed in Chapter 2. Thus, when the empirical H/V ratio is utilized in site model, vertical kappa must be used as diminution effect (Motazedian, 2006).

For this reason, vertical kappa value predicted as 0.047 is used for Duzce by Ugurhan and Askan (2010).

3.4.3. Comparison of the Simulated and Recorded Ground Motions of the 1999 Duzce Earthquake

Figure 3.6 provides the comparisons of FAS and acceleration-time series of the recorded and simulated time histories of 1999 Duzce earthquake. The comparison of acceleration time series generally indicates a satisfactory match between the individual synthetic PGA values and the real ones. The duration of the accelerograms is accurately defined at stations DZC, IZN, and IZT, while at the far station YPT it is not well produced, due to the complex propagation effects. Surface waves that originate from basin effects can be the reason of long durations in real accelerograms compared to simulated ones because the stochastic approach uses only the shear waves in simulations. Through the comparison of synthetic and observed Fourier spectra at DZC station in Figure 3.6, the synthetic FAS is observed to be below the recorded one for frequencies less than 1 Hz. The waveforms at the stations close to the fault plane of November 12, 1999 Duzce earthquake can be expressed by the variations in rupture velocity (Konca et al., 2010). So, the differences at low frequencies in the near source stations is expected, since the variety in rupture velocity is not included in the finite-fault approach. At stations GYN, IZN and IZT an obvious spectral consistency is obtained at high frequencies. But, the high frequency band of the synthetic spectra is lower than the actual ones at DZC station while it is overestimated at YPT station. The inadequate modeling of site effects could be the main cause of these differences, because soft sites can show nonlinearity under strong ground shaking. It should also be noted that all strong-motion recording devices were not located at free field during the 1999 Duzce earthquake. So, possible dynamic responses of the buildings could affect the amplitude and frequency content of real data, which are not possible to simulate herein.

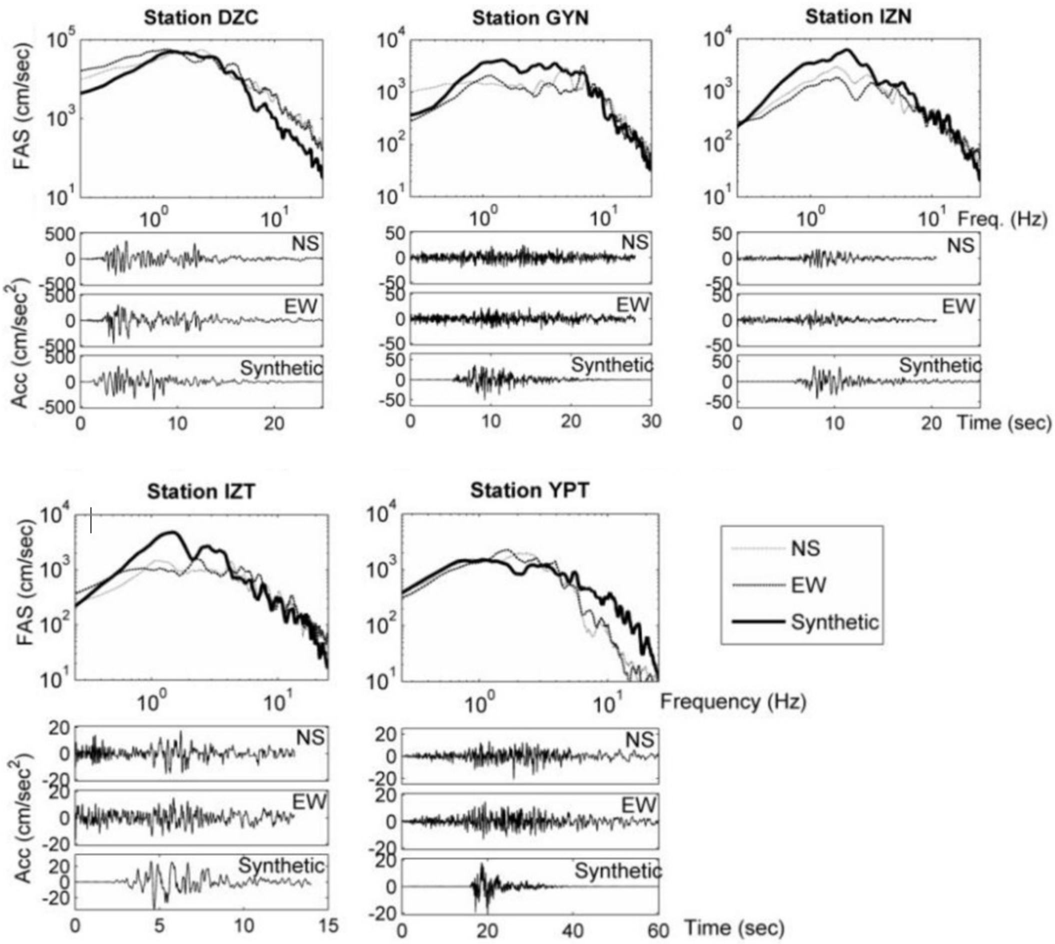

Figure 3.6. Comparisons of Fourier amplitude spectra and acceleration time series of the real and synthetic accelerograms of 1999 Duzce earthquake (Adapted from Ugurhan and Askan, 2010)

3.4.4. Simulated Ground Motion Database for Duzce Region

Scenario earthquakes in Duzce are simulated for magnitudes M_w 5.0, 5.5, 6.0, 6.5, 7.0, 7.1 (1999 event) and 7.5 by Ugurhan and Askan (2010) and Karimzadeh et al. (2017b). In these simulations, the rupture propagation and site models are adapted from Ugurhan and Askan (2010) while source variables (stress drop and fault geometry) are physically selected for each M_w value. Table 3.4 displays the input parameters for the simulations.

Duzce area is lies within a rectangular box localized by 40°-41° Northern latitudes, 30°-32° Eastern longitudes. For generating the synthetic ground motions, 370 nodes are chosen in Duzce region: 24 grid points around the earthquake epicenter are located 1 km away from each other, 57 nodes on a wider region are 20 km away from each other, and the rest of 289 points are approximately 3 km away from each other. Figure 3.7 presents the distribution of 312 points in Duzce area where 289 of them symbolized by red circles, 24 of them shown by green triangular symbols, and the 57 points with a grid distance of 20 km cannot be shown on the same figure due to scaling reasons. Finally, 5810 simulated ground motion records are obtained in Duzce region to use in the development of GMPEs.

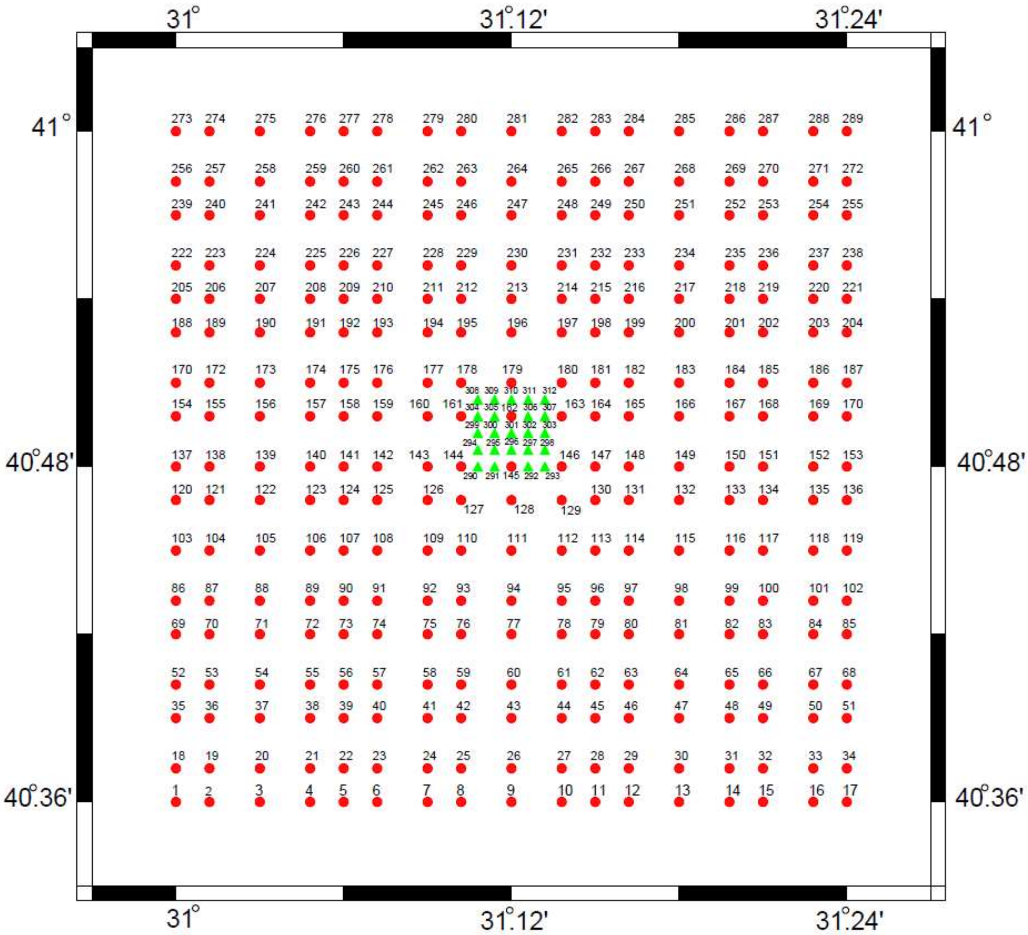

Figure 3.7. Distribution of the selected nodes in Duzce area

CHAPTER 4

GROUND MOTION PREDICTION EQUATIONS BASED ON SIMULATED DATA FROM THE ERZINCAN AND DUZCE REGIONS

4.1. Introduction

Ground Motion Prediction Equations (GMPEs) give an understanding of ground shaking level with a degree of uncertainty for a specific region or globally, depending on earthquake magnitude, faulting mechanism, source-to-site distance, soil properties etc. Ground motion estimates (or Ground Motion Intensity Measures, GMIMs) are compatible with the past earthquakes, and can be used to estimate the ground excitations of future earthquakes. For most of the applications, ground motion models are developed from ground motion databases that include real (i.e., observed or recorded) ground motion data. The distribution of ground motion data generally displays differences with respect to the areas of interest in terms of basically magnitude and source-to-site distance. In areas such as Japan, Western North America and Pan-European region (Turkey, Iran, Italy, Greece), the data distribution is almost satisfactory to develop a ground motion model. However, there are many regions such as Eastern North America, Georgia, Jordan, etc. that suffer from reliable amount of ground motion data to model new predictive relations. In these regions, the common practice is to employ seismological models using stochastic ground motion simulation methods (e.g.: Atkinson and Boore, 2006; Atkinson and Macias, 2009; Yenier and Atkinson, 2015).

Although the problematic case is considered as the latter one mentioned in the previous paragraph, the former approach may have some limitations for reliable estimations of GMIMs. The model development ground motion databases of the NGA-West2 GMPEs (Abrahamson et al., 2014; Boore et al., 2014; Campbell and

Bozorgnia, 2014; Chiou and Youngs, 2014; Idriss, 2014), the Turkish local models of Akkar and Çağnan (2010) and Kale et al. (2015), and the Pan-European regional models of Akkar et al. (2014) and Bindi et al. (2014) can be assessed to investigate the possible limitations. NGA-West2 models have a reliable data coverage with respect to distance and magnitude; however, most of the large magnitude events (magnitude greater than M_w 7.2) are from areas outside Western North America (i.e., Alaska, Iran, Turkey, Taiwan, and China). The ground motion databases of the Turkish local models include only two large magnitude earthquakes (Duzce M_w 7.1 and Kocaeli M_w 7.6) which have limited data in the near field region (R_{JB} < 20 km) and low-amplitude peaks when compared to similar size earthquakes in the shallow active crustal regions (Kagawa et al., 2004, Akkar and Cagnan, 2010). Akkar et al. (2014) and Bindi et al. (2014) has a ground motion database with $4.0 \leq M_w \leq 7.6$ magnitude range. The number of records with magnitudes up to nearly M_w 7.0 is sufficient, but large magnitude ground motions are only from three large strike-slip earthquakes (Duzce M_w 7.1, Kocaeli M_w 7.6, and Manjil M_w 7.4). In this case, the near source ground motion data is also limited as in the case of Turkish local models. Specifically, the number of recordings from large earthquakes and close distances can be considered as the main deficiency encountered in the regional or global ground motion databases to reflect the regional characteristics on GMIM estimates. In addition, the regional ground motion databases are well represented by the recordings from small-to-moderate magnitude earthquakes and with near-to-moderate (20 km < R < 50 km), moderate (50 km < R < 80 km) and far distances (R > 80 km).

There are some alternative approaches in literature to overcome the issues related to no or poor ground motion data regions or poor ground motion data parts of the model development databases. The simulation-based approach is the most commonly used method in which the ground motion recordings are simulated by considering a wide range of magnitude and distance as well as different site conditions. The predictive models are then developed in accordance with the simulated spectral amplitudes. Stochastic finite-fault or deterministic wave propagation methods can be employed in the simulation process as described in the previous chapters (Chapter 1.1, 1.2 and Chapter 2). The hybrid empirical method is another alternative to obtain a GMPE which is appropriate to the target region (i.e., data-poor region). This method can be employed in two different ways. In the first application, a well-constrained predictive model derived from a data-rich region (i.e., host region) is calibrated by considering adjustment factors calculated from spectral ratios of stochastic simulations in order to use in a data-poor region (Campbell, 2003; Douglas et al, 2006; Pezeshk et al., 2011; Shahjouei and Pezeshk, 2016, Tsereteli et al., 2016). In the second application which is called as the referenced empirical approach (Atkinson, 2008), adjustment factors are obtained by the spectral ratios of recorded data in the host region instead of using stochastic simulations (Atkinson, 2008, 2010; Atkinson and Boore, 2011, Atkinson and Motazedian, 2013; Hassani and Atkinson, 2015). As a combination of the methods mentioned above, Yenier and Atkinson (2015) developed a regionally adjustable generic ground motion model. Some of the recent studies employ the integration of observed (real) and simulated ground motion data to develop ground motion models that can be considered as hybrid GMPEs (Anbazhagan et al., 2013; Sharma and Harbindu, 2014; D'Amico et al., 2018). To propose a new GMPE, this approach provides enrichment of the ground motion databases in the areas with totally or partly poor observed ground motion data. The studies of Anbazhagan et al. (2013), and Sharma and Harbindu (2014) develop hybrid GMPEs for the Himalayan region which can be considered as a data-poor region, whereas D'Amico et al. (2018) improve the near field conditions of the moderate-to-large magnitude events in the recorded dataset of Southern Italy.

This study focuses on the potential gaps (i.e. poor ground motion data parts) in the recorded ground motion dataset of Turkey. The studies of Ugurhan and Askan (2010), Askan et al. (2013), Askan et al. (2015), Karimzadeh et al. (2017b) and Karimzadeh et al. (2018) provide considerable amount of simulated ground motion records from Erzincan and Duzce regions that can be considered as the representative of main source mechanism of the Turkish earthquake characteristics. When large magnitude and close distance ground motion data deficiencies of the Turkish dataset is considered, the current simulated dataset could be used to increase data coverage of the recorded database. However, firstly, the general predictive capabilities of the simulated database should be investigated by comprehensive regression analysis.

The development of the GMPEs derived from the simulated ground motion database of the Erzincan and Duzce regions and assessment of this model with the up-to-date local Turkish GMPEs (Kale et al., 2015) are presented in this chapter. First, simulated ground motion database with main features is explained. Then, definitions of predictor variables (independent variables; i.e., moment magnitude, source to site distance, soil conditions etc.) as well as response variables (dependent variables or ground motion intensity parameters; i.e., PGA, PGV and 5% damped PSA response spectra etc.) that are used in the functional forms are given. The functional form that is optimized according to estimator parameters and the simulated ground motion database is presented as well. Regression analysis approach is also explained in general manner. Model coefficients and standard deviation (i.e., sigma) values obtained from regression analysis are listed, as well. In following subsection, median ground motion estimations, standard deviations and residuals are evaluated. Final subsection presents the evaluation of proposed ground motion model against existing recorded ground motion dataset of Turkey (Kale et al., 2015) as well as previous global and regional ground motion predictive models.

4.2. Simulated Ground Motion Database Used in the Development of GMPEs

The simulation process yields a single horizontal component for each earthquake scenario at every station. A total of 7397 records are simulated from Duzce and Erzincan regions for regression analyses including different soil conditions, magnitude and distance values. Simulated ground motions are generated for several earthquake scenarios. FAS of all simulated records are plotted to see the frequency content and noise level. Stochastic simulation methodology provides free field simulated ground motions, and the simulated records do not include any significant noise at low and high frequency levels. Therefore, the band-pass filtering process is not applied to the simulated recordings in the database.

Figure 4.1 displays the moment magnitude (M_w) versus Joyner-Boore distance (R_{JB}) distribution of the simulated database in terms of soil conditions. Figure 4.2 presents the histograms for magnitude, distance and V_{S30} data distribution of the simulated database. The magnitude range of the simulated database is $5.0 \leq M_w \leq 7.5$ whereas the upper R_{JB} value is 136 km (Figure 4.1). In the simulated database, there is no records from small magnitude earthquakes (i.e., $M_w < 5$) but there is a considerable number of recordings from moderate-to-large magnitude events (Figure 4.2.a). The distance distribution is better constrained at all close and moderate distances. The database is mainly composed of simulated accelerograms of stations located in the distance range of 0 to 20 km. However, the data distribution is not sufficient and uniform for moderate and moderate-to-large distances (i.e., $R_{JB} > 80$ km) (Figure 4.2.b). As the main regression coefficients are calculated for distances up to 80 km, the weak distance distribution of the simulated database for $R_{JB} > 80$ km does not have a major effect on the regression results.

In the simulations of the scenario earthquakes the sites are modeled with $V_{S30} = 255$ m/s (NEHRP 2009, Class D), $V_{S30} = 310$ m/s (NEHRP 2009, Class D) and $V_{S30} = 520$ m/s (NEHRP 2009, Class C). For all V_{S30} values there is a uniform distribution in magnitude versus distance space as shown in Figure 4.1. However, V_{S30} values in the database are not randomly distributed, rather they are accumulated in V_{S30} values of 255 m/s and 520 m/s (Figure 4.2.c). In the simulation process, the detailed velocity profiles at selected sites are found with a microtremor array technique for Erzincan region by Askan et al. (2015). V_{S30} values of these sites are assigned to all generated points by considering the distance. This perspective produced uncertainty to the simulations, but due to the proximity of the nodes, the ultimate error can be ignored. In Duzce region, the site amplification values suggested by Ugurhan and Askan (2010) based on the H/V approach and generic amplifications by Boore and Joyner (1997) are used at recording stations. For validation, PGA, PGV, and FAS values obtained from the real data are compared with the simulated ones generated with two alternative types of site amplification factors. The empirical H/V factors show better consistency between generated and observed recordings at four stations. However, for one station, generic amplification factors by Boore and Joyner (1997) for NEHRP-D (NEHRP, 2009) site class produces simulated ground motion more consistent with the real one. Duzce and Erzincan regions are located on alluvial basins, and their local soil conditions are varying between stiff and soft soil which result in relatively lower V_{S30} values. Therefore, the V_{S30} values assigned to the generated nodes in simulation process is between $255 \leq V_{S30} \leq 520$ m/s.

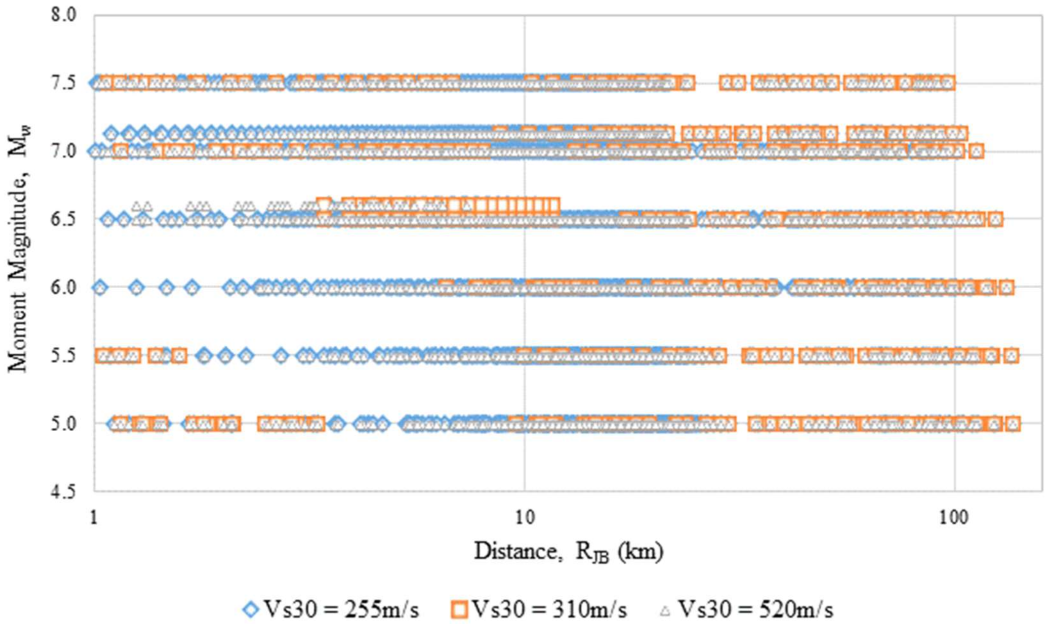

Figure 4.1. Magnitude (M_w) versus distance (R_{JB}) distribution of the simulated database in terms of the V_{S30} values. The V_{S30} range of simulated dataset is 255 m/s $\leq V_{S30} \leq$ 520 m/s

There is a single faulting mechanism used in the ground motion simulations which is strike-slip (SS), since both 1992 Erzincan and 1999 Duzce earthquake cases used in the simulation process are strike-slip earthquakes. Note that, the North Anatolian and East Anatolian fault zones which are the major tectonic structures in Turkey, generate predominantly strike-slip events.

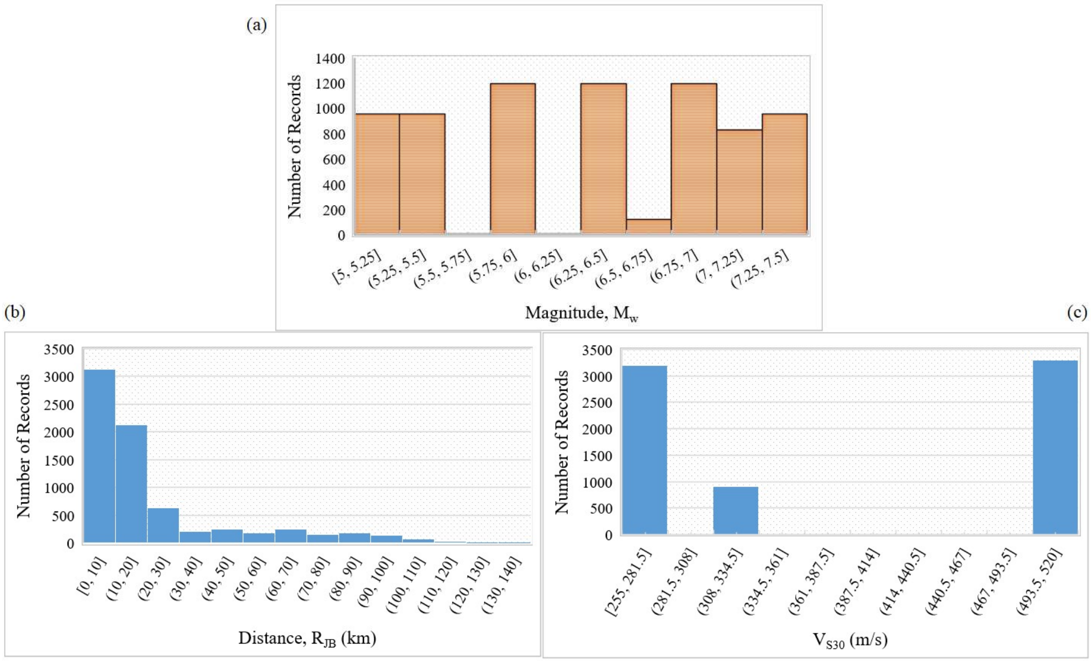

Figure 4.2. Ground motion data distribution of simulated database (a) magnitude, (b) distance, and (c) V_{S30} site parameter.

Figure 4.3 presents the hypocentral depth distribution of the simulated database in terms of magnitude scale. 1992 Erzincan mainshock (M_w 6.6) has a hypocentral depth of 9 km (Bernard et al., 1997), while the hypocentral depth of 1999 Duzce earthquake (M_w 7.1) is 12.5 km (Milkereit et al., 1999). For each scenario earthquake, hypocentral depths are calculated with respect to geometrical features of the fault plane (i.e., fault depth to upper edge, dip angle and sub-fault width). The deepest hypocentral depth in the simulated database is 18 km for the Duzce scenario earthquake with moment magnitude 5.0, whereas 7 km is the shallowest hypocentral depth for the Erzincan scenario earthquake with moment magnitude 6.0. The hypocentral depth values of the earthquakes in the simulated database are vary between 7 km and 18 km. Akkar and

Cagnan (2010) database consists of the earthquakes in hypocentral depth range of 0-30 km. Hypocentral depth contributions in the studies of Akkar and Cagnan (2010) and Kale et al. (2015) indicate that the Turkish recorded ground motion database includes relatively deeper events than the ground motion databases of NGA-West1 and West2 models (Power et al., 20018; Gregor et al., 2014). Therefore, the hypocentral depth distribution of the simulated database (Figure 4.3) can be considered as consistent.

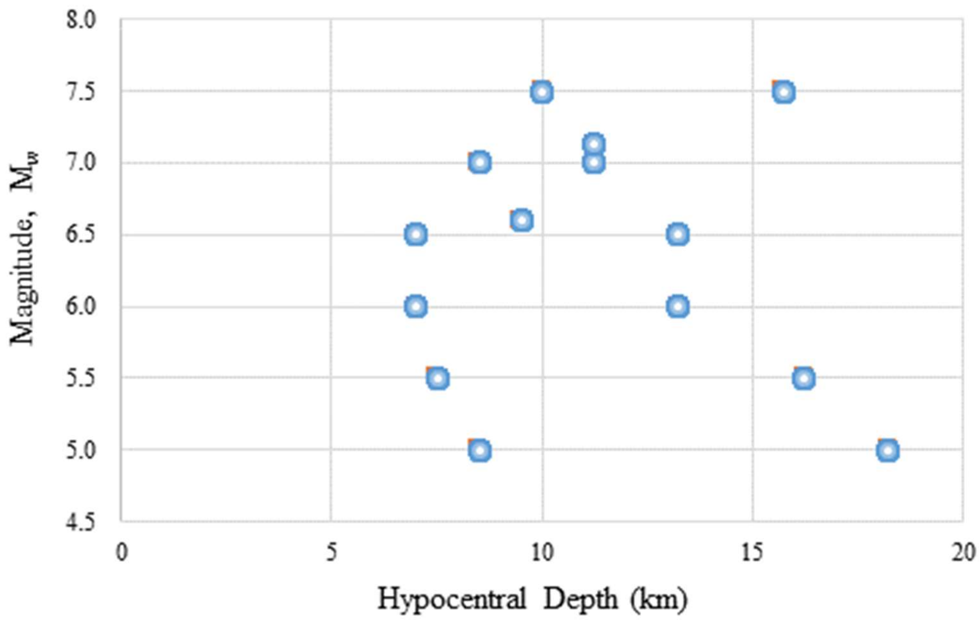

Figure 4.3. Magnitude versus hypocentral depth distribution of the simulated ground motion database.

Figure 4.4 displays the variations of PGA values with respect to magnitude for the simulated database. This distribution enables to determine the hinging magnitude value of the magnitude scaling function that indicates magnitude saturation effects after this specific magnitude value. When the ground motion data trends are investigated in this figure, the hinging magnitude value of 6.75 could be considered as an acceptable selection. Note that, this value is same with the hinging magnitude values used in the studies of Akkar et al. (2014) and Kale et al. (2015).

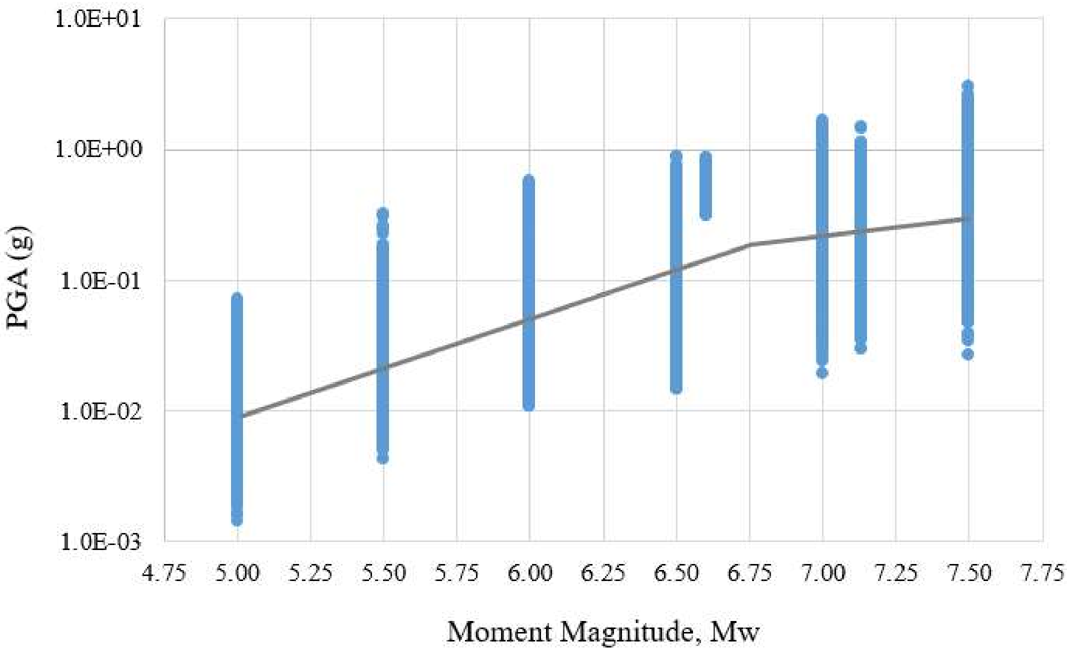

Figure 4.4. Magnitude versus PGA variations of the simulated database at distances smaller than 80 km (R_{JB} < 80 km).

Figures 4.5-4.7 present the magnitude and distance dependence of PGA and PSA at periods 0.2, 0.5, 1, 2 and 4 s, for sites with V_{S30} = 255, 310 and 520 m/s, respectively, in the simulated ground motion dataset. The comparisons are done for $5 \leq M_w < 6$, $6 \leq M_w < 7$, and $7 \leq M_w < 8$ magnitude intervals. These figures represent the general behavior of the simulated database to take into account the development of functional form. The use of a magnitude-dependent geometric spreading term can be observed from these plots. It also can be observed that the simulated database (maximum R_{JB} = 136 km) is not sufficient to consider the anelastic attenuation term in the functional form because a significant amplitude decay beyond distances about 80 km cannot be observed.

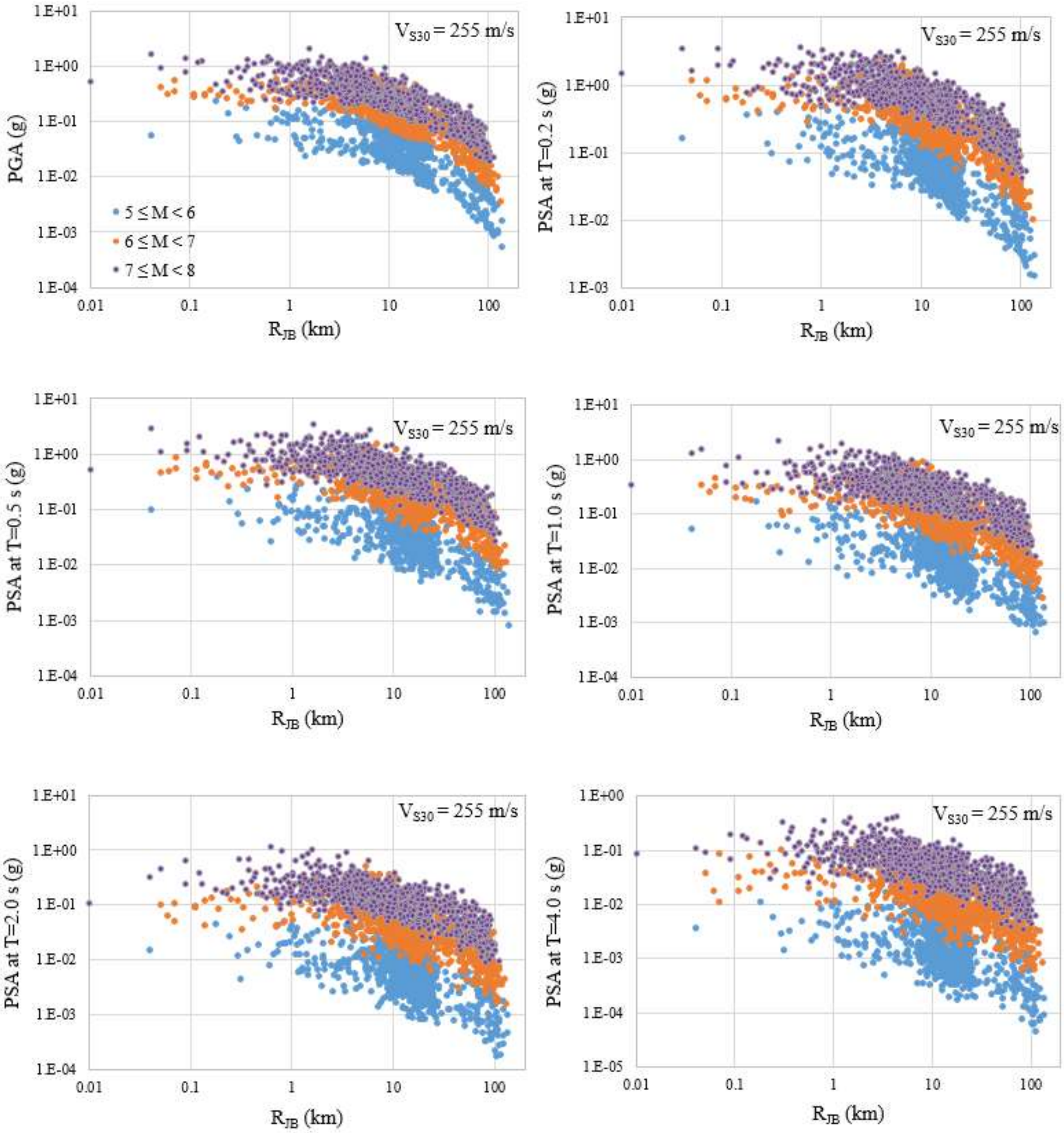

Figure 4.5. Magnitude and distance dependence of PGA and PSA at periods 0.2 s, 0.5 s, 1 s, 2 s and 4 s, for sites with V_{S30} = 255 m/s.

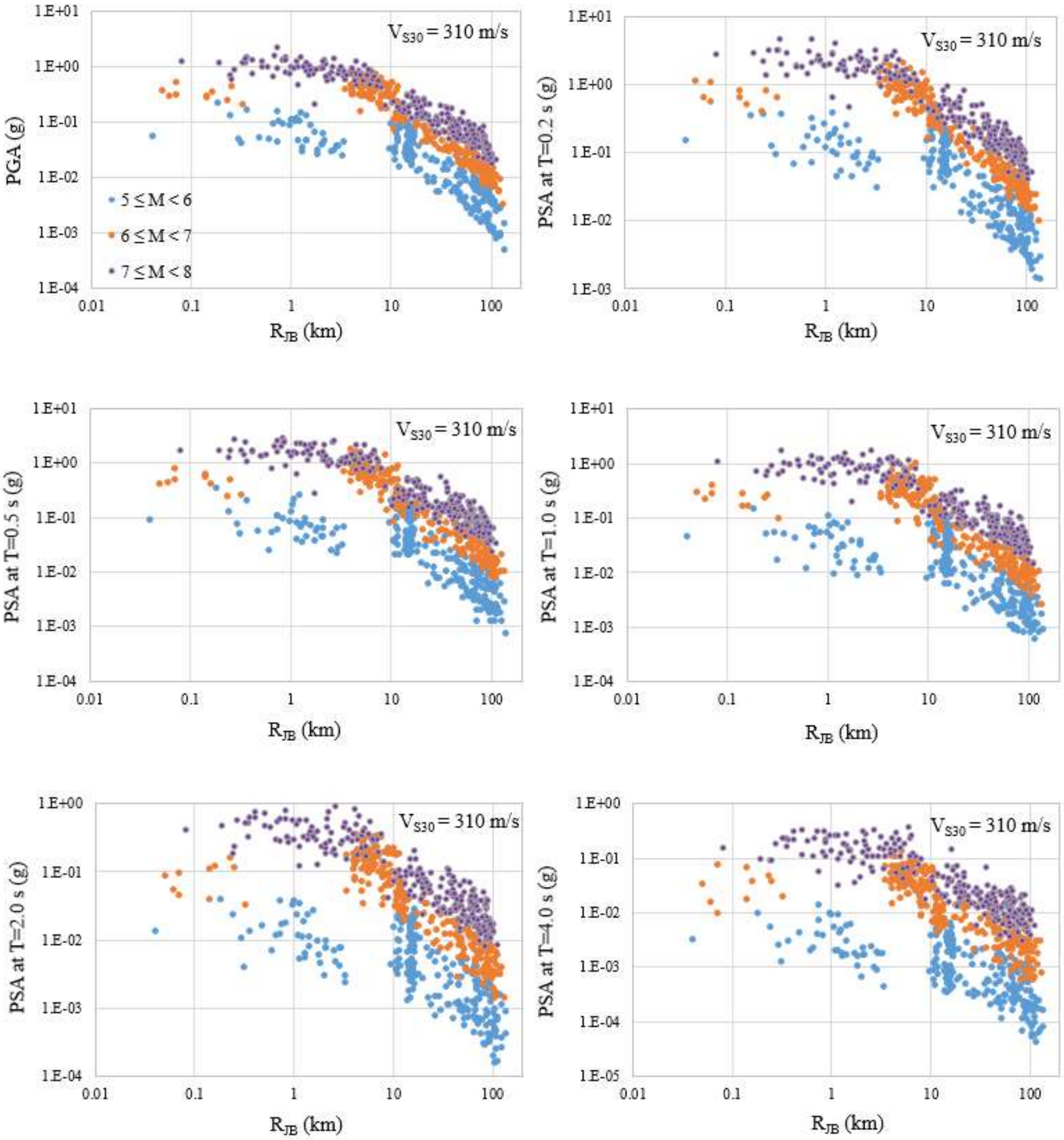

Figure 4.6. Magnitude and distance dependence of PGA and PSA at periods 0.2 s, 0.5 s, 1 s, 2 s and 4 s, for sites with V_{S30} = 310 m/s.

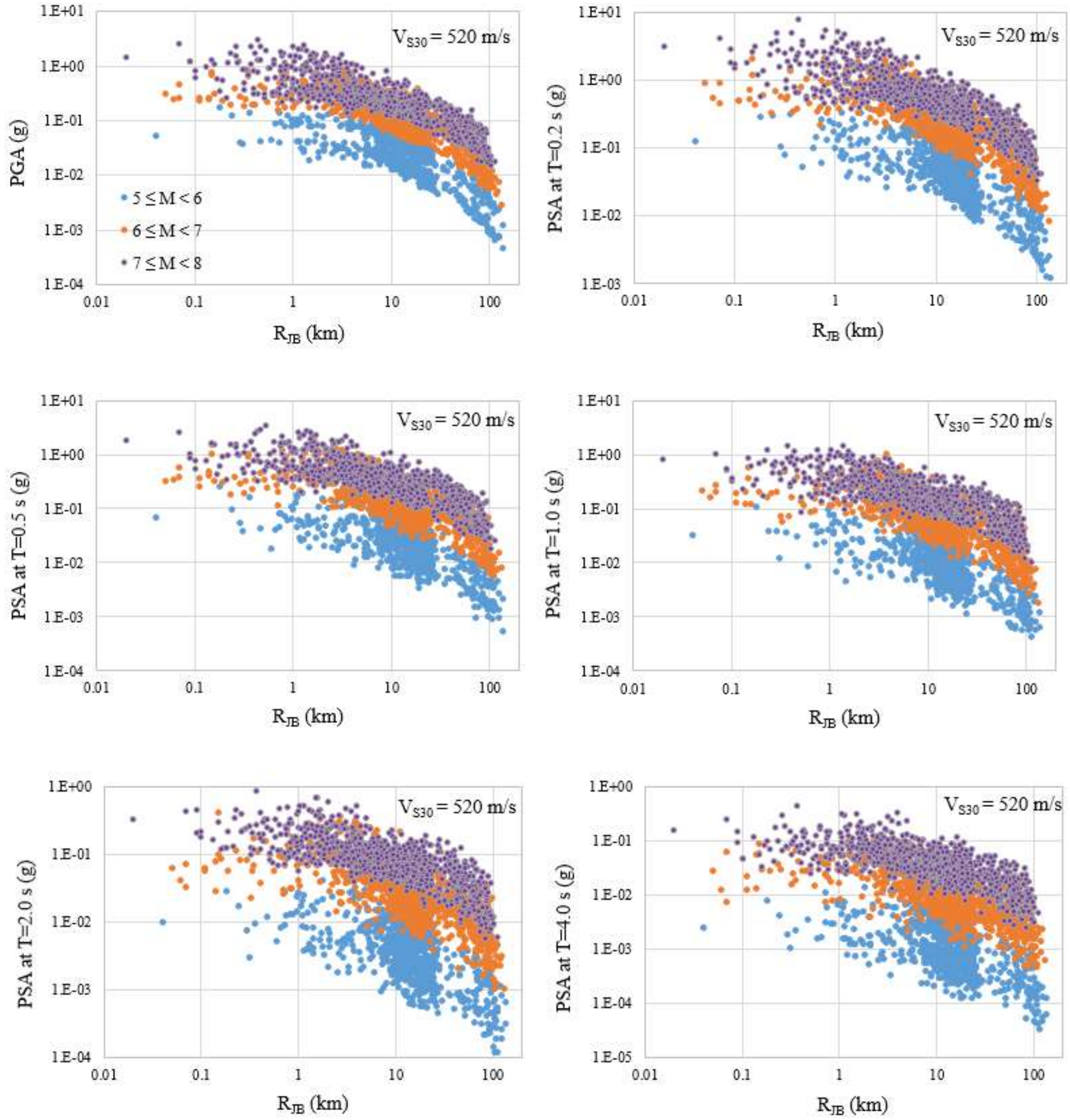

Figure 4.7. Magnitude and distance dependence of PGA and PSA at periods 0.2 s, 0.5 s, 1 s, 2 s and 4 s, for sites with V_{S30} = 520 m/s.

4.3. Response and Predictor Variables

The ground motion intensity measures (GMIMs) are the dependent variables (response variables) of the GMPEs which can be listed as peak ground acceleration (PGA), peak ground velocity (PGV), and 5% damped pseudo acceleration (PSA) response spectra. In the past applications, the response variables are proposed as larger component or geometric mean of the two horizontal components (Kalkan and Gulkan, 2004; Boore et al., 1997; Akkar and Cagnan, 2010; Kale et al., 2015). Then, GMPEs developer teams of the NGA-West1 project used the intensity measure GMRotI50, rotation-independent average horizontal component (Boore et al., 2006). Lastly, with the evaluation of NGA-West2 project RotD50 is started to be used, it is defined as the 50th-percentile of the rotated orientation-independent, period-dependent combined horizontal components (Boore, 2010). The difference between RotD50 (in NGA-West2) and GMRotI50 (in NGA-West1) is small for GMPE progress (Boore, 2010). The stochastic simulation technique utilized in this study provides only one horizontal component, by considering the motion as independent of direction. Therefore, this study proposes the GMIMs for PGA, PGV, and 5%-damped PSA for periods between 0.01 s and 4 s without considering any component definition. Note that, the GMIMs proposed for T > 1s may be biased considering the theoretical background of stochastic simulation processes since stochastic method provides solutions to the high frequency band of ground motions which has an arbitrary character constituted of random phases. Deterministic simulation techniques, which is not within the scope of this thesis, can accurately model the low frequency (long period) band, and they need precise source characteristics and wave velocity patterns (Hanks and Mc Guire, 1981).

The primary predictor variables in ground motion predictions are moment magnitude, measures of the source to site distance (i.e., R_{EPI}: epicentral distance, R_{HYP}: hypocentral distance, R_{JB}: closest distance to the surface projection of the fault plane, R_{RUP}: closest distance to the fault rupture plane), V_{S30} site response and faulting style (i.e., normal, reverse and strike-slip). Secondary parameters in general include event type classified as mainshock and aftershock, depth to top of fault rupture, basin response, hanging wall effect, directivity effects and other source parameters. The metadata information of observed earthquakes that the simulations are based on and the resulted simulated database do not provide information about complex parameters, therefore secondary estimator parameters are not included in the proposed GMPEs.

Within this study, the moment magnitude, R_{JB} distance, site parameter V_{S30} and faulting mechanism are used as predictor variables. It should be noted that, all the earthquakes in the simulated database are strike-slip, since both 1992 Erzincan and 1999 Duzce earthquakes used in the simulations are strike-slip earthquakes. Thus, the fault mechanism term is excluded from the equations.

4.4. Functional Form of the GMPEs and Regression Analyses

GMPEs are typically derived from regression analysis of ground motion data with considered estimator variables. The sophistication of GMPEs has been modified in time due to increased size of ground motion datasets and quality of their metadata information. The older GMPEs provide only peak ground acceleration that depends on only magnitude and distance with quite simple functional forms (Douglas, 2003). The new predictive models estimate various ground motion intensity measures (i.e., PGA, PGV, spectral acceleration, etc.) as functions of magnitude, distance, site characteristics, style of faulting and some more additional independent variables such as hanging wall effect, depth to top of rupture, depth to basement rock (Power et al., 2008; Gregor et al., 2014).

In this thesis, the use of the regional GMPEs developed from the simulated ground motion database is evaluated by comparing the proposed model with the Turkish model of Kale et al (2015) which is developed from the observed ground motion data. Therefore, the same functional form of Kale et al (2015) is directly employed in the proposed GMPEs to remove the epistemic uncertainty related to the selection of functional form and to make accurate comparisons. As mentioned in Kale et al (2015), because of the limitations of the metadata information of the database, the complex estimator variables (i.e., depth to top of fault rupture, basin response, hanging wall effect, directivity effects, etc.) are not used in the functional form of the GMPEs. This functional form is a similar version of the basic function of Akkar and Cagnan (2010) and Abrahamson and Silva (2008).

The functional form for the estimations of peak horizontal ground acceleration, PGA (in the unit of g), of peak horizontal ground velocity, PGV (in cm/s), and pseudo acceleration spectral ordinates, PSA (in the unit of g) is presented in Equation 4.1.

$$\ln(\overline{\mathrm{Y}}) = f_{mag} + f_{dis} + f_{site} \tag{4.1}$$

The model includes magnitude scaling (f_{mag}), geometric decay (f_{dis}) and site effects (f_{site}) to estimate the natural logarithmic mean ($\ln(\overline{\mathrm{Y}})$, median) of the above intensity measures. Style of faulting term (f_{sof}) is not included since the fault mechanisms of all earthquakes in the simulated database are strike-slip. The aleatory variability in the predictions is presented by the standard deviation (σ, sigma) which is discussed in the following paragraphs. Equations 4.2-4.3 display f_{mag} and f_{dis}, respectively. In the beginning, anelastic attenuation (f_{aat}) is also considered in the functional form but the attenuation effect is not observed from the regression analysis. This may be due to the lower upper distance limit of the simulated dataset which is 136 km or using only two different quality factors in simulations. The f_{mag} functional form includes linear and quadratic magnitude scaling terms. In f_{dis}, the multiplier of the logarithmic distance term indicates the magnitude-dependent ground motion decay. The hinging magnitude term (c_1) in Equation 4.2 indicates magnitude saturation effects after $M_w > c_1$. It is selected as M_w 6.75 which depends on observed trend in the simulated data for different magnitude and distance interval (Figure 4.4).

$$f_{mag} = \begin{matrix} b_1 + b_2(M_w - c_1) + b_3(8.5 - M_w)^2\,;\ M_w \le c_1 \\ b_1 + b_7(M_w - c_1) + b_3(8.5 - M_w)^2\,;\ M_w > c_1 \end{matrix} \tag{4.2}$$

$$f_{dis} = [b_4 + b_5(M_w - c_1)] \ln \sqrt{R_{JB}^2 + b_6^2} \tag{4.3}$$

The coefficient b_6 in Equation 4.3 is the fictitious depth which is considered in the regression to avoid overlap in the curves for large magnitude events at very short distances. The logarithmic distance term can never be less than the fictitious depth. In regression analysis, variations in fictitious depth are found to be minimal in the spectral period band; as a result, this coefficient is considered as period-independent and taken as 4.5 km. The fictitious depth coefficient is considered as period-dependent or independent in the recent empirical ground motion models. In Akkar and Cagnan (2010) the fictitious depth coefficient has increasing values from 7.33 for PGA to 9.61 for T = 0.2 s, and beyond this period it has decreasing values till 3.88 for T = 2 s. This coefficient is taken as constant with a value of 7.5 in Akkar et al. (2014) and 8.0 in Kale et al. (2015), due to the minimal variations in the spectral period band of these models in regression analyses. The fictitious depth in Abrahamson et al. (2014) is constant with a value of 4.5. Boore et al. (2014) take this coefficient as period-dependent from 4.5 for PGA to 5.74 for T = 1 s, and to 9.66 for T = 10 s. In Campbell and Bozorgnia (2014), the pseudo-depth coefficient is varied in between 5.52-8.54 for a period range of T = 0-10 s. The period-independent fictitious depth value (4.5 km) of the proposed model is lower than those from aforementioned Turkish models. The reason of this can be the high number of large earthquakes (i.e., M_w 6.5-7.5) at short distances in the simulated database. Besides, the pseudo-depth values of the NGA-West2 models can also be considered as low for the short-to-intermediate period range. Note that, these models are derived from an extensive ground motion database in distance and magnitude ranges, even for larger events at short distances compared to the local databases.

The nonlinear site function introduced by Sandikkaya et al. (2013) which is derived for the broader Europe is utilized to take into account the site effects (f_{site}). The site effects model of Sandikkaya et al. (2013) is provided in Equation 4.4. The period-dependent regression coefficients (s_{b1} and s_{b2}) of the nonlinear site function are taken from Kale et al. (2015) which are the smoothed version of original coefficients provided by Sandikkaya et al. (2013). The reference V_{S30} (i.e., V_{REF}) is 750 m/s in the nonlinear site function and V_{CON} = 1000 m/s accounts to limit the V_{S30} after which the site amplification is constant. The reference rock site PGA (PGA_{REF}) is computed from the reference ground motion model in Equations 4.2 and 4.3. It is the revised version of PGA_{REF} model provided in Sandikkaya et al. (2013) by taking into account the specific magnitude, faulting mechanism and distance distributions of the simulated database. Regressions are carried out initially by scaling the spectral ordinates to reference rock conditions. The coefficients c and n are period-independent with values c =2.5 and n =3.2 and are taken from the Sandikkaya et al. (2013) model. The transition between higher and lower ground motion amplitudes is defined by the coefficient c, while the soil nonlinearity is represented by n. Table 4.1 lists the period-dependent s_{b1} and s_{b2} coefficients for some selected periods in the proposed model. It should be noted that Sandikkaya et al. (2013) site model is limited with 150 m/s ≤ V_{S30} ≤ 1200 m/s. The site model is only used to compute soil response over the reference rock condition that is estimated by the proposed GMPE, since the V_{S30} values in the simulated database do not fall outside of its V_{S30} limits, possible biases in the estimates are prevented.

$$f_{site} = \begin{cases} sb_1 \ln\left(\frac{V_{S30}}{V_{REF}}\right) + sb_2 \ln\left(\frac{PGA_{REF}+c(V_{S3}\ /V_{REF})^n}{(PGA_{REF}+c)+(V_{S3}\ /V_{REF})^n}\right), & V_{S30} < V_{REF} \\ sb_1 \ln\left(\frac{min(V_{S30},V_{CON})}{V_{REF}}\right), & V_{S3}\ \geq V_{REF} \end{cases} \tag{4.4}$$

The total aleatory variability of the model is defined by σ that consists of between-event (τ, inter-event) and within-event (ϕ, intra-event) standard deviations.

$$\sigma = \sqrt{\tau^2 + \phi^2} \tag{4.5}$$

Between-event standard deviation describes the variability from one earthquake to the next in the database (earthquake-to-earthquake variability). On the other hand, within-event standard deviation is the variability among recordings within an event.

Table 4.1. *Period-Dependent f_{site} Coefficients*

Period (s)	sb1	sb2
PGA	-0.41997	-0.28846
PGV	-0.72057	-0.19688
0.01	-0.41729	-0.28685
0.02	-0.39998	-0.28241
0.03	-0.34799	-0.26842
0.04	-0.27572	-0.24759
0.05	-0.21231	-0.22385
0.075	-0.13909	-0.17798
0.1	-0.26492	-0.28832
0.15	-0.48496	-0.39525
0.2	-0.64239	-0.44574
0.3	-0.82052	-0.45287
0.4	-0.90568	-0.41105
0.5	-0.95097	-0.37956
0.75	-1.00027	-0.32233
1	-1.01881	-0.28172
1.5	-0.96317	-0.22449
2	-0.91305	-0.18388
3	-0.84242	-0.12665
4	-0.79231	-0.08605

(Adapted from Kale et al., 2015)

Magnitude dependence of standard deviations is sought by performing pure error analysis (Draper and Smith, 1981) before starting the regression analysis. The simulated ground motion database is divided into 0.5 magnitude bins for conducting this analysis. The investigations obtained from the pure error analysis results suggest that the standard deviations do not depend on magnitude. Accordingly, the weighting functions obtained in Kale et al. (2015) model are implemented in unity. It means that weighted regression is not performed in this study.

Table 4.2. *Period-Independent Hinging Magnitude and Regression Coefficients*

c1	b2	b5	b6	b7
6.75	0.585	0.053	4.5	-0.08

Table 4.3. *Period-Dependent Regression Coefficients*

Period (s)	b1	b3	b4
PGA	1.49363	-0.12517	-1.04879
PGV	5.51025	-0.17197	-0.90738
0.01	1.49637	-0.12499	-1.04859
0.02	1.52215	-0.12434	-1.04919
0.03	1.59512	-0.12239	-1.05013
0.04	1.73669	-0.11978	-1.05452
0.05	1.86901	-0.11629	-1.04998
0.075	2.16294	-0.1137	-1.04991
0.1	2.34622	-0.12448	-1.05259
0.15	2.40726	-0.13758	-1.05484
0.2	2.32386	-0.14437	-1.0544
0.3	2.02111	-0.15131	-1.0279
0.4	1.71654	-0.15584	-1.00237
0.5	1.47234	-0.15969	-0.98178
0.75	0.99388	-0.16839	-0.94342
1	0.62856	-0.1767	-0.91614
1.5	0.11612	-0.19307	-0.87875
2	-0.23544	-0.20934	-0.85363
3	-0.7105	-0.24182	-0.82103
4	-1.02045	-0.27427	-0.80023

The mixed-effects regression algorithm proposed by Abrahamson and Youngs (1992) is applied in the regression analysis. The spectral periods in the range of 0.0 s (PGA) to 4.0 s (at 63 discrete spectral periods) and PGV are predicted by the proposed GMPEs. The predictive model is developed in two steps. In the first part, the GMPEs is developed by using the close-distance database (R_{JB} < 80 km) which has the main importance for engineering purposes (Campbell and Bozorgnia, 2014). Therefore, the magnitude dependent regression coefficients of b_2, b_3, b_5, b_6, and b_7 are obtained in this step. In the second step, the distance effects are modeled by the regression analysis by using the entire simulated ground motion database. At larger distances (R_{JB} > 80 km), change in characteristics of crustal structure can highly influence the ground motions, resulting a modification in the attenuation at large distances (e.g., Q term) (Abrahamson et al., 2014). Anelastic attenuation effect is investigated in this step in order to account for such differences; however, the anelastic attenuation effect cannot be modeled appropriately because of the upper distance limit of the database. Thus, this term is not included in the proposed ground motion model. Application of second step regression analysis yield the distance scaling term (b_4), regression constant term (b_1), and aleatory variability components (τ and ϕ).

The regression coefficients of the new model at some chosen periods are listed in Table 4.2 and 4.3. After each regression step, the smoothing is applied to the obtained coefficients to remove jagged variation of response spectra estimations. Table 4.4 lists the between-evet (τ) and within-event (ϕ) standard deviations for selected periods. The total lists of regression coefficients for the proposed GMPEs are provided in Appendix A.

Table 4.4. *Period-Dependent Standard Deviation Values*

Period (s)	ϕ	τ
PGA	0.2937	0.2935
PGV	0.311	0.3108
0.01	0.2935	0.2933
0.02	0.2931	0.2929
0.03	0.291	0.2907
0.04	0.2887	0.2885
0.05	0.289	0.2888
0.075	0.2948	0.2946
0.1	0.3037	0.3035
0.15	0.3214	0.3211
0.2	0.3341	0.3338
0.3	0.3487	0.3484
0.4	0.3553	0.355
0.5	0.363	0.3628
0.75	0.3786	0.3783
1	0.3917	0.3914
1.5	0.4096	0.3952
2	0.4219	0.3569
3	0.4469	0.2967
4	0.4651	0.2561

4.5. Prediction Results of the Proposed GMPEs

In this section, the proposed prediction equations are verified by residual analysis. The residuals of proposed GMPEs are evaluated under the model development database (i.e., the simulated database) of this study and recorded database of Kale et al (2015) model. Note that, the total residuals are the differences between the natural logarithm of observed data and the natural logarithm of ground motion estimates. The mixed effects regression algorithm (Abrahamson and Youngs, 1992) is utilized to separate total residuals into between-event (η_i) and within-event (ε_{ij}) components where index i indicates the earthquakes and index j represents recordings in the dataset. In the evaluations, the residuals are grouped into distance, magnitude and V_{S30} bins to obtain mean binned residuals for each predictor variable. Additionally, 95% confidence intervals for the mean binned residual groups are also computed for detecting any systematic trend in the behavior of residuals. Fluctuations of the mean binned residuals and their confidence limits about zero indicates agreement between the predictions of the GMPE and the ground motion database being considered. As seen from the figures, GMPEs display different residual behaviors (e.g., underestimation or overestimation) for different magnitude bins. The residual evaluations are made by considering PGA and PSA at T = 0.2 s, 0.5 s and 1.0 s. In the comparative plots, mean binned residuals are represented by solid circles, whereas confidence intervals are displayed as error bars.

Figure 4.8 represents the between-event (inter-event) and within-event (intra-event) residuals of the proposed GMPEs under simulated database. The between-event residuals for M_w and within-event residuals for V_{S30} are not randomly distributed instead they show systematic distributions as a result of simulated database features. Only, within-event residuals for R_{JB} show random distributions with high number of very close distance events. But still, the corresponding mean residuals fluctuate about zero without any significant trends and indicates that the proposed model fits the simulated data well. Besides, the 95% confidence intervals of between-event residuals are high due to the very small number of earthquakes in the simulated database.

The between-event and within-event residuals of the proposed model under the recorded database of Kale et al. (2015) are given in Figure 4.9. Only strike-slip earthquakes from development database of Kale et al. (2015) are considered for residual analysis to prevent additional biases as the proposed model is derived only for strike-slip faulting simulated events. The residuals for M_w as well as for R_{JB} and V_{S30} show random distribution. In general, the between-event and within-event residuals are larger in the recorded data, and they display more dispersive behavior compared to those in the simulated dataset. The between-event mean residuals fluctuate about zero for magnitudes larger than M_w 5.0 and show a positive bias for small magnitudes, which indicates that the proposed model underestimates the small magnitude earthquakes. This underestimation does not reflect the expected behavior of the proposed model since the lower magnitude limit of the model development database is M_w 5.0. This observation is more significant at short periods. The within-event residuals for R_{JB} also fluctuate about zero at almost all distances while at close distances positive and negative biases are observed. This can be due to the fact that the proposed model is derived from a database that contains a large number of close-distance earthquakes ($R_{JB} \leq 30$ km). For V_{S30}, the within-event mean residuals fluctuate about zero and indicates that the estimates of proposed GMPEs are unbiased with respect to site parameter while a negative bias is shown for large V_{S30} values that points out over prediction. The bias in larger V_{S30} values is likely to be caused by the low upper limit of the site parameter in the model development database (maximum $V_{S30} = 520$ m/s).

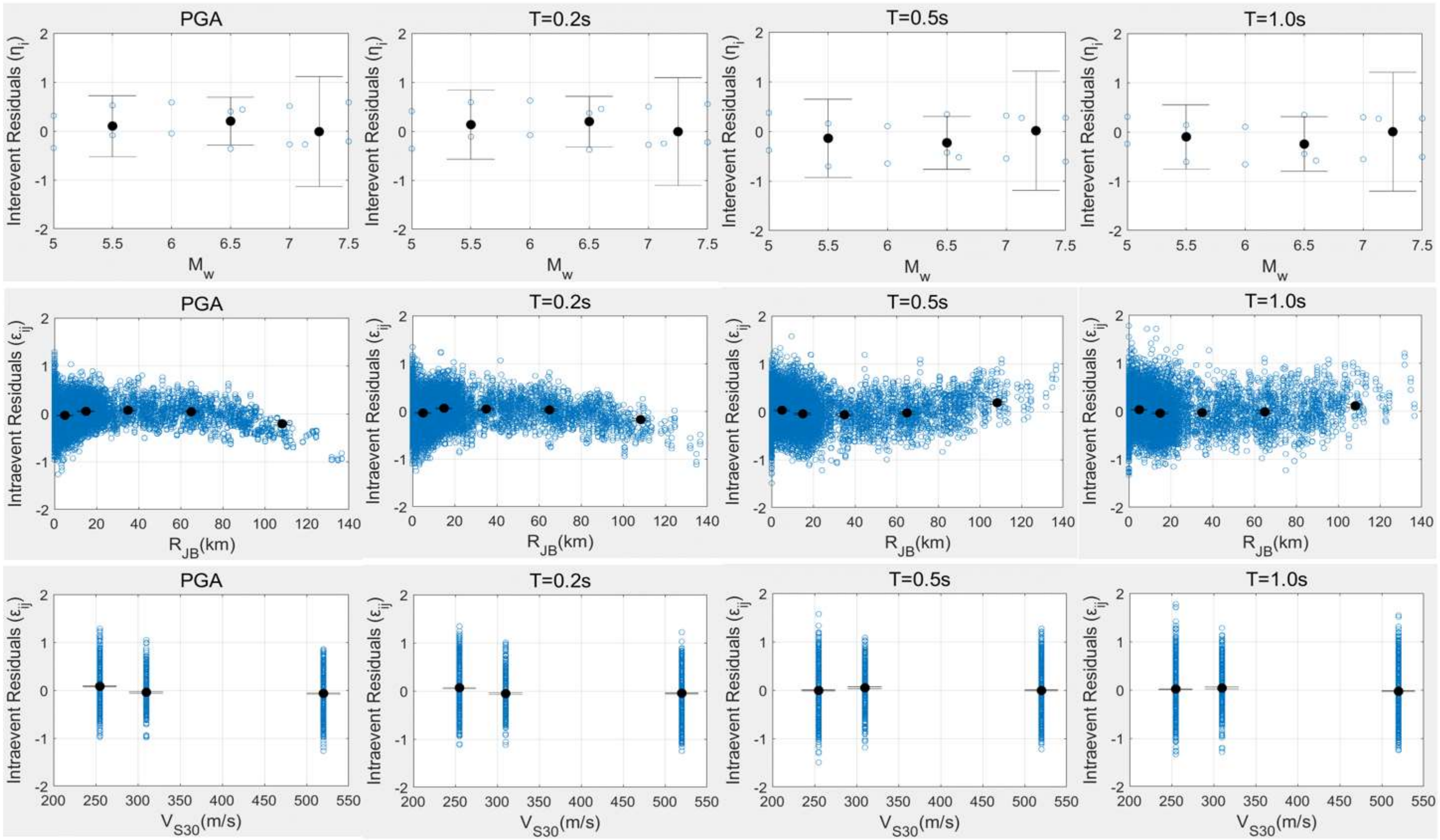

Figure 4.8. Between-event (first row) and within-event (second and third rows) residuals of the proposed GMPEs for simulated dataset.

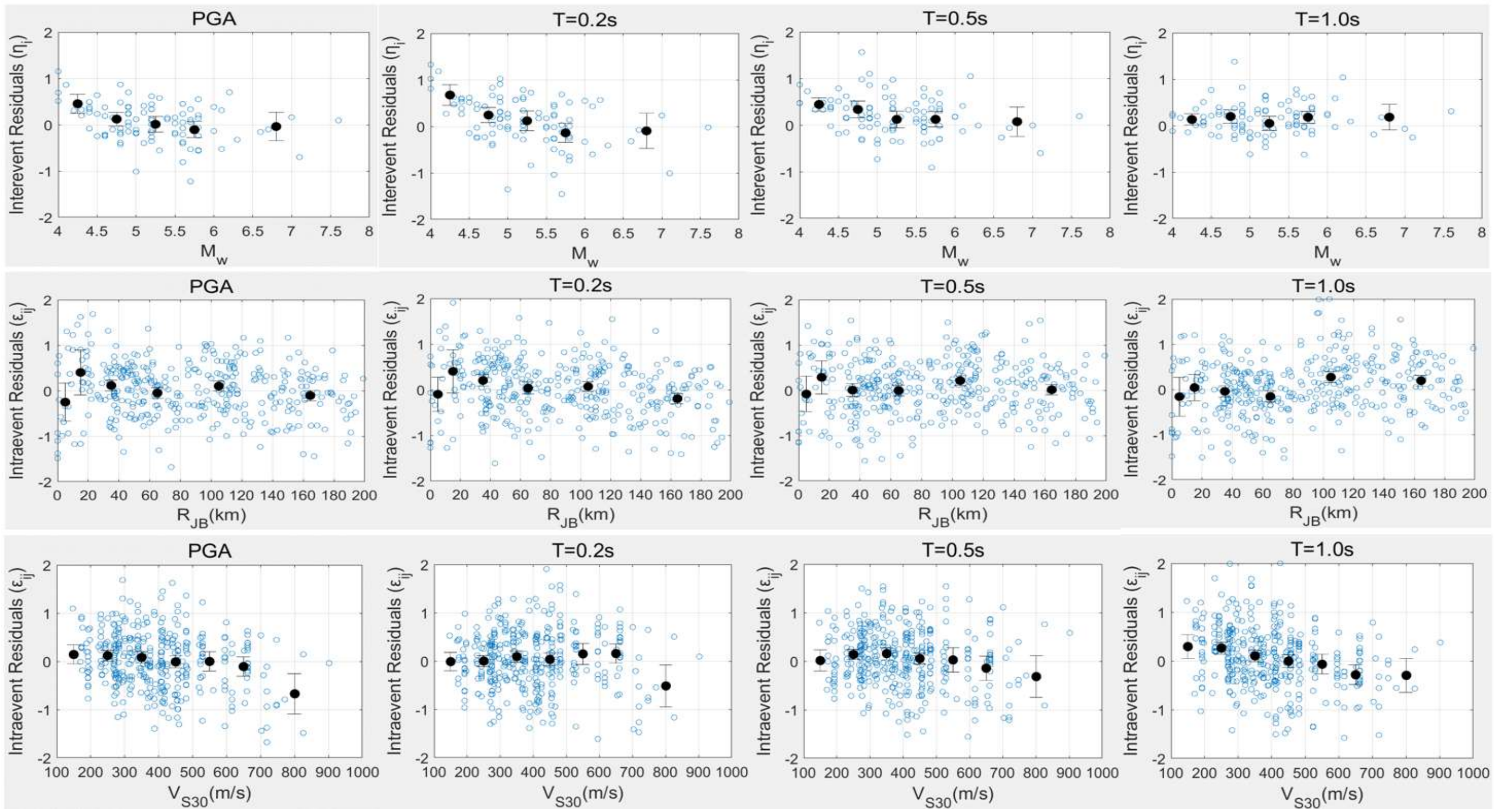

Figure 4.9. Between-event (first row) and within-event (second and third rows) residuals of the proposed model for the recorded database of Kale et al. (2015) considering only strike-slip faulting earthquakes.

Figures 4.10-4.12 show a series of example plots that display how the proposed median ground motion model scales with M_w, R_{JB}, V_{S30}, and spectral periods. Figure 4.10 presents the distance scaling (attenuation) of the proposed model for magnitudes of 5, 6, 7 and 8 for a strike slip fault on rock site (V_{S30} =760 m/s). The plots show similar trends for all magnitudes at all given spectral periods. The plots show similar trends and similar magnitude-dependent distance slope for all periods. Magnitude saturation is not observed for large magnitudes at very short distances. For R_{JB} > 10 km, the distance attenuation shows a linear slope for all periods. A downward curvature in the lines cannot be obtained towards large distances at short periods, which indicates that anelastic attenuation is not observed, due to the lower upper distance limit of the simulated database.

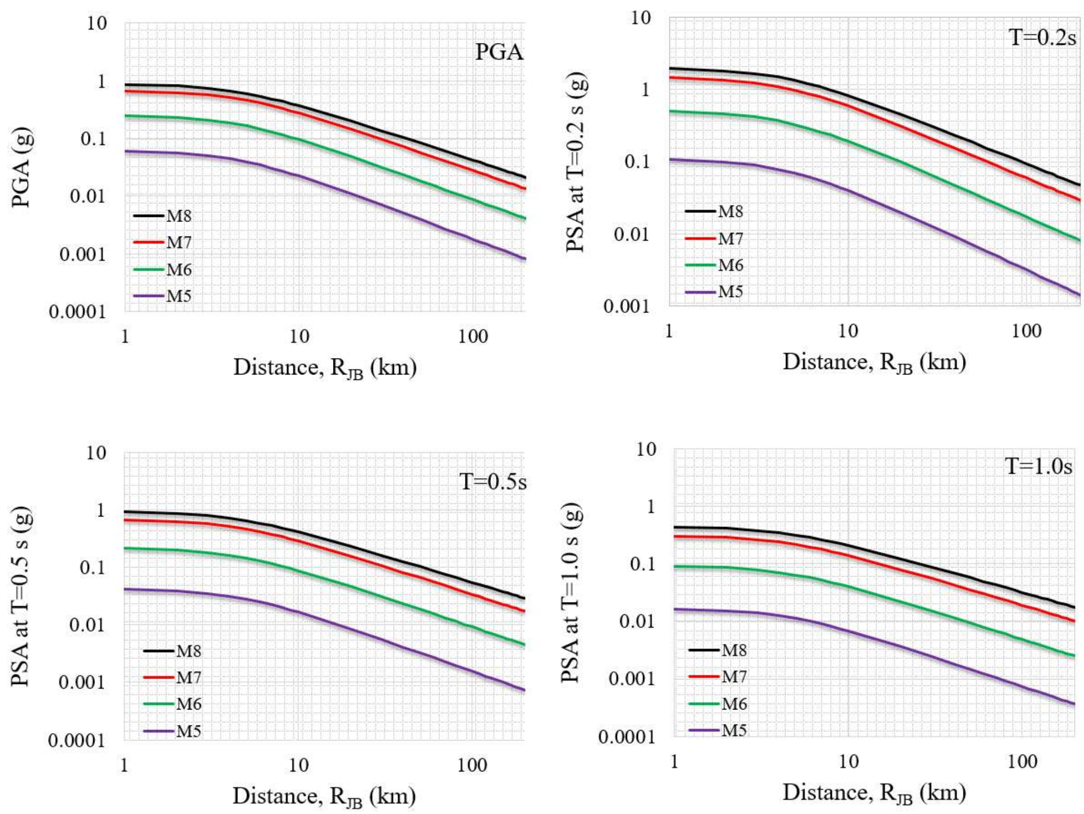

Figure 4.10. Distance scaling of the proposed GMPE at different spectral ordinates (PGA, PSA at T = 0.2s, 0.5s and 1s) for magnitude range between M_w 5 and M_w 8. The comparisons are done for a reference rock site V_{S30} = 760 m/s.

The magnitude scaling of the proposed model is given in Figure 4.11 for strike-slip earthquakes on rock sites (V_{S30} =760 m/s) for T=0.2 s and T=1.0 s. There is no weak scaling of the short period motion at short distances, indicates there is no significant saturation with magnitude, due to the high number of short distance events for all considered magnitudes in the simulated database. The dependence of the spectra on the V_{S30} for magnitudes M_w 5, 6, 7 and 8 strike-slip faults at R_{JB} = 30 km is provided in Figure 4.12. The plots show the V_{S30} site dependence of the peak period in the spectrum. For V_{S30} = 760 m/s, the peak period ranges from approximately 0.18 s for M_w 5 to 0.20 s as the magnitude increase, which is in the acceleration-sensitive spectral region. Besides, for the soft site (i.e., V_{S30} = 255 m/s), the peak period ranges from 0.21 s for M_w 5 to 0.25 s for M_w 8. The response spectra show similar trends for all magnitudes, with more differences between compared site parameters at intermediate to long periods. Besides, the amplification from rock to soft soil is increasing significantly towards the longer periods for all magnitudes.

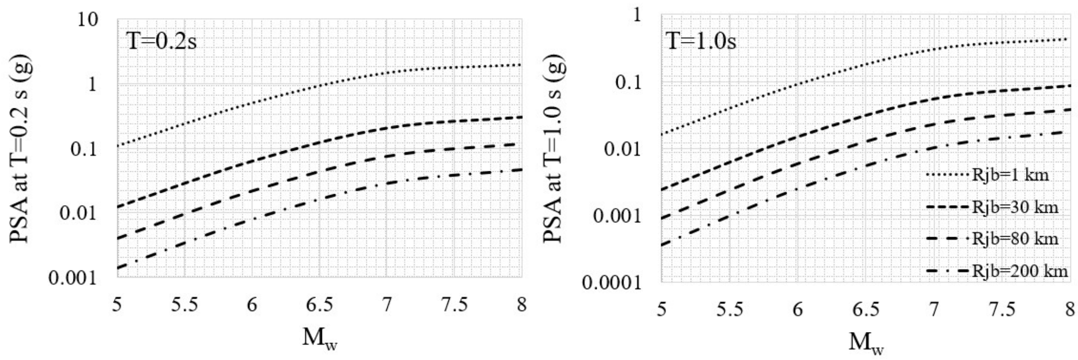

Figure 4.11. Magnitude scaling of the proposed GMPE at spectral ordinates T = 0.2s and T = 1s for distance ranges R_{JB} = 1, 30, 80 and 200 km. The comparisons are done for a reference rock site, V_{S30} = 760 m/s on a strike slip fault.

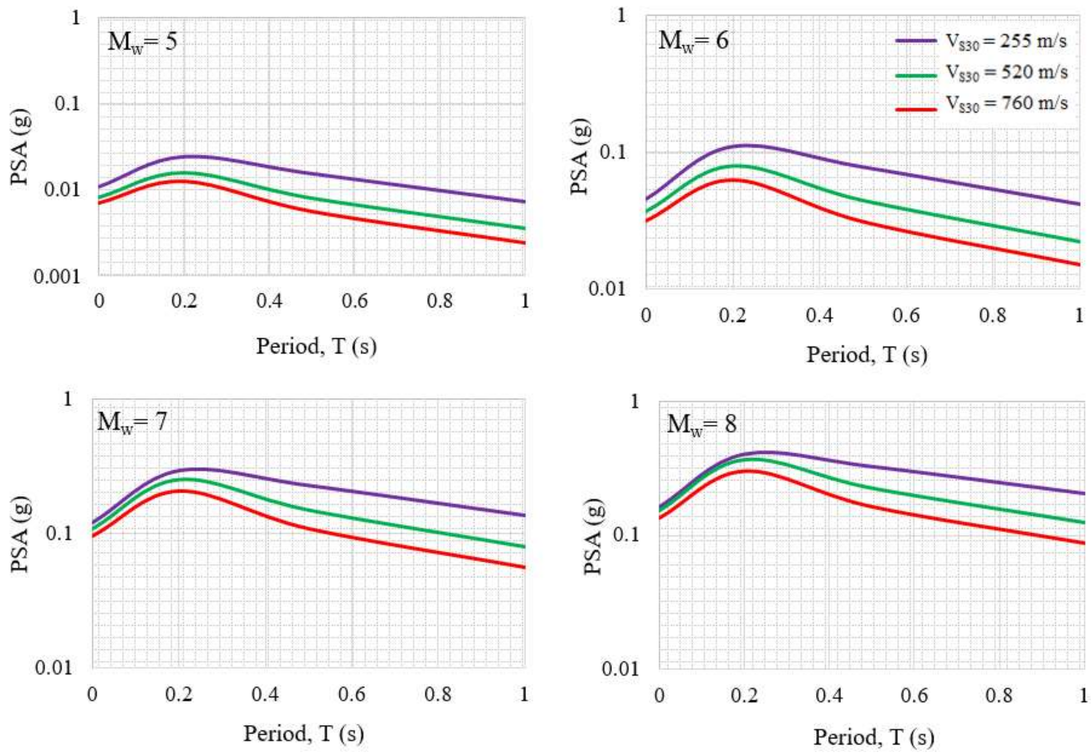

Figure 4.12. Period scaling of proposed GMPE for different soil sites (V_{S30} = 255, 520, 760 m/s). The comparisons are done for R_{JB} = 30 km from a strike slip fault for magnitudes M_w 5, 6, 7 and 8.

The period-dependent variations of between-event (τ, inter-event), within-event (ϕ, intra-event) and total standard deviations (σ) of the proposed GMPEs based on simulated database are provided in Figure 4.13. It is globally known that within-event standard deviations are much larger than the between-event component for GMPEs whose datasets consist of recorded ground motions (Strasser et al., 2009). But for the standard deviations of the proposed model derived from the simulated database, the within-event and between-event standard deviations are almost equal, while the within-event sigma is just slightly larger than the between-event component. In the simulated database, a systematic distribution is dominated in terms of magnitude, distance and soil properties, and the database consists of 7397 records from 1195 stations for 14 earthquakes. The pure error analysis showed unbiased weighting for the binned magnitudes of the simulated database. This results in similar and magnitude-independent within-event and between-event standard deviations due to the simulated database features. Also, standard deviations of the proposed GMPEs show a period-dependent behavior since they increase with the period. The total aleatory variability (σ) of the new model has values ranging from 0.42 natural log units for PGA and to 0.55 natural log units for T= 1s.

Furthermore, as mentioned in Akkar and Cagnan (2010) standard deviations of Turkish models are generally larger than the NGA models significantly for larger magnitudes. This may be due to the differences in functional forms with respect to predictor variables or database features. The low number of large earthquakes in Turkish database increases the aleatory variability of Turkish GMPEs. However, all standard deviations computed from the proposed model are significantly lower than those obtained from the previous Turkish models as well as NGA-West2 GMPEs, and note that the main difference is between the within-event uncertainty values. Figure 4.14 compares the total sigma values for the new model, the regional model of Akkar et al. (2014) and local model of Kale et al. (2015). The total variabilities of the new model derived from the simulated database are lower than those obtained from the evaluated GMPEs, with a reduction of about 20% to 30%. Besides, the total variabilities of Kale et al. (2015) model for large magnitudes are also smaller than those obtained from Akkar et al. (2014), possibly due to the magnitude-dependent standard deviation modeling of Kale et al. (2015). The reason of low standard deviation estimates of current model can be the simulated database features and the considerable number of simulated records from moderate-to-large earthquakes (i.e., M_w 6.0-7.5).

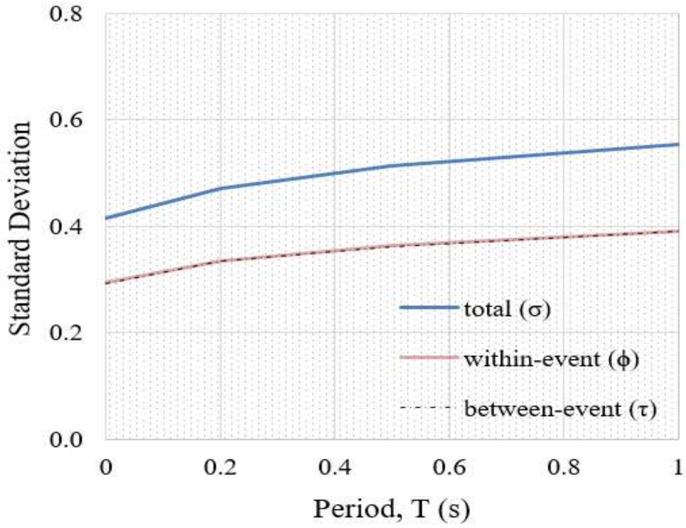

Figure 4.13. The within-event, between-event and total standard deviations of the proposed GMPEs.

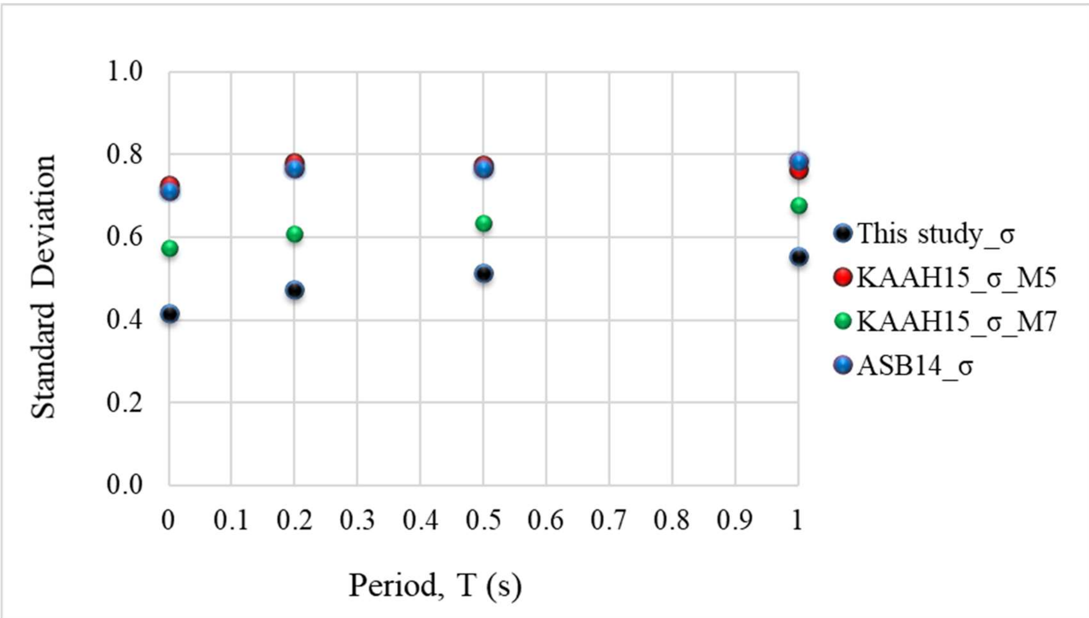

Figure 4.14. Comparisons of total standard deviations (σ) for the new GMPEs, the regional model of Akkar et al. (2014) and local model of Kale et al. (2015).

4.6. Comparisons with the Local, Regional and Global GMPEs

Ground-motion estimations of the proposed model are compared with the regional model of Akkar et al. (2014) [hereafter referred to as ASB14], local model of Kale et al. (2015) - KAAH15 and global GMPEs of Abrahamson et al. (2014) - ASK14, Boore et al. (2014) - BSSA14, Campbell and Bozorgnia (2014) - CB14, and Chiou and Youngs (2014) - CY14. The basic estimator parameters of the proposed GMPEs are adequate for comparisons with the regional model of ASB14 and the local model of KAAH15. For the comparisons with the NGA-West2 GMPEs additional predictor variables such as R_{RUP} distance measure, depth to top of rupture (Z_{TOR}), hypocentral depth, down-dip rupture width (W), basin/sediment depths ($z_{1.0}$: depth from the ground surface to the 1.0 km/s shear-wave horizon beneath the site, and $z_{2.5}$: depth to the 2.5 km/s shear wave velocity horizon) are required. These additional parameters are estimated consistently with the empirical relations given in the studies of Wells and Coppersmith (1994) and Kaklamanos et al. (2011). The recommended basin depth of each model developer is used to compare the simulated database with the NGA-West2 models. The reference site class with V_{S30} = 760 m/s is utilized for the overall comparisons due to the nonconformity in site classification between the evaluated GMPEs. Vertical (dip = 90°) strike-slip faulting is considered in the comparisons.

Figure 4.15 shows distance scaling comparisons between ASB14 and KAAH15 ground motion models and proposed model for PGA and spectral periods of 0.2 s, 0.5 s and 1.0 s. The median ground motions from strike slip faults on rock site (V_{S30} = 760 m/s) are plotted for four different magnitudes (M_w 5, 6, 7 and 8). The remarkable observation shown from the comparative plots presented in Figure 4.15 is that the proposed ground motion estimations are lower for small magnitudes particularly at short periods with respect to previous regional and local models. The apparent inconsistency in small magnitudes highly reduces with increasing magnitude. This small magnitude bias of the proposed model may be due to using low stress drop or lack of observed near field pulses in the simulations. Moreover, the small magnitude bias can arise from the use of stochastic finite-fault simulation at small magnitudes instead of stochastic point-source technique, because theoretically finite-fault method can underestimate the ground motion amplitudes from small magnitude events. The stochastic point-source simulation is more adequate to generate accelerograms for small magnitude earthquakes. In general, the plots show similar trends for all magnitudes at selected spectral periods; however, the proposed GMPEs tends to estimate higher spectral amplitudes at close distances (i.e., R_{JB} < 10km) for large magnitudes (i.e., M_w 7 and 8) at selected spectral periods. The reason for the overestimation of the new model for large magnitudes at close distances can be considerable number of close distance simulated data since the stochastic method is capable of simulating near-field ground motions from large magnitude earthquakes. Besides, the new model underestimates the spectral amplitudes at R_{JB} distances greater than 10 km for large magnitudes (i.e., M_w 7 and 8) particularly at intermediate to long spectral periods (i.e., T=0.5s and 1.0s), possibly due to the insufficient low frequency modeling of stochastic approach. ASB14 and KAAH15 predictions converge and even overlap by showing similar predictions for all magnitudes and for selected spectral periods although ASB14 is on the safe side for magnitudes M_w 5 and M_w 6 at distances of R_{JB} < 60 km.

NGA-West2 GMPEs are included to comparisons in Figure 4.16 which shows distance scaling comparisons at selected spectral ordinates (PGA, PSA at T= 0.2 s, 0.5 s and 1 s) for magnitudes M_w 5 (representing small magnitude events) and M_w 7 (representing large magnitude events). The evaluations are again for a reference rock site, V_{S30} = 760 m/s. For small magnitude, all evaluated GMPEs show great variation with respect to one another at all periods, although the new model and KAAH15 predict smaller amplitudes at all distances for all periods, and median estimations of ASB14 is much closer to NGA-West2 models. In general, the new GMPEs is on the low side for M_w 5 at almost all distances. For large magnitude, the comparisons provide good agreement between the new GMPEs and evaluated models, but the proposed model estimates higher spectral values at close distances (i.e., R_{JB} < 10 km) for short periods and lower spectral values at large distances for long periods. For large magnitude (M_w 7), spectral amplitudes predicted by all GMPEs generally converge and overlap by showing similar prediction.

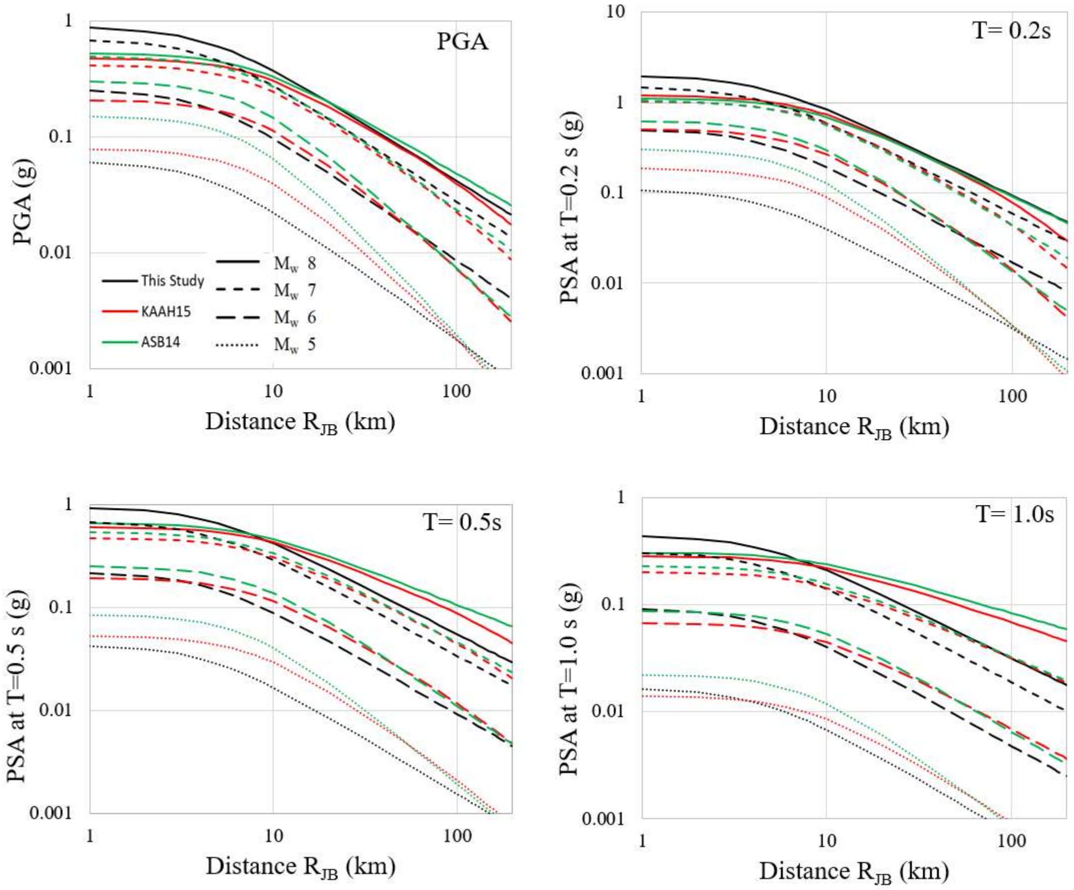

Figure 4.15. Distance scaling comparisons between ASB14 and KAAH15 GMPEs and the proposed model at different spectral ordinates (PGA, PSA at T = 0.2s, 0.5s and 1s) for M_w 5, 6, 7 and 8. The comparisons are done for a reference rock site, V_{S30} = 760 m/s.

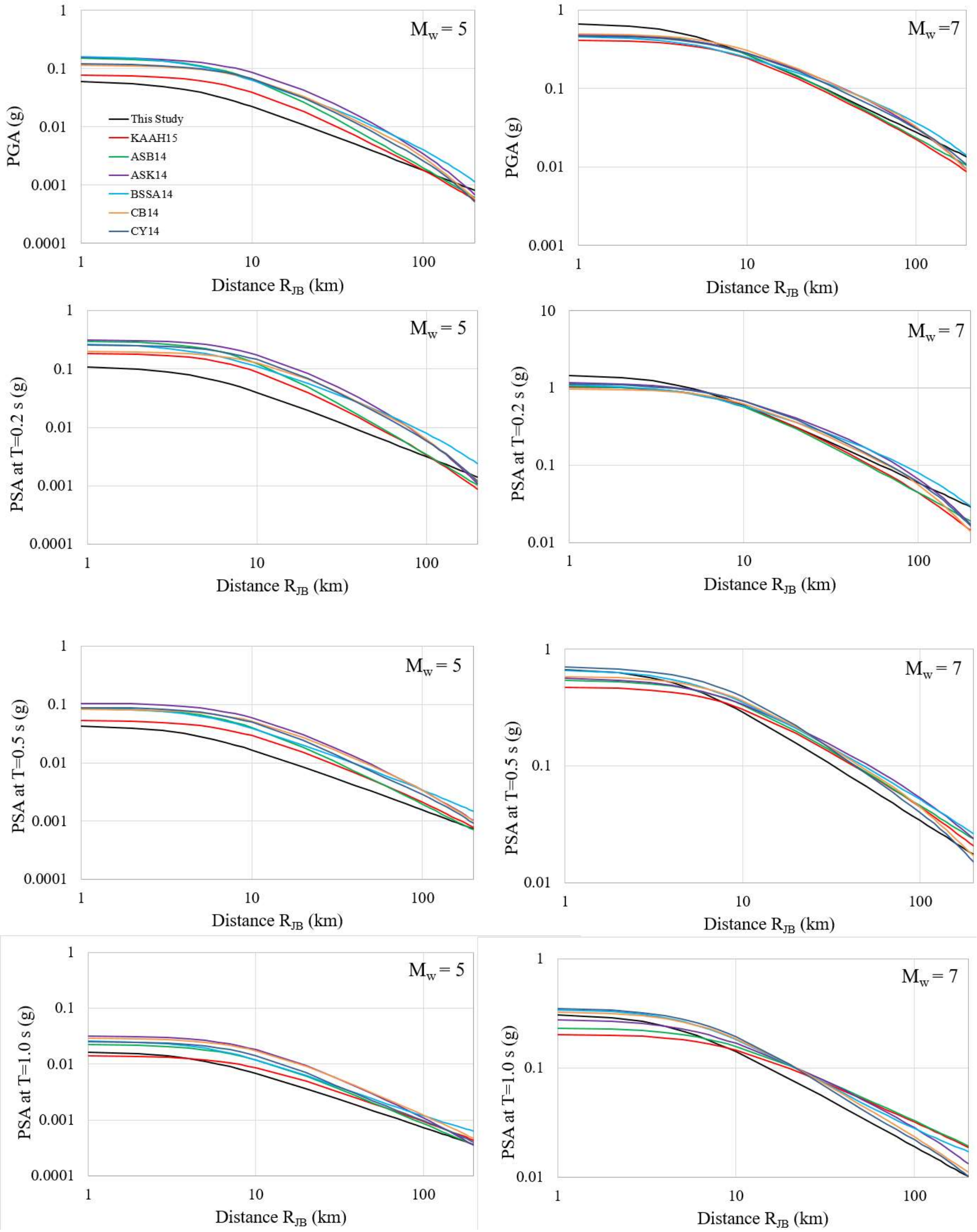

Figure 4.16. Distance *scaling comparisons between the proposed model and ASB14, KAAH15 ground motion models and NGA-West2 GMPEs (ASB14, BSSA14, CB14 and CY14) at different spectral ordinates (PGA, PSA at T = 0.2s, 0.5s and 1s). The comparisons are done for magnitudes M_w 5 and M_w 7 for V_{S30} = 760 m/s from a strike slip fault.*

The magnitude scaling comparisons between ASB14 and KAAH15 models and the proposed model for PGA and spectral periods of 0.2 s, 0.5 s and 1.0 s are presented in

Figure 4.17. The comparisons are done at a distance of R_{JB} = 10 km for a reference rock site, V_{S30} = 760 m/s from a strike slip fault. The magnitude scaling predicted by the new model derived from the simulated database is very similar to those from ASB14 and KAAH15 particularly at large magnitudes ($M_w \geq 6.5$) for all spectral periods, probably due to the accurate estimates of stochastic technique for near-field ground motions from large earthquakes. It is noticeable that the new model underestimates the spectral ordinates at magnitudes smaller than M_w 6 for $T \leq 0.5$s. As stated previously, the small magnitude bias of the proposed model can be due to using the low stress drop parameter or employing the finite-fault method for small magnitudes in simulations.

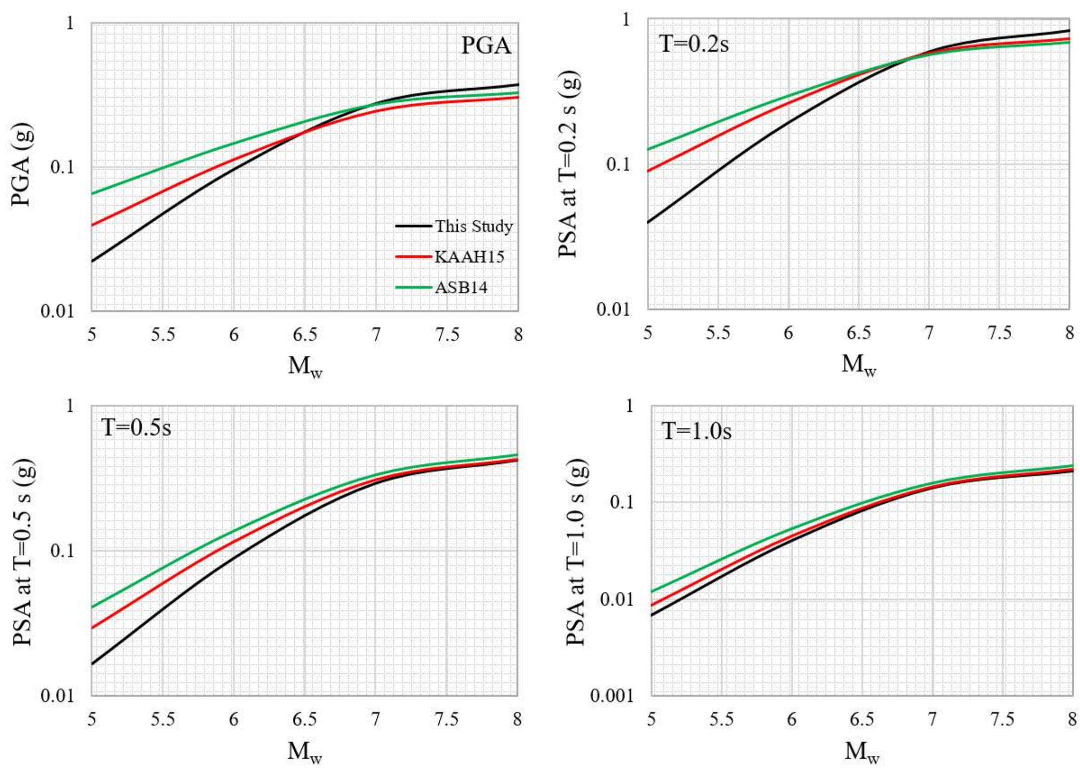

Figure 4.17. Magnitude scaling comparisons between ASB14 and KAAH15 models and the proposed GMPEs at different spectral ordinates (PGA, PSA at T = 0.2s, 0.5s and 1s). The comparisons are done for a reference rock site, V_{S30} = 760 m/s at R_{JB} = 10 km from a strike slip fault.

Figure 4.18 also shows magnitude scaling comparisons between previous models and the proposed model for PGA and spectral periods of 0.2 s, 0.5 s and 1.0 s but this time at distance R_{JB} = 80 km. The comparisons are done for V_{S30} = 760 m/s from a strike slip fault. For the upper bound of the geometric attenuation, the magnitude scaling predicted by the new GMPEs is very similar to those from ASB14 and KAAH15 models at all magnitudes particularly for $T \leq 0.2$ s. Although, the proposed GMPE is slightly on the low side at large magnitudes for intermediate to long periods (i.e., T = 0.5 s and 1 s). The small magnitude bias of the new GMPE does not shown for R_{JB} = 80km.

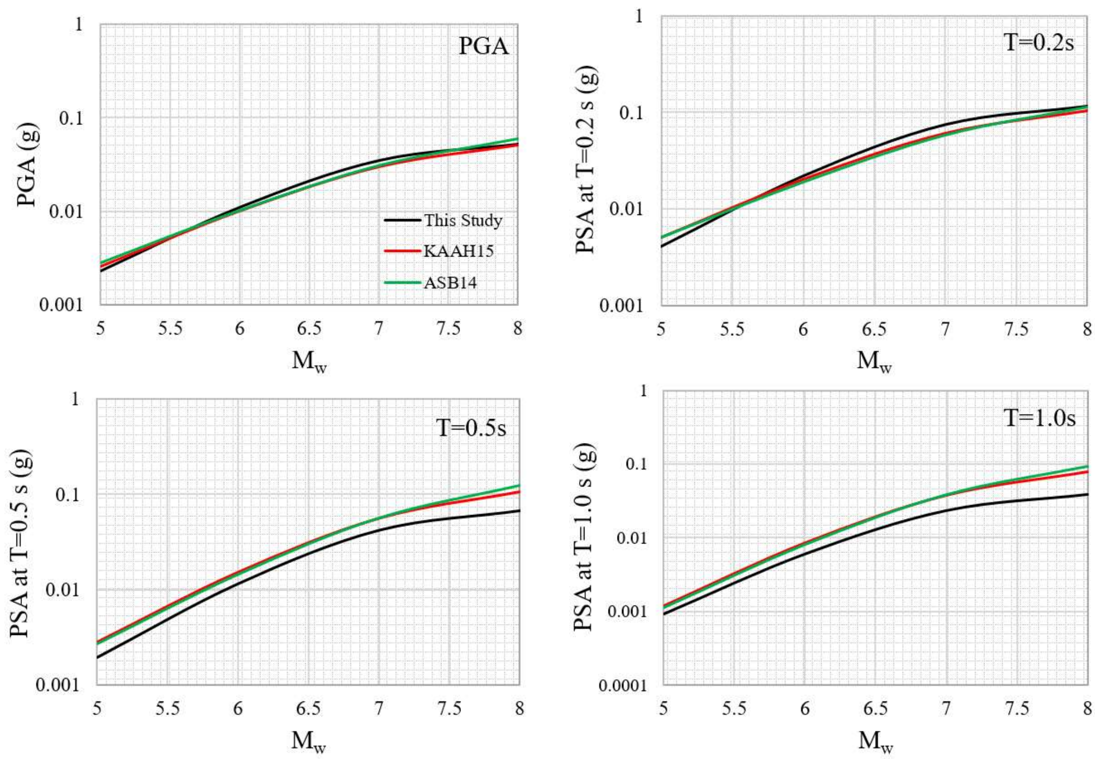

Figure 4.18. Magnitude scaling comparisons between ASB14 and KAAH15 GMPEs and the proposed model at different spectral ordinates (PGA, PSA at T = 0.2s, 0.5s and 1s). The comparisons are done for a reference rock site, V_{S30} = 760 m/s at R_{JB} = 80 km from a strike slip fault.

Figure 4.19 presents magnitude scaling comparisons of proposed GMPEs with previous local GMPEs and NGA-West2 models for PGA and spectral periods of 0.2 s, 0.5 s and 1.0 s. The comparisons are done for a reference rock site, V_{S30} = 760 m/s at a distance of R_{JB} = 10 km from a strike slip fault. For the close distance (i.e., R_{JB} = 10 km), the magnitude scaling of evaluated GMPEs are comparable at all magnitudes for T = 1.0 s, while the new study estimates lower spectral amplitudes than compared

GMPEs for T ≤ 0.5 s at small magnitudes (i.e., $M_w < 6$). The new GMPE is on the low side at small magnitudes for selected periods. In general, regional differences, GMPEs parametric form variations and the differences in lower magnitude limits as well as the small magnitude close distance data numbers of the model development databases can be the reason of the discrepancies between evaluated models at periods T ≤ 0.5 s.

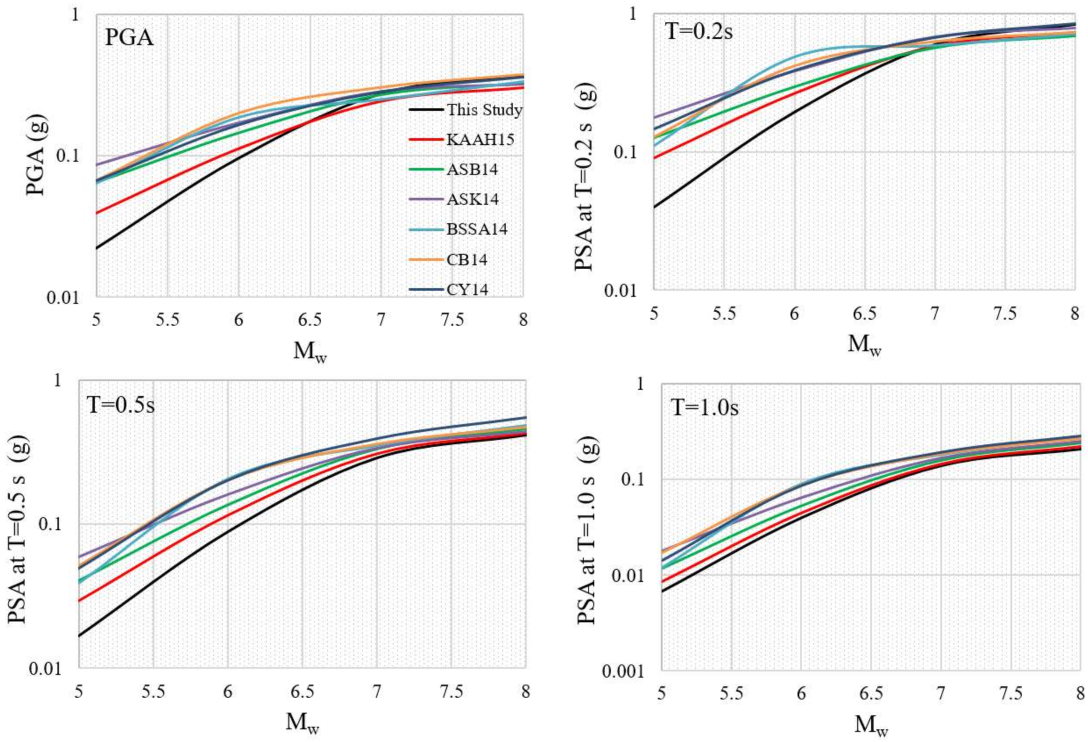

Figure 4.19. Magnitude scaling comparisons of the new model with NGA-West2 GMPEs, previous local and regional models at different spectral ordinates (PGA, PSA at T = 0.2s, 0.5s and 1 s). The comparisons are done for V_{S30} = 760 m/s at R_{JB} = 10 km from a strike slip fault.

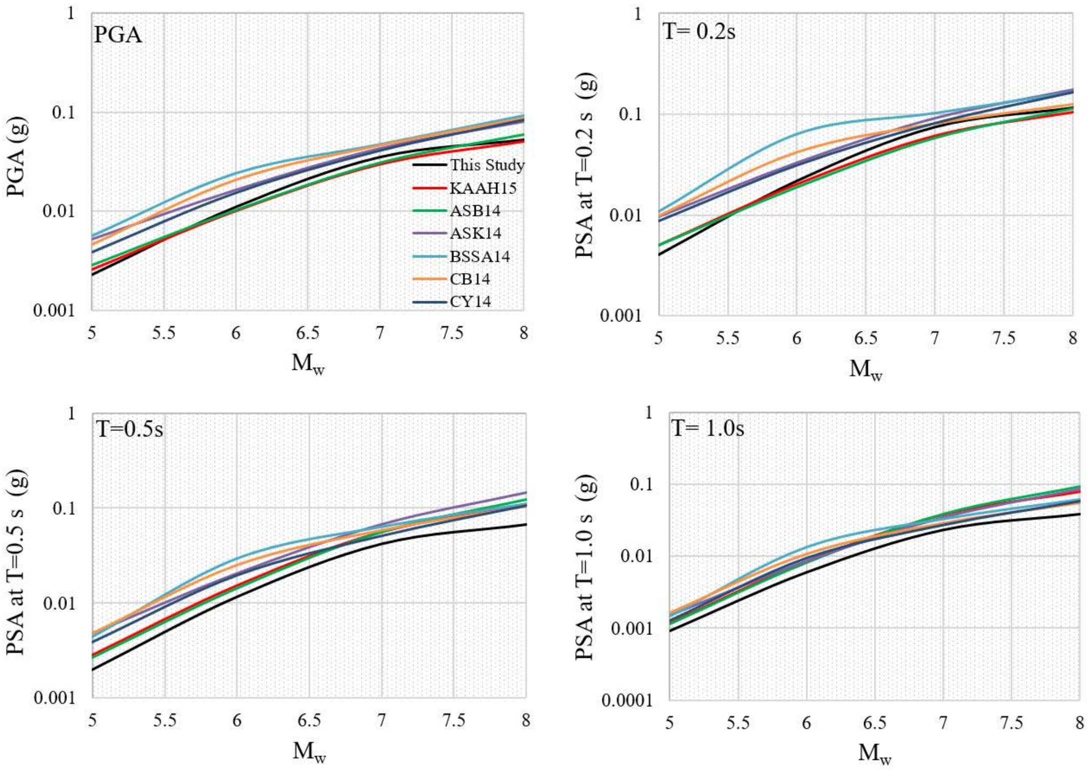

Figure 4.20. Magnitude scaling comparisons of the new GMPEs with NGA-West2 models and ASB14 and KAAH15 ground motion models at different spectral ordinates (PGA, PSA at T = 0.2s, 0.5s and 1s). The comparisons are done for V_{S30} = 760 m/s at a distance of R_{JB} = 80 km from a strike slip fault.

Magnitude scaling comparisons of the new GMPEs with previous local models and NGA-West2 models for PGA and spectral periods of 0.2s, 0.5s and 1.0s are presented in Figure 4.20 at a distance of R_{JB} = 80 km from a strike slip fault (V_{S30} = 760 m/s). All evaluated models show similar magnitude scaling at selected spectral periods. Although, the plots show the slightly lower spectral estimates of the proposed model at all magnitudes for the spectral period T = 0.5 s, and slightly higher estimates of BSSA14 for M_w < 6.5 at T = 0.2s.

Figure 4.21 shows the comparisons of spectral ordinates from the new model with previous local and regional predictive models and NGA-West2 GMPEs. The comparisons are done for sites with V_{S30} = 255, 520 and 760 m/s at R_{JB} = 30 km from a strike slip fault for magnitudes M_w 5 and M_w 7. The comparisons for all sites indicate good agreement at large magnitudes (i.e., M_w 7), although the proposed GMPEs tend to estimate relatively small spectral amplitudes at intermediate to long periods. For magnitude M_w 5, there is variation between all compared models particularly at short periods while the proposed model with ASB14 and KAAH15 models predict the lowest spectral amplitudes at all periods. The small magnitude bias of the proposed model that possibly originates from the low stress drop simulation parameters and the lower ground motion amplitude estimates of the finite-fault technique for small magnitude events, can also be seen in these plots. The new model also estimates lower spectral periods for large magnitudes (M_w 7) particularly at $T \geq 0.5$s. This can be due to the fact that stochastic method is limited at low frequencies that are highly influenced by the source mechanism of large magnitude earthquakes (Askan et al., 2013). Complex source behavior cannot be fully included in stochastic finite-fault method, since source effects are quite complicated and uncertain in compare to all other seismic properties.

Figure 4.22 presents magnitude scaling comparisons between ASB14 and KAAH15 ground motion models and the proposed GMPEs at selected spectral ordinates (PGA, PSA at T = 0.2 s, 0.5 s and 1 s) for distances R_{JB} = 1, 30 and 80 km. The comparisons are done for a reference rock site, V_{S30} = 760 m/s on a strike slip fault. The figure display little weak scaling of the short period motion at very short distances, indicates there is little saturation with magnitude. ASB14 and KAAH15 reflect the saturation with magnitude more than the proposed model. At long periods, saturation is not significant. Discrepancy between the estimates of three models occur mostly for M_w < 6 at close and intermediate distances (i.e., R_{JB} = 1 and 30 km) at short spectral periods, and for M_w > 7 at the closest distance (i.e., R_{JB} = 1 km) at all selected periods.

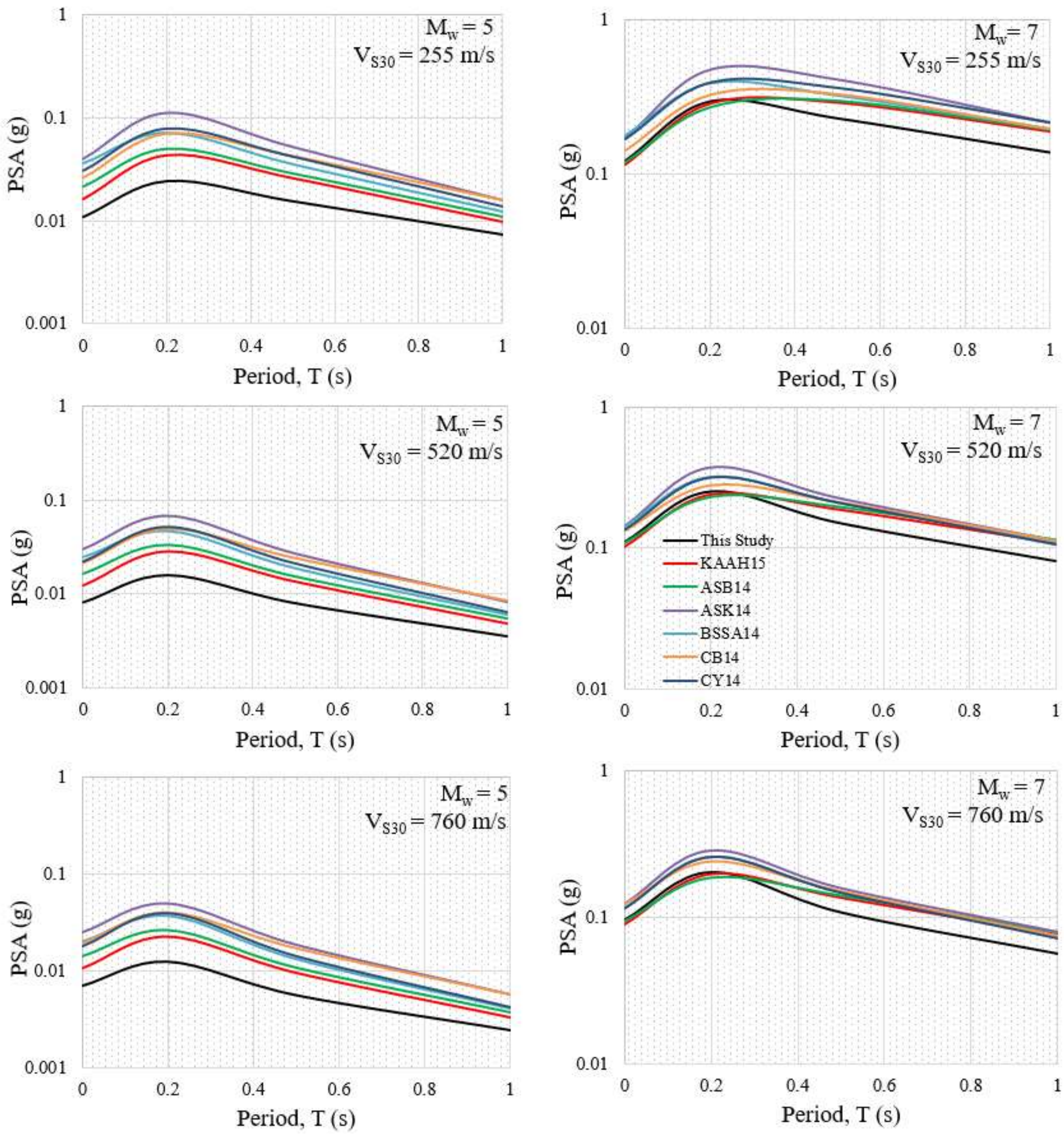

Figure 4.21. Comparisons of spectral ordinates from the proposed model with NGA-West2 models, ASB14 and KAAH15 predictive models. The comparisons are done for V_{S30} = 255, 520 and 760 m/s at R_{JB} = 30 km from a strike slip fault for magnitudes M_w 5 and 7.

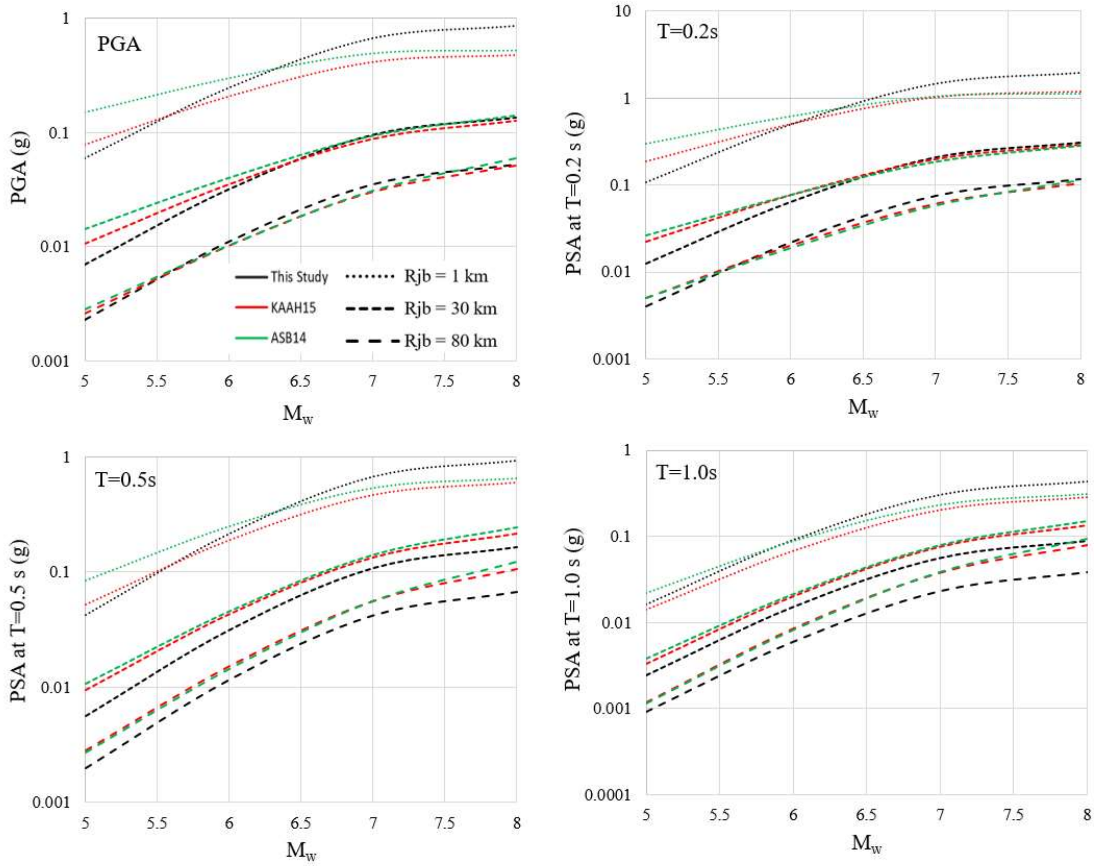

Figure 4.22. Magnitude scaling comparisons between ASB14, KAAH15 models and the proposed GMPEs at different spectral ordinates (PGA, PSA at T = 0.2s, 0.5s and 1s) for distance ranges R_{JB} = 1, 30 and 80 km. The comparisons are done for V_{S30} = 760 m/s on a strike slip fault.

Additional figures that provide the median ground motion comparisons between the proposed model and ASB14, KAAH15 models and NGA-West2 prediction models (ASK14, BSSA14, CB14 and CY14) considering different V_{S30} values, and R_{JB} distances are included in Appendix B.

CHAPTER 5

CONCLUSIONS

5.1. Summary

This thesis evaluates the use of regional GMPEs derived from the simulated ground motion database of the Erzincan and Duzce regions by comparing the proposed model with the up-to-date local Turkish GMPEs (Kale et al., 2015) and other previous regional and global predictive models. Ground motions are simulated from the Erzincan and Duzce regions which are located on the Eastern and Western territories of seismically active North Anatolian Fault zone, respectively. These target areas can be considered as representative of source mechanisms for most of the Turkish earthquake characteristics. The synthetic database is implemented from the past studies (Ugurhan and Askan, 2010; Askan et al., 2013; Askan et al., 2015; Karimzadeh et al., 2017b; Karimzadeh et al., 2018). Simulated ground motion records are generated from the 1992 Erzincan (M_w 6.6) and the 1999 Duzce (M_w 7.1) earthquakes with stochastic finite-fault technique. Validated simulation models are used to produce a large number of potential scenario earthquakes. The regional GMPEs is derived from this generated synthetic database. Functional form is structured with the number of estimator parameters limited by the simulated database. The proposed GMPEs derived from the synthetic database are assessed by comparing the proposed model with the observed local GMPEs of Kale et al. (2015). The same functional form of Kale et al. (2015) is employed in the proposed model to remove the epistemic uncertainty that results from the functional form selection and to make reliable comparisons. Regression analysis is performed to obtain the model coefficients and standard deviation values. Residual analyses are presented for the model development synthetic database and the recorded Turkish ground motion database. Finally, the proposed ground motion model is evaluated against the existing local, regional and global GMPEs.

5.2. Conclusions

The main conclusions obtained in this study are listed as follows:

- The finite-fault simulations can efficiently model the near-source ground motions of large magnitude earthquakes, particularly the significant effect of finite-fault features (rupture geometry, spatial slip variation, rupture directivity) on ground motion characteristics. This feature of the finite-fault simulations is important since the recordings from large earthquakes at close distances are the main deficiency of the GMPEs based on regional real ground motion databases.

- Examining residuals for the simulated database indicates that the proposed model fits the simulated data well, and show unbiased estimations with respect to the predictor parameters with near-zero mean residuals. The proposed GMPEs also agree well with recorded database of Kale et al. (2015); however, a tendency to positive or negative residuals are observed for small magnitude events (i.e., $M_w < 5$), for close distances (i.e., $R_{JB} < 20$ km), and for large site parameter values (i.e., $V_{S30} > 700$ m/s), possibly resulting from the model development database features.

- It is observed that the within-event and between-event variabilities of the new model are almost equal. The total aleatory variability (σ) of the proposed model derived from the simulated database is magnitude-independent and period-dependent with values ranging from 0.42 natural log units for PGA and to 0.55 natural log units for T = 1 s. The calculated uncertainties are lower than those obtained from the selected empirical GMPEs, where the main difference is between the within-event uncertainty values. The lower sigma values of the current model can be due to the systematic features of the simulated database and considerable number of records from moderate to large earthquakes.

- The median estimation comparisons between the proposed model and regional predictive models as well as global GMPEs indicate good agreements in general. However, the median estimations of the proposed GMPEs show some biases when they are compared to the selected models. Significant observations related to the median estimations are given as follows:

  - The proposed model underestimates the spectral amplitudes for small magnitudes (i.e., M_w 5) particularly at short periods. This small magnitude bias can arise from using low stress drop, lack of observed near field pulses in the simulations or use of finite-fault simulation method instead of point-source technique for small magnitude earthquake simulations.

  - The new model yields relatively lower spectral amplitude estimates for large magnitudes (i.e., $M_w > 7$) particularly at $T > 0.5$ s. This underestimation results from the theoretical background of stochastic simulation processes, since the stochastic methods are inherently limited to generate the coherent motions of long periods.

  - The proposed GMPEs tends to estimate higher spectral amplitudes at close distances (i.e., $R_{JB} < 10$km) for large magnitudes (i.e., M_w>7) for all spectral periods. This overestimation is possibly due to the considerable number of simulated near-source data. Thus, it can be stated that the stochastic method can successfully simulate near-field ground motions from large earthquakes.

- The proposed ground motion model is evaluated by comparing with local, regional and global GMPEs for magnitude, distance and V_{S30} limits of M_w = 5–8.0, $R_{JB} \leq 200$ km, and V_{S30} = 255–760 m/s, respectively. However, the largest magnitude in the simulated database is M_w 7.5. Besides, the upper distance limit of the comparisons is beyond the data limits of the simulated database, and the proposed model is not well constrained for distances larger than 120 km as observed from the residual analysis. Note that, the proposed model is considered as applicable for $V_{S30} \leq 760$ m/s, but the upper limit of the model development database is $V_{S30} = 520$ m/s and the proposed model should be used with caution for sites above this limit. The equations are presented for the prediction of peak ground acceleration, peak ground velocity, and 5%-damped pseudo-absolute-acceleration spectra at oscillator periods between 0.01 s and 4 s.

- Overall, the comparable median estimations between the proposed model and the selected GMPEs indicates that the simulated ground motions with physical earthquake source, propagation, and site effects can be contributed in developing GMPEs.

5.3. Suggestions for Future Research

- In this dissertation, only strike-slip faulting is used in the model development database since the observed earthquakes used for simulations have strike-slip mechanism. When the earthquakes with normal and reverse faulting are simulated, it is possible to expand the country-based synthetic database to contain the style of faulting differences.

- The long period bias of the median estimations for large magnitudes is originated from the insufficient low frequency modeling of stochastic approach. The stochastic technique provides solutions to the high frequency band of ground motions which has an arbitrary character constituted of random phases. However, deterministic simulations can accurately model the low frequencies (long period) by using precise source characteristics and wave velocity patterns. It is possible to use the deterministic methods in areas that are well studied seismologically.

- Hybrid methods can successfully model the broadband ground motions with the whole frequency range by combining the low and high frequencies generated from deterministic and stochastic methods, respectively. The current local simulated database can be enhanced with simulated ground motions by using the hybrid simulation methods.

- The structure of the ground motion database, such as distributions in magnitude and distance, may affect the ground motion estimates. Empirical databases can be extended by adding ground motion records from small-to-moderate magnitude earthquakes. Eventually, hybrid ground motion databases can be constituted by integration of the available real ground motion data from small-to-moderate size earthquakes and simulated ground motions at close distances from large earthquakes to develop more reliable ground motion relations.

REFERENCES

Abrahamson, N. A. and Silva, W. J. (1997). Empirical response spectral attenuation relations for shallow crustal earthquakes. Seismological Research Letters, 68(1), 94–127.

Abrahamson, N. and Silva, W. (1993). Attenuation of long period strong ground motions. In American Society of Mechanical Engineers, Pressure Vessels and Piping Division (Publication) PVP.

Abrahamson, N. A., Silva, W. J. and Kamai, R. (2014). Summary of the ASK14 ground motion relation for active crustal regions. Earthquake Spectra, 30(3), 1025–1055.

Abrahamson, N. A. and Youngs, R. R. (1992). A stable algorithm for regression analyses using the random effects model. Bulletin of the Seismological Society of America, 82(1), 505–510.

Abrahamson, N. and Silva, W. (2008). Summary of the Abrahamson & Silva NGA ground-motion relations. Earthquake Spectra, 24(1), 67–97.

Aki, K. (1967). Scaling law of seismic spectrum. Journal of Geophysical Research, 72(4), 1217–1231.

Aki, K. (1968). Seismic displacements near a fault. Journal of Geophysical Research, 73(16), 5359–5376.

Aki, K. (1980). Attenuation of shear-waves in the lithosphere for frequencies from 0.05 to 25 Hz. Physics of the Earth and Planetary Interiors, 21(1), 50–60.

Aki, K. and Richards, P. G. (1980). Quantative seismology: Theory and methods. New York, 801.

Akinci, A. and Antonioli, A. (2012). Observations and stochastic modelling of strong ground motions for the 2011 October 23 Mw 7.1 Van, Turkey, earthquake. Geophysical Journal International, 192(3), 1217–1239.

Akinci, A., Malagnini, L., Herrmann, R. B., Pino, N. A., Scognamiglio, L. and Eyidogan, H. (2001). High-frequency ground motion in the Erzincan region, Turkey: Inferences from small earthquakes. Bulletin of the Seismological Society of America, 91(6), 1446–1455.

Akkar, S., Sandikkaya, M. A. and Bommer, J. J. (2014). Empirical ground-motion models for point-and extended-source crustal earthquake scenarios in Europe and the Middle East. Bulletin of Earthquake Engineering, 12(1), 359–387.

Akkar, S. and Bommer, J. J. (2010). Empirical equations for the prediction of PGA, PGV, and spectral accelerations in Europe, the Mediterranean region, and the Middle East. Seismological Research Letters, 81(2), 195–206.

Akkar, S. and Bommer, J. J. (2007). Empirical prediction equations for peak ground velocity derived from strong-motion records from Europe and the Middle East. Bulletin of the Seismological Society of America, 97(2), 511–530.

Akkar, S. and Cagnan, Z. (2010). A local ground-motion predictive model for Turkey, and its comparison with other regional and global ground-motion models. Bulletin of the Seismological Society of America, 100(6), 2978–2995.

Akyol, N. and Karagoz, O. (2009). Empirical attenuation relationships for western Anatolia, Turkey. Turkish Journal of Earth Sciences, 18(3), 351–382.

Akyuz, H. S., Hartleb, R., Barka, A., Altunel, E., Sunal, G., Meyer, B. and Armijo, v R. (2002). Surface rupture and slip distribution of the 12 November 1999 Duzce earthquake (M 7.1), North Anatolian fault, Bolu, Turkey. Bulletin of the Seismological Society of America, 92(1), 61–66.

Allen, T. I. (2012). Stochastic ground-motion prediction equations for southeastern Australian earthquakes using updated source and attenuation parameters. Geoscience Australia Record, 69, 55.

Ambraseys, N. N. (1995). The prediction of earthquake peak ground acceleration in Europe. Earthquake Engineering & Structural Dynamics, 24(4), 467–490.

Ambraseys, N. N. (1990). Uniform magnitude re-evaluation of European earthquakes associated with strong-motion records. Earthquake Engineering & Structural Dynamics, 19(1), 1–20.

Ambraseys, N. N. (1975). Trends in engineering seismology in Europe. In Proceedings of fifth European conference on earthquake engineering (Vol. 3, pp. 39–52).

Ambraseys, N. N., Douglas, J., Sarma, S. K. and Smit, P. M. (2005). Equations for the estimation of strong ground motions from shallow crustal earthquakes using data from Europe and the Middle East: horizontal peak ground acceleration and spectral acceleration. Bulletin of Earthquake Engineering, 3(1), 1–53.

Ambraseys, N. N. (1978). Middle East—A reappraisal of the seismicity. Quarterly Journal of Engineering Geology and Hydrogeology, 11(1), 19–32.

Ambraseys, N. N., Simpson, K. A. u and Bommer, J. J. (1996). Prediction of horizontal response spectra in Europe. Earthquake Engineering & Structural Dynamics, 25(4), 371–400.

Ameri, G., Drouet, S., Traversa, P., Bindi, D. and Cotton, F. (2017). Toward an empirical ground motion prediction equation for France: accounting for regional differences in the source stress parameter. Bulletin of Earthquake Engineering, 15(11), 4681–4717.

Anbazhagan, P., Kumar, A. and Sitharam, T. G. (2013). Ground motion prediction equation considering combined dataset of recorded and simulated ground motions. Soil Dynamics and Earthquake Engineering, 53, 92–108.

Anderson, J. G. and Hough, S. E. (1984). A model for the shape of the Fourier amplitude spectrum of acceleration at high frequencies. Bulletin of the Seismological Society of America, 74(5), 1969–1993.

Ansal, A., Akinci, A., Cultrera, G., Erdik, M., Pessina, V., Tonuk, G. and Ameri, G. (2009). Loss estimation in Istanbul based on deterministic earthquake scenarios of the Marmara Sea region (Turkey). Soil Dynamics and Earthquake Engineering, 29(4), 699–709.

Askan, A., Karimzadeh, S., Asten, M., Kilic, N., Sisman, F. N. and Erkmen, C. (2015). Assessment of seismic hazard in the Erzincan (Turkey) region: construction of local velocity models and evaluation of potential ground motions. Turkish Journal of Earth Sciences, 24(6), 529–565.

Askan, A., Karimzadeh, S., Bilal, M. (2016). Seismic intensity maps for North Anatolian Fault Zone (Turkey) based on recorded and simulated ground motion data, Book Chapter, Neotectonics and Earthquake Potential of the Eastern Mediterranean Region, AGU Books.

Askan, A., Sisman, F. N. and Ugurhan, B. (2013). Stochastic strong ground motion simulations in sparsely-monitored regions: A validation and sensitivity study on the 13 March 1992 Erzincan (Turkey) earthquake. Soil Dynamics and Earthquake Engineering, 55, 170–181.

Assatourians, K. and Atkinson, G. M. (2007). Modeling variable-stress distribution with the stochastic finite-fault technique. Bulletin of the Seismological Society of America, 97(6), 1935–1949.

Asten, M.W., T. Dhu, A. Jones and T. Jones (2003). Comparison of shear velocities measured from microtremor array studies and SCPT data acquired for earthquake site hazard classification in the northern suburbs of Perth W.A., Proceedings of a Conference of the Australian Earthquake Engineering Soc., 12 p., Melbourne.

Atkinson, G. M. (1984). Attenuation of strong ground motion in Canada from a random vibrations approach. Bulletin of the Seismological Society of America, 74(6), 2629–2653.

Atkinson, G. M. (2004). Empirical attenuation of ground-motion spectral amplitudes in southeastern Canada and the northeastern United States. Bulletin of the Seismological Society of America, 94(3), 1079–1095.

Atkinson, G. M. (2006). Single-station sigma. Bulletin of the Seismological Society of America, 96(2), 446–455.

Atkinson, G. M. (2008). Ground-motion prediction equations for eastern north America from a referenced empirical approach: implications for epistemic uncertainty. Bulletin of the Seismological Society of America, 98(3), 1304–1318.

Atkinson, G. M. (2010). Ground-motion prediction equations for Hawaii from a referenced empirical approach. Bulletin of the Seismological Society of America, 100(2), 751–761.

Atkinson, G. M., Assatourians, K., Boore, D. M., Campbell, K. and Motazedian, D. (2009). A guide to differences between stochastic point-source and stochastic finite-fault simulations. Bulletin of the Seismological Society of America, 99(6), 3192–3201.

Atkinson, G. M. and Boore, D. M. (2003). Empirical ground-motion relations for subduction-zone earthquakes and their application to Cascadia and other regions. Bulletin of the Seismological Society of America, 93(4), 1703–1729.

Atkinson, G. M. and Boore, D. M. (2006). Earthquake ground-motion prediction equations for eastern North America. Bulletin of the Seismological Society of America, 96(6), 2181–2205.

Atkinson, G. M. and Boore, D. M. (2011). Modifications to existing ground-motion prediction equations in light of new data. Bulletin of the Seismological Society of America, 101(3), 1121–1135.

Atkinson, G. M. and Goda, K. (2010). Inelastic seismic demand of real versus simulated ground-motion records for Cascadia subduction earthquakes. Bulletin of the Seismological Society of America, 100(1), 102–115.

Atkinson, G. M., Goda, K. and Assatourians, K. (2011). Comparison of nonlinear structural responses for accelerograms simulated from the stochastic finite-fault approach versus the hybrid broadband approach. Bulletin of the Seismological Society of America, 101(6), 2967–2980.

Atkinson, G. M. and Macias, M. (2009). Predicted ground motions for great interface earthquakes in the Cascadia subduction zone. Bulletin of the Seismological Society of America, 99(3), 1552–1578.

Atkinson, G. M. and Mereu, R. F. (1992). The shape of ground motion attenuation curves in southeastern Canada. Bulletin of the Seismological Society of America, 82(5), 2014–2031.

Atkinson, G. M. and Motazedian, D. (2013). Ground-motion amplitudes for earthquakes in Puerto Rico. Bulletin of the Seismological Society of America, 103(3), 1846–1859.

Atkinson, G. M. and Silva, W. (2000). Stochastic modeling of California ground motions. Bulletin of the Seismological Society of America, 90(2), 255–274.

Aydan O., Sedaki M., Yarar R. (1996). The seismic characteristics of Turkish earthquakes. Proceedings of Eleventh World Conference on Earthquake Engineering Paper no. 1270.

Aydan, O. (2001) 'Comparison of suitability of submerged tunnel and shield tunnel for subsea passage of Bosphorus', Geological Engineering Journal of Turkey, 25(1), pp. 1–17.

Baumann, C. and Dalguer, L. A. (2014). Evaluating the compatibility of dynamic rupture-based synthetic ground motion with empirical ground-motion prediction equation. Bulletin of the Seismological Society of America, 104(2), 634–652.

Bazzurro, P., Sjoberg, B. and Luco, N. (2004). Post-elastic response of structures to synthetic ground motions. Report for Pacific Earthquake Engineering Research (PEER) Center Lifelines Program Project, 65–112.

Beresnev, I. A. and Atkinson, G. M. (1997). Modeling finite-fault radiation from the ω n spectrum. Bulletin of the Seismological Society of America, 87(1), 67–84.

Beresnev, I. A. and Atkinson, G. M. (1998a). FINSIM--a FORTRAN program for simulating stochastic acceleration time histories from finite faults. Seismological Research Letters, 69(1), 27–32.

Beresnev, I. A. and Atkinson, G. M. (1998b). Stochastic finite-fault modeling of ground motions from the 1994 Northridge, California, earthquake. I. Validation on rock sites. Bulletin of the Seismological Society of America, 88(6), 1392–1401.

Bernard, P., Gariel, J.-C. and Dorbath, L. (1997). Fault location and rupture kinematics of the magnitude 6.8, 1992 Erzincan earthquake, Turkey, from strong ground motion and regional records. Bulletin of the Seismological Society of America, 87(5), 1230–1243.

Bindi, D., Luzi, L., Massa, M. and Pacor, F. (2010). Horizontal and vertical ground motion prediction equations derived from the Italian Accelerometric Archive (ITACA). Bulletin of Earthquake Engineering, 8(5), 1209–1230.

Bindi, D., Massa, M., Luzi, L., Ameri, G., Pacor, F., Puglia, R., and Augliera, P. (2014). Pan-European ground-motion prediction equations for the average horizontal component of PGA, PGV, and 5%-damped PSA at spectral periods up to 3.0 s using the RESORCE dataset. Bulletin of Earthquake Engineering, 12(1), 391–430.

Boatwright, J. and Choy, G. L. (1992). Acceleration source spectra anticipated for large earthquakes in northeastern North America. Bulletin of the Seismological Society of America, 82(2), 660–682.

Bommer, J. J., Stafford, P. J., Alarcón, J. E. and Akkar, S. (2007). The influence of magnitude range on empirical ground-motion prediction. Bulletin of the Seismological Society of America, 97(6), 2152–2170.

Boore, D. M. (2009). Comparing stochastic point-source and finite-source ground-motion simulations: SMSIM and EXSIM. Bulletin of the Seismological Society of America, 99(6), 3202–3216.

Boore, D. M. (1983). Stochastic simulation of high-frequency ground motions based on seismological models of the radiated spectra. Bulletin of the Seismological Society of America, 73(6A), 1865–1894.

Boore, D. M. (2003). Simulation of ground motion using the stochastic method. Pure and Applied Geophysics, 160(3–4), 635–676.

Boore, D. M. (1984). Use of seismoscope records to determine ML and peak velocities. Bulletin of the Seismological Society of America, 74(1), 315–324.

Boore, D. M. (2010). Orientation-independent, nongeometric-mean measures of seismic intensity from two horizontal components of motion. Bulletin of the Seismological Society of America, 100(4), 1830–1835.

Boore, D. M. and Atkinson, G. M. (2008). Ground-motion prediction equations for the average horizontal component of PGA, PGV, and 5%-damped PSA at spectral periods between 0.01 s and 10.0 s. Earthquake Spectra, 24(1), 99–138.

Boore, D. M. and Atkinson, G. M. (1987). Stochastic prediction of ground motion and spectral response parameters at hard-rock sites in eastern North America. Bulletin of the Seismological Society of America, 77(2), 440–467.

Boore, D. M. and Joyner, W. B. (1982). The empirical prediction of ground motion. Bulletin of the Seismological Society of America, 72(6B), S43–S60.

Boore, D. M. and Joyner, W. B. (1997). Site amplifications for generic rock sites. Bulletin of the Seismological Society of America, 87(2), 327–341.

Boore, D. M. and Joyner, W. B. (1991). Estimation of ground motion at deep-soil sites in eastern North America. Bulletin of the Seismological Society of America, 81(6), 2167–2185.

Boore, D. M., Joyner, W. B. and Fumal, T. E. (1994). Estimation of response spectra and peak accelerations from western North American earthquakes: an interim report. US Department of the Interior, US Geological Survey.

Boore, D. M., Joyner, W. B. and Fumal, T. E. (1997). Equations for estimating horizontal response spectra and peak acceleration from western North American earthquakes: A summary of recent work. Seismological Research Letters, 68(1), 128–153.

Boore, D. M., Stewart, J. P., Seyhan, E. and Atkinson, G. M. (2014). NGA-West2 equations for predicting PGA, PGV, and 5% damped PSA for shallow crustal earthquakes. Earthquake Spectra, 30(3), 1057–1085.

Bora, S. S., Cotton, F., Scherbaum, F., Edwards, B. and Traversa, P. (2017). Stochastic source, path and site attenuation parameters and associated variabilities for shallow crustal European earthquakes. Bulletin of Earthquake Engineering, 15(11), 4531–4561.

Bozorgnia, Y., Abrahamson, N. A., Atik, L. Al, Ancheta, T. D., Atkinson, G. M., Baker, J. W., … Chiou, B. S.-J. (2014). NGA-West2 research project. Earthquake Spectra, 30(3), 973–987.

Brune, J. N. (1970). Tectonic stress and the spectra of seismic shear waves from earthquakes. Journal of Geophysical Research, 75(26), 4997–5009.

Brune J. N. (1971). Correction [to "Tectonic stress and the spectra, of seismic shear waves from earthquakes"]. Journal of Geophysical Research, 76(20), 5002-5002.

Bydlon, S. A., Gupta, A. and Dunham, E. M. (2017) 'Using Simulated Ground Motions to Constrain Near-Source Ground-Motion Prediction Equations in Areas Experiencing Induced Seismicity', Bulletin of the Seismological Society of America, 107(5), pp. 2078–2093.

Campbell, K. W. and Bozorgnia, Y. (2000). New empirical models for predicting near-source horizontal, vertical, and V/H response spectra: Implications for design. In Proceedings of the Sixth International Conference on Seismic Zonation.

Campbell, K. W. (1981). Near-source attenuation of peak horizontal acceleration. Bulletin of the Seismological Society of America, 71(6), 2039–2070.

Campbell, K. W. (2003). Prediction of strong ground motion using the hybrid empirical method and its use in the development of ground-motion (attenuation) relations in eastern North America. Bulletin of the Seismological Society of America, 93(3), 1012–1033.

Campbell, K. W. (1989). The dependence of peak horizontal acceleration on magnitude, distance, and site effects for small-magnitude earthquakes in California and eastern North America. Bulletin of the Seismological Society of America, 79(5), 1311–1346.

Campbell, K. W. and Bozorgnia, Y. (2003). Updated near-source ground-motion (attenuation) relations for the horizontal and vertical components of peak ground acceleration and acceleration response spectra. Bulletin of the Seismological Society of America, 93(1), 314–331.

Campbell, K. W. and Bozorgnia, Y. (2014). NGA-West2 ground motion model for the average horizontal components of PGA, PGV, and 5% damped linear acceleration response spectra. Earthquake Spectra, 30(3), 1087–1115.

Campbell, K. W. and Bozorgnia, Y. (2008). NGA ground motion model for the geometric mean horizontal component of PGA, PGV, PGD and 5% damped linear elastic response spectra for periods ranging from 0.01 to 10 s. Earthquake Spectra, 24(1), 139–171.

Castro, R. R., Pacor, F., Franceschina, G., Bindi, D., Zonno, G. and Luzi, L. (2008). Stochastic strong-motion simulation of the M w 6 Umbria–Marche earthquake of September 1997: Comparison of different approaches. Bulletin of the Seismological Society of America, 98(2), 662–670.

Chiou, B. S.-J. and Youngs, R. R. (2014). Update of the Chiou and Youngs NGA model for the average horizontal component of peak ground motion and response spectra. Earthquake Spectra, 30(3), 1117–1153.

Chiou, B., Darragh, R., Gregor, N. and Silva, W. (2008). NGA project strong-motion database. Earthquake Spectra, 24(1), 23–44.

Chiou, B.-J. and Youngs, R. R. (2008). An NGA model for the average horizontal component of peak ground motion and response spectra. Earthquake Spectra, 24(1), 173–215.

Chopra, S., Kumar, D., Choudhury, P. and Yadav, R. B. S. (2012). Stochastic finite fault modelling of M w 4.8 earthquake in Kachchh, Gujarat, India. Journal of Seismology, 16(3), 435–449.

D'Amico, M., Lanzano, G., Santulin, M., Puglia, R., Felicetta, C., Tiberti, M. M., Gomez-Capera, A. A. and Russo, E. (2018) 'Hybrid GMPEs for Region Specific PSHA in Southern Italy', Geosciences (2076-3263), 8(6).

Danciu, L. and Tselentis, G.-A. (2007). Engineering ground-motion parameters attenuation relationships for Greece. Bulletin of the Seismological Society of America, 97(1B), 162–183.

Douglas, J. (2003). Earthquake ground motion estimation using strong-motion records: a review of equations for the estimation of peak ground acceleration and response spectral ordinates. Earth-Science Reviews, 61(1–2), 43–104.

Douglas, J., Bungum, H., and Scherbaum, F. (2006). Ground-motion prediction equations for southern Spain and southern Norway obtained using the composite model perspective. Journal of Earthquake Engineering, 10(01), 33–72.

Draper, N. R., and H. Smith (1981). Applied Regression Analysis, Second Ed., John Wiley & Sons, New York, New York.

Durukal, E. (2002). Critical evaluation of strong motion in Kocaeli and Duzce (Turkey) earthquakes. Soil Dynamics and Earthquake Engineering, 22(7), 589–609.

Edwards, B. and Fäh, D. (2013). A stochastic ground-motion model for Switzerland. Bulletin of the Seismological Society of America, 103(1), 78–98.

Erdik, M. and Durukal, E. (2001). A hybrid procedure for the assessment of design basis earthquake ground motions for near-fault conditions. Soil Dynamics and Earthquake Engineering, 21(5), 431–443.

Esteva, L. and Rosenblueth, E. (1964). Espectros de temblores a distancias moderadas y grandes. Boletin Sociedad Mexicana de Ingenieria Sesmica, 2(1), 1–18, in Spanish.

Frankel, A. (2009). A constant stress-drop model for producing broadband synthetic seismograms: Comparison with the Next Generation Attenuation relations. Bulletin of the Seismological Society of America, 99(2A), 664–680.

Galasso, C. and Zareian, F. (2014). Engineering validation of hybrid broadband ground motion simulation using historical events. In NCEE 2014-10th US National Conference on Earthquake Engineering: Frontiers of Earthquake Engineering.

Galasso, C., Zhong, P., Zareian, F., Iervolino, I. and Graves, R. W. (2013). Validation of ground-motion simulations for historical events using MDoF systems. Earthquake Engineering & Structural Dynamics, 42(9), 1395–1412.

Ghofrani, H., Atkinson, G. M., Goda, K. and Assatourians, K. (2013). Stochastic finite-fault simulations of the 2011 Tohoku, Japan, earthquake. Bulletin of the Seismological Society of America, 103(2B), 1307–1320.

Goda, K., Kurahashi, S., Ghofrani, H., Atkinson, G. M. and Irikura, K. (2015). Nonlinear response potential of real versus simulated ground motions for the 11 March 2011 Tohoku-oki earthquake. Earthquake Spectra, 31(3), 1711–1734.

Goda, K., Petrone, C., De Risi, R. and Rossetto, T. (2017). Stochastic coupled simulation of strong motion and tsunami for the 2011 Tohoku, Japan earthquake. Stochastic Environmental Research and Risk Assessment, 31(9), 2337–2355.

Graves, R. W. and Pitarka, A. (2010). Broadband ground-motion simulation using a hybrid approach. Bulletin of the Seismological Society of America, 100(5A), 2095–2123.

Gregor, N., Abrahamson, N. A., Atkinson, G. M., Boore, D. M., Bozorgnia, Y., Campbell, K. W., Chiou, B. S-J., Idriss, I.M., Kamai, R. and Seyhan, E. (2014). Comparison of NGA-West2 GMPEs. *Earthquake Spectra*, *30*(3), 1179–1197.

Grosser, H., Baumbach, M., Berckhemer, H., Baier, B., Karahan, A., Schelle, H., … Demirtas, R. (1998). The Erzincan (Turkey) earthquake (Ms 6.8) of March 13, 1992 and its aftershock sequence. Pure and Applied Geophysics, 152(3), 465–505.

Gulkan, P. and Kalkan, E. (2002). Attenuation modeling of recent earthquakes in Turkey. Journal of Seismology, 6(3), 397–409.

Hanks, T. C. (1979). b value and 6 ‘seismic source models: implication for tectonic stress variation along active crustal fault zone and the estimation of high frequency strong ground motion. Journal of Geophysical Research.

Hanks, T. C. (1982). f max. Bulletin of the Seismological Society of America, 72(6A), 1867–1879.

Hanks, T. C. and Boore, D. M. (1984). Moment-magnitude relations in theory and practice. Journal of Geophysical Research: Solid Earth, 89(B7), 6229–6235.

Hanks, T. C. and Kanamori, H. (1979). A moment magnitude scale. Journal of Geophysical Research: Solid Earth, 84(B5), 2348–2350.

Hanks, T. C. and McGuire, R. K. (1981). The character of high-frequency strong ground motion. Bulletin of the Seismological Society of America, 71(6), 2071–2095.

Hartzell, S. H. (1978). Earthquake aftershocks as Green's functions. Geophysical Research Letters, 5(1), 1–4.

Hartzell, S., Guatteri, M., Mai, P. M., Liu, P.-C. and Fisk, M. (2005). Calculation of broadband time histories of ground motion, Part II: Kinematic and dynamic modeling using theoretical Green's functions and comparison with the 1994 Northridge earthquake. Bulletin of the Seismological Society of America, 95(2), 614–645.

Hartzell, S., Harmsen, S., Frankel, A. and Larsen, S. (1999). Calculation of broadband time histories of ground motion: Comparison of methods and validation using strong-ground motion from the 1994 Northridge earthquake. Bulletin of the Seismological Society of America, 89(6), 1484–1504.

Haskell, N. A. (1964). Total energy and energy spectral density of elastic wave radiation from propagating faults. Bulletin of the Seismological Society of America, 54(6A), 1811–1841.

Haskell, N. A. (1960). Crustal reflection of plane SH waves. Journal of Geophysical Research, 65(12), 4147–4150.

Hassani, B. and Atkinson, G. M. (2015). Referenced empirical ground-motion model for eastern North America. Seismological Research Letters, 86(2A), 477–491.

Hays, W. W. (1980). Procedures for estimating earthquake ground motions. US Govt. Print. Off., 1980.

Herrmann, R. B. (1985). An extension of random vibration theory estimates of strong ground motion to large distances. Bulletin of the Seismological Society of America, 75(5), 1447–1453.

Hirasawa, T. and Stauder, W. (1965). On the seismic body waves from a finite moving source. Bulletin of the Seismological Society of America, 55(2), 237–262.

Hisada, Y. (2008). Broadband strong motion simulation in layered half-space using stochastic Green's function technique. Journal of Seismology, 12(2), 265–279.

Holzer, T. L. (2000). Implications for earthquake risk reduction in the United States from the Kocaeli, Turkey, earthquake of August 17, 1999 (Vol. 1193). US Government Printing Office.

Hough, S. E. and Dreger, D. S. (1995). Source parameters of the 23 April 1992 M 6.1 Joshua Tree, California, earthquake and its aftershocks: empirical Green's function analysis of GEOS and TERRAscope data. Bulletin of the Seismological Society of America, 85(6), 1576–1590.

Housner, G. W. (1947). Characteristics of strong-motion earthquakes. Bulletin of the Seismological Society of America, 37(1), 19–31.

Housner, G. W. (1955). Properties of strong ground motion earthquakes. Bulletin of the Seismological Society of America, 45(3), 197–218.

Huang, H.-C. and Teng, T.-L. (1999). An evaluation on H/V ratio vs. spectral ratio for site-response estimation using the 1994 Northridge earthquake sequences. Pure and Applied Geophysics, 156(4), 631–649.

Idriss, I. M. (1978). Characteristics of earthquake ground motions. In Proceedings of the ASCE geotechnical engineering division speciality conference: earthquake engineering and soil dynamics (Vol. 3, pp. 1151–1265).

Idriss, I. M. (1991). Selection of Earthquake Ground Motions at Rock Sites. Report Prepared for the Structures Division, Building and Fire Research Laboratory, National Institute of Standards and Technology, Department of Civil Engineering, University of California, Davis.

Inan, E., Colakoglu, Z., Koc, N., Bayulke, N. and Coruh, E. (1996) 'Earthquake Catalogs with Acceleration Records from 1976 to 1996. General Directorate of Disaster Affairs, Earthquake Research Division, Ankara, Turkey, 98 pp'. Turkish.

Joyner, W. B. and Boore, D. M. (1996). Recent developments in strong-motion attenuation relationships. NIST SPECIAL PUBLICATION SP, 101–116.

Joyner, W. B. and Boore, D. M. (1988). Measurement, characterization, and prediction of strong ground motion. In Earthquake Engineering and Soil Dynamics II, Proceedings of American Society of Civil Engineers Geotechnical Engineering Division Specialty Conference, Park City, Utah (pp. 43–102).

Joyner, W. B. and Boore, D. M. (1981). Peak horizontal acceleration and velocity from strong-motion records including records from the 1979 Imperial Valley, California, earthquake. Bulletin of the Seismological Society of America, 71(6), 2011–2038.

Joyner, W., and T. Fumal (1985). Predictive mapping of ground motion in Evaluating Earthquake Hazards in the Los Angeles Region, Ziony (Editor), U.S. Geol. Surv. Prof. Pap. 1360, 203–220.

Kale, O., Akkar, S., Ansari, A. and Hamzehloo, H. (2015). A ground-motion predictive model for Iran and Turkey for horizontal PGA, PGV, and 5% damped response spectrum: Investigation of possible regional effects. Bulletin of the Seismological Society of America, 105(2A), 963–980.

Kalkan, E. and Gulkan, P. (2004). Site-dependent spectra derived from ground motion records in Turkey. Earthquake Spectra, 20(4), 1111–1138.

Kaklamanos, J., Baise, L. G., and Boore, D. M. (2011). Estimating unknown input parameters when implementing the NGA ground-motion prediction equations in engineering practice. *Earthquake Spectra*, *27*(4), 1219–1235.

Kamae, K., Irikura, K. and Pitarka, A. (1998). A technique for simulating strong ground motion using hybrid Green's function. Bulletin of the Seismological Society of America, 88(2), 357–367.

Karimzadeh, S., (2016). Use of Simulated Strong Ground Motion Records in Earthquake Engineering Applications. Middle East Technical University.

Karimzadeh, S. and Askan, A. (2018). Modeling of a historical earthquake in Erzincan, Turkey (Ms~ 7.8, in 1939) using regional seismological information obtained from a recent event. Acta Geophysica, 1–12.

Karimzadeh, S., Askan, A., Erberik, M. A. and Yakut, A. (2018). Seismic damage assessment based on regional synthetic ground motion dataset: a case study for Erzincan, Turkey. Natural Hazards, 1–27.

Karimzadeh, S., Askan, A., Yakut, A. and Ameri, G. (2017a). Assessment of alternative simulation techniques in nonlinear time history analyses of multi-story frame buildings: A case study. Soil Dynamics and Earthquake Engineering, 98, 38–53.

Karimzadeh, S., Askan, A. and Yakut, A. (2017b). Assessment of simulated ground motions in earthquake engineering practice: A case study for Duzce (Turkey). Pure and Applied Geophysics, 174(9), 3589–3607.

Karimzadeh, S., Kadas, K., Askan, A., Erberik, M. A. and Yakut, A. (2017c). A study on fragility analyses of masonry buildings in Erzincan (Turkey) utilizing simulated and real ground motion records. Procedia Engineering, 199, 188–193.

Kennett, B.L.N. (1983). Seismic wave propagation in a stratified half-space, Cambridge University Press, Cambridge.

Konca, A. O., Leprince, S., Avouac, J.-P. and Helmberger, D. V. (2010). Rupture process of the 1999 M w 7.1 Duzce earthquake from joint analysis of SPOT, GPS, InSAR, strong-motion, and teleseismic data: A supershear rupture with variable rupture velocity. Bulletin of the Seismological Society of America, 100(1), 267–288.

Kramer, S. L. (1996). Geotechnical Earthquake Engineering. Engineering (Vol. 6). Prentice Hall Upper Saddle River, NJ.

Krishnan, S., Ji, C., Komatitsch, D. and Tromp, J. (2006a). Case studies of damage to tall steel moment-frame buildings in southern California during large San Andreas earthquakes. Bulletin of the Seismological Society of America, 96(4A), 1523–1537.

Krishnan, S., Ji, C., Komatitsch, D. and Tromp, J. (2006b). Performance of two 18-story steel moment-frame buildings in southern California during two large simulated San Andreas earthquakes. Earthquake Spectra, 22(4), 1035–1061.

Lav, A., A. Erken, R. Iyisan and A. Ansal (1993). The Local Soil Conditions in Erzincan and Its Effects on Structural Damage, Proc. of XII. Technical Conference of Turkish Civil Engineering, Ankara, Turkey, 25-38, in Turkish.

Lay, T. and Wallace, T. C. (1995). Modern Global Seismology, Volume 58 (International Geophysics). Academic Press, San Diego.

Legrand, D. and Delouis, B. (1999). Determination of the fault plane using a single near-field seismic station with a finite-dimension source model. Geophysical Journal International, 138(3), 801–808.

Lermo, J. and Chávez-García, F. J. (1994). Are microtremors useful in site response evaluation? Bulletin of the Seismological Society of America, 84(5), 1350–1364.

Louie, J. N. (2001). Faster, better: shear-wave velocity to 100 meters depth from refraction microtremor arrays. Bulletin of the Seismological Society of America, 91(2), 347–364.

Mahood, M., Akbarzadeh, N. and Hamzehloo, H. (2014). Simulation of the first earthquake August 11, 2012 Ahar-Varzaghan using stochastic finite fault method.

Mai, P. M. and Beroza, G. C. (2003). A hybrid method for calculating near-source, broadband seismograms: Application to strong motion prediction. Physics of the Earth and Planetary Interiors, 137(1–4), 183–199.

Mai, P. M., Imperatori, W. and Olsen, K. B. (2010). Hybrid broadband ground-motion simulations: Combining long-period deterministic synthetics with high-frequency multiple S-to-S backscattering. Bulletin of the Seismological Society of America, 100(5A), 2124–2142.

Margaris, B. N. and Boore, D. M. (1998). Determination of Δσ and κ 0 from response spectra of large earthquakes in Greece. Bulletin of the Seismological Society of America, 88(1), 170–182.

McGuire, R. K. (1976). FORTRAN computer program for seismic risk analysis. US Geological Survey.

McGuire, R. K. (1977). Seismic design spectra and mapping procedures using hazard analysis based directly on oscillator response. Earthquake Engineering & Structural Dynamics. https://doi.org/10.1002/eqe.4290050302.

Milkereit, C., Zunbul, S., Karakisa, S., Iravul, Y., Zschau, J., Baumbach, M., … Kuru, T. (1999). Preliminary aftershock analysis of the Mw= 7.4 Izmit and Mw= 7.1 Duzce earthquake in western Turkey. The, 179–187.

Mohammadioun, B., & Serva, L. (2001). Stress drop, slip type, earthquake magnitude, and seismic hazard. *Bulletin of the Seismological Society of America*, *91*(4), 694–707.

Motazedian, D. (2006). Region-specific key seismic parameters for earthquakes in northern Iran. Bulletin of the Seismological Society of America, 96(4A), 1383–1395.

Motazedian, D. and Atkinson, G. M. (2005). Stochastic finite-fault modeling based on a dynamic corner frequency. Bulletin of the Seismological Society of America, 95(3), 995–1010.

Motazedian, D. and Moinfar, A. (2006). Hybrid stochastic finite fault modeling of 2003, M6. 5, Bam earthquake (Iran). Journal of Seismology, 10(1), 91–103.

Nakamura, Y. (1989). A method for dynamic characteristics estimation of subsurface using microtremor on the ground surface. QR Railway Tech. Res. Inst., 30(1), 25–33.

Ozbey, C., Sari, A., Manuel, L., Erdik, M. and Fahjan, Y. (2004). An empirical attenuation relationship for northwestern Turkey ground motion using a random effects approach. Soil Dynamics and Earthquake Engineering, 24(2), 115–125.

Ozlu, E., Karimzadeh, S., Askan, A. (2018). Broadband ground motion simulation within the city of Duzce (Turkey) and building response simulation. Eleventh U.S. National Conference on Earthquake Engineering, Integrating Science, Engineering & Policy, California.

Ozsarac, V., Karimzadeh, S., Erberik, M. A. and Askan, A. (2017). Energy-based response of simple structural systems by using simulated ground motions. Procedia Engineering, 199, 236–241.

Pacor, F., Cultrera, G., Mendez, A. and Cocco, M. (2005). Finite fault modeling of strong ground motions using a hybrid deterministic–stochastic approach. Bulletin of the Seismological Society of America, 95(1), 225–240.

Papageorgiou, A. S. and Aki, K. (1983). A specific barrier model for the quantitative description of inhomogeneous faulting and the prediction of strong ground motion. I. Description of the model. Bulletin of the Seismological Society of America, 73(3), 693–722.

Park, C. B., Miller, R. D. and Xia, J. (1999). Multichannel analysis of surface waves. Geophysics, 64(3), 800–808.

Pezeshk, S., Zandieh, A., and Tavakoli, B. (2011). Hybrid empirical ground-motion prediction equations for eastern North America using NGA models and updated seismological parameters. Bulletin of the Seismological Society of America, 101(4), 1859–1870.

Pitarka, A., Irikura, K., Iwata, T. and Sekiguchi, H. (1998). Three-dimensional simulation of the near-fault ground motion for the 1995 Hyogo-ken Nanbu (Kobe), Japan, earthquake. Bulletin of the Seismological Society of America, 88(2), 428–440.

Power, M., Chiou, B., Abrahamson, N., Bozorgnia, Y., Shantz, T. and Roblee, C. (2008). An overview of the NGA project. Earthquake Spectra, 24(1), 3–21.

Raghukanth, S. T. G. and Nadh Somala, S. (2009). Modeling of strong-motion data in northeastern India: Q, stress drop, and site amplification. Bulletin of the Seismological Society of America, 99(2A), 705–725.

Saragoni, G. R. and Hart, G. C. (1973). Simulation of artificial earthquakes. Earthquake Engineering & Structural Dynamics, 2(3), 249–267.

Romero, S. and Rix, G. J. (2001). Regional variations in near surface shear wave velocity in the Greater Memphis area. Engineering Geology, 62(1–3), 137–158.

Rosenblad, B. L. and Li, J. (2009). Comparative study of refraction microtremor (ReMi) and active source methods for developing low-frequency surface wave dispersion curves. Journal of Environmental and Engineering Geophysics, 14(3), 101–113.

Roumelioti, Z., Kiratzi, A. and Theodulidis, N. (2004). Stochastic strong ground-motion simulation of the 7 September 1999 Athens (Greece) earthquake. Bulletin of the Seismological Society of America, 94(3), 1036–1052.

Sanchez-Sesma, F. J. (1987). Site effects on strong ground motion. Soil Dynamics and Earthquake Engineering, 6(2), 124–132.

Sandikkaya, M. A., Akkar, S. and Bard, P. (2013). A nonlinear site-amplification model for the Next Pan-European ground-motion prediction equations. Bulletin of the Seismological Society of America, 103(1), 19–32.

Schmidt, R. (1986). Multiple emitter location and signal parameter estimation. IEEE Transactions on Antennas and Propagation, 34(3), 276–280.

Shahjouei, A. and Pezeshk, S. (2016). Alternative hybrid empirical ground-motion model for central and eastern North America using hybrid simulations and NGA-West2 models. Bulletin of the Seismological Society of America, 106(2), 734–754.

Sharma, M. L. and Harbindu, A. (2014) 'Ground Motion Prediction In Himalayas Using Observed and Simulated Datasets', in 10th US National Conference on Earthquake Engineering. Anchorage, Alaska.

Shoja-Taheri, J. and Ghofrani, H. (2007). Stochastic finite-fault modeling of strong ground motions from the 26 December 2003 Bam, Iran, earthquake. Bulletin of the Seismological Society of America, 97(6), 1950–1959.

Silva, W. J., Darragh, R. (1995). Engineering Characterization of Earthquake Strong Ground Motion Recorded at Rock Sites. Electric Power Research Institute, Palo Alto, California.

Silva, W. J. and Lee, K. (1987). State-of-the-Art for Assessing Earthquake Hazards in the United States. Report 24. WES RASCAL Code for Synthesizing Earthquake Ground Motions. WOODWARD-CLYDE CONSULTANTS WALNUT CREEK CA.

Sisman, F. N., Askan, A. and Asten, M. (2018). Evaluation of site response with alternative methods: a case study for engineering implications. Pure and Applied Geophysics, 175(1), 257–273.

Sørensen, M. B. and Lang, D. H. (2015). Incorporating simulated ground motion in seismic risk assessment: Application to the Lower Indian Himalayas. Earthquake Spectra, 31(1), 71–95.

Stokoe K., Wright S., Bay J.A., Roesset J. M. (1994) Characterization of geotechnical sites by SASW method, ISSMFE Technical Committee #10 for XIII ICSMFE, Geophysical characterization of sites. A. A. Balkema Publishers/Rotterdam & Brookfield, Netherlands. 15-25.

Strong Ground Motion Database of Turkey, http://kyhdata.deprem.gov.tr/2K/kyhdata_v4.php , (last visited on July 2018).

Sucuoglu, H., Anderson, J. G. and Zeng, Y. (2003). Predicting intensity and damage distribution during the 1995 Dinar, Turkey, earthquake with generated strong motion accelerograms. Bulletin of the Seismological Society of America, 93(3), 1267–1279.

Suzuki, T., Adachi, Y. and Tanaka, M. (1995). Application of microtremor measurements to the estimation of earthquake ground motions in Kushiro city during the Kushiro-Oki earthquake of 15 january 1993. Earthquake Engineering & Structural Dynamics, 24(4), 595–613.

Thomson, W. T. (1959). Spectral aspect of earthquakes. Bulletin of the Seismological Society of America, 49(1), 91–98.

Toro, G. R. and McGUIRE, R. K. (1987). An investigation into earthquake ground motion characteristics in eastern North America. Bulletin of the Seismological Society of America, 77(2), 468–489.

Trifunac, M. D. and Brady, A. G. (1975). On the correlation of peak acceleration of strong motion with earthquake magnitude, epicentral distance and site conditions. In Proceedings of the US national conference on earthquake engineering (pp. 43–52).

Trifunac, M. D. and Brady, A. G. (1976). Correlations of peak acceleration, velocity and displacement with earthquake magnitude, distance and site conditions. Earthquake Engineering & Structural Dynamics. https://doi.org/10.1002/eqe.4290040504.

Tsereteli, N., Askan, A., & Hamzehloo, H. (2016). Hybrid-empirical ground motion estimations for Georgia. Acta Geophysica, 64(5), 1225–1256.

Ugurhan, B. and Askan, A. (2010). Stochastic strong ground motion simulation of the 12 November 1999 Duzce (Turkey) earthquake using a dynamic corner frequency approach. Bulletin of the Seismological Society of America, 100(4), 1498–1512.

Ugurhan, B., Askan, A., Akinci, A. and Malagnini, L. (2012). Strong-ground-motion simulation of the 6 April 2009 L'Aquila, Italy, earthquake. Bulletin of the Seismological Society of America, 102(4), 1429–1445.

Ugurhan, B., Askan, A. and Erberik, M. A. (2011). A methodology for seismic loss estimation in urban regions based on ground-motion simulations. Bulletin of the Seismological Society of America, 101(2), 710–725.

Ulusay, R., Tuncay, E., Sonmez, H. and Gokceoglu, C. (2004). An attenuation relationship based on Turkish strong motion data and iso-acceleration map of Turkey. Engineering Geology, 74(3–4), 265–291.

Ulutas, E. and Ozer, M. F. (2010). Empirical attenuation relationship of peak ground acceleration for Eastern Marmara region in Turkey. Arabian Journal for Science and Engineering, 35(1), 187.

Umutlu, N., Koketsu, K. and Milkereit, C. (2004). The rupture process during the 1999 Duzce, Turkey, earthquake from joint inversion of teleseismic and strong-motion data. Tectonophysics, 391(1–4), 315–324.

Wells, D. L. and Coppersmith, K. J. (1994). New empirical relationships among magnitude, rupture length, rupture width, rupture area, and surface displacement. *Bulletin of the Seismological Society of America*, *84*(4), 974–1002.

Yalcinkaya E. Stochastic finite-fault modeling of ground motions from the June 27, 1998 Adana-Ceyhan earthquake. Earth Planets Sp. 2005; 57(2): 107-115.

Yenier, E. and Atkinson, G. M. (2015). Regionally adjustable generic ground-motion prediction equation based on equivalent point-source simulations: Application to central and eastern North America. Bulletin of the Seismological Society of America, 105(4), 1989–2009.

Zengin, E. and Cakti, E. (2014). Ground motion simulations for the 23 October 2011 Van, Eastern Turkey earthquake using stochastic finite fault approach. Bulletin of Earthquake Engineering, 12(2), 627–646.

Zhang, L., Li, S. and Lyu, Y. (2018). The ground motion simulation of Kangding Mw6. 0, 2014 by the stochastic finite-fault model. In IOP Conference Series: Earth and Environmental Science (Vol. 108, p. 32044). IOP Publishing.

Zhao, Z., Zhao, Z., Xu, J., Kubota, R. and Liu, L. (2007). Strong ground motion simulation for seismic hazard assessment in an urban area. Journal of Geophysics and Engineering, 4(3), 308.

APPENDICES

APPENDIX A

ENTIRE LIST OF THE REGRESSION COEFFICIENTS OF THE PROPOSED MODEL

The whole list of the regression coefficients of the predictive model provided in Chapter 4 is presented in this appendix.

Table A.1. *Period-Dependent f_{site} Coefficients (Kale et al., 2015)*

Period (s)	sb1	sb2
0	-0.41997	-0.28846
-1	-0.72057	-0.19688
0.01	-0.41729	-0.28685
0.02	-0.39998	-0.28241
0.03	-0.34799	-0.26842
0.04	-0.27572	-0.24759
0.05	-0.21231	-0.22385
0.075	-0.13909	-0.17798
0.1	-0.26492	-0.28832
0.11	-0.31346	-0.31798
0.12	-0.36002	-0.34246
0.13	-0.40424	-0.36297
0.14	-0.44592	-0.38036
0.15	-0.48496	-0.39525
0.16	-0.52137	-0.40811
0.17	-0.5552	-0.4193
0.18	-0.58656	-0.42911
0.19	-0.61558	-0.43774
0.2	-0.64239	-0.44574
0.22	-0.69002	-0.45499
0.24	-0.73062	-0.45939
0.26	-0.7653	-0.45988
0.28	-0.79499	-0.45739
0.3	-0.82052	-0.45287
0.32	-0.84256	-0.44255
0.34	-0.86167	-0.43399
0.36	-0.87832	-0.42592
0.38	-0.89288	-0.41829
0.4	-0.90568	-0.41105
0.42	-0.91697	-0.40417
0.44	-0.92698	-0.3976
0.46	-0.93589	-0.39133

Period (s)	sb1	sb2
0.48	-0.94384	-0.38532
0.5	-0.95097	-0.37956
0.55	-0.96584	-0.3661
0.6	-0.97746	-0.35382
0.65	-0.9867	-0.34252
0.7	-0.99416	-0.33206
0.75	-1.00027	-0.32233
0.8	-1.00532	-0.31322
0.85	-1.00956	-0.30466
0.9	-1.01314	-0.29659
0.95	-1.01619	-0.28896
1	-1.01881	-0.28172
1.1	-1.0172	-0.26827
1.2	-1.00204	-0.25599
1.3	-0.9881	-0.24469
1.4	-0.97519	-0.23423
1.5	-0.96317	-0.22449
1.6	-0.95193	-0.21538
1.7	-0.94136	-0.20682
1.8	-0.93141	-0.19876
1.9	-0.92199	-0.19112
2	-0.91305	-0.18388
2.2	-0.89645	-0.17043
2.4	-0.88129	-0.15815
2.6	-0.86735	-0.14685
2.8	-0.85444	-0.13639
3	-0.84242	-0.12665
3.2	-0.83118	-0.11754
3.4	-0.82062	-0.10899
3.6	-0.81066	-0.10092
3.8	-0.80124	-0.09329
4	-0.79231	-0.08605

Table A.2. *Period-Dependent Regression Coefficients*

Period	b1	b3	b4
0	1.49363	-0.12517	-1.04879
-1	5.51025	-0.17197	-0.90738
0.01	1.49637	-0.12499	-1.04859
0.02	1.52215	-0.12434	-1.04919
0.03	1.59512	-0.12239	-1.05013
0.04	1.73669	-0.11978	-1.05452
0.05	1.86901	-0.11629	-1.04998
0.075	2.16294	-0.1137	-1.04991
0.1	2.34622	-0.12448	-1.05259
0.11	2.3719	-0.12613	-1.05459
0.12	2.4008	-0.12996	-1.05696
0.13	2.41361	-0.13302	-1.05689
0.14	2.41346	-0.13551	-1.05623
0.15	2.40726	-0.13758	-1.05484
0.16	2.39825	-0.13934	-1.05476
0.17	2.39488	-0.14085	-1.05791
0.18	2.37648	-0.14217	-1.05834
0.19	2.34986	-0.14333	-1.05653
0.2	2.32386	-0.14437	-1.0544
0.22	2.27774	-0.14617	-1.05373
0.24	2.20887	-0.1477	-1.04668
0.26	2.14376	-0.14903	-1.04006
0.28	2.083	-0.15022	-1.03381
0.3	2.02111	-0.15131	-1.0279
0.32	1.95449	-0.15232	-1.02229
0.34	1.89149	-0.15326	-1.01696
0.36	1.83297	-0.15416	-1.01187
0.38	1.77221	-0.15502	-1.00702
0.4	1.71654	-0.15584	-1.00237
0.42	1.66577	-0.15665	-0.99792
0.44	1.61535	-0.15743	-0.99365
0.46	1.56523	-0.1582	-0.98954

Table A.2. *Cont'd.*

Period	b1	b3	b4
0.48	1.51699	-0.15895	-0.98559
0.5	1.47234	-0.15969	-0.98178
0.55	1.36207	-0.16149	-0.97284
0.6	1.25863	-0.16326	-0.96463
0.65	1.16626	-0.16499	-0.95703
0.7	1.07954	-0.1667	-0.94999
0.75	0.99388	-0.16839	-0.94342
0.8	0.9146	-0.17007	-0.93728
0.85	0.83966	-0.17174	-0.93152
0.9	0.7674	-0.1734	-0.92609
0.95	0.69605	-0.17505	-0.92098
1	0.62856	-0.1767	-0.91614
1.1	0.50535	-0.17999	-0.90719
1.2	0.39819	-0.18327	-0.8991
1.3	0.29849	-0.18654	-0.89173
1.4	0.20471	-0.18981	-0.88497
1.5	0.11612	-0.19307	-0.87875
1.6	0.03457	-0.19633	-0.87299
1.7	-0.03913	-0.19959	-0.86764
1.8	-0.10832	-0.20284	-0.86266
1.9	-0.17504	-0.20609	-0.858
2	-0.23544	-0.20934	-0.85363
2.2	-0.34621	-0.21584	-0.84565
2.4	-0.44879	-0.22234	-0.83852
2.6	-0.54311	-0.22883	-0.83212
2.8	-0.63161	-0.23533	-0.82631
3	-0.7105	-0.24182	-0.82103
3.2	-0.78125	-0.24831	-0.81618
3.4	-0.84691	-0.2548	-0.81173
3.6	-0.90854	-0.26129	-0.80761
3.8	-0.96598	-0.26778	-0.80378
4	-1.02045	-0.27427	-0.80023

Table A.3. *Period-Dependent Standard Deviation Values*

Period (s)	ϕ	τ
0	0.2937	0.2935
-1	0.311	0.3108
0.01	0.2935	0.2933
0.02	0.2931	0.2929
0.03	0.291	0.2907
0.04	0.2887	0.2885
0.05	0.289	0.2888
0.075	0.2948	0.2946
0.1	0.3037	0.3035
0.11	0.3053	0.305
0.12	0.3118	0.3116
0.13	0.3164	0.3162
0.14	0.3192	0.319
0.15	0.3214	0.3211
0.16	0.3252	0.325
0.17	0.3279	0.3276
0.18	0.3317	0.3314
0.19	0.333	0.3327
0.2	0.3341	0.3338
0.22	0.3331	0.3328
0.24	0.3406	0.3404
0.26	0.348	0.3478
0.28	0.3516	0.3513
0.3	0.3487	0.3484
0.32	0.3464	0.3461
0.34	0.3489	0.3486
0.36	0.3501	0.3499
0.38	0.3534	0.3531
0.4	0.3553	0.355
0.42	0.3573	0.357
0.44	0.3591	0.3589
0.46	0.361	0.3607

Period (s)	ϕ	τ
0.48	0.362	0.3617
0.5	0.363	0.3628
0.55	0.3673	0.367
0.6	0.3692	0.3689
0.65	0.3722	0.3719
0.7	0.3749	0.3746
0.75	0.3786	0.3783
0.8	0.3817	0.3814
0.85	0.3846	0.3843
0.9	0.3873	0.387
0.95	0.3896	0.3893
1	0.3917	0.3914
1.1	0.3977	0.3974
1.2	0.4019	0.4016
1.3	0.4038	0.4035
1.4	0.4069	0.4018
1.5	0.4096	0.3952
1.6	0.4121	0.3868
1.7	0.4152	0.3786
1.8	0.4175	0.3705
1.9	0.4204	0.3641
2	0.4219	0.3569
2.2	0.4241	0.3419
2.4	0.4277	0.3269
2.6	0.4337	0.3142
2.8	0.4411	0.304
3	0.4469	0.2967
3.2	0.4505	0.2882
3.4	0.4544	0.2817
3.6	0.4577	0.2732
3.8	0.4616	0.2644
4	0.4651	0.2561

APPENDIX B

ADDITIONAL COMPARISON FIGURES

This appendix presents additional median ground motion comparison plots between proposed ground motion model and Akkar et al. (2014), Kale et al. (2015) predictive models and NGA-West2 GMPEs (Abrahamson et al., 2014; Boore et al., 2014; Campbell and Bozorgnia, 2014; Chiou and Youngs, 2014).

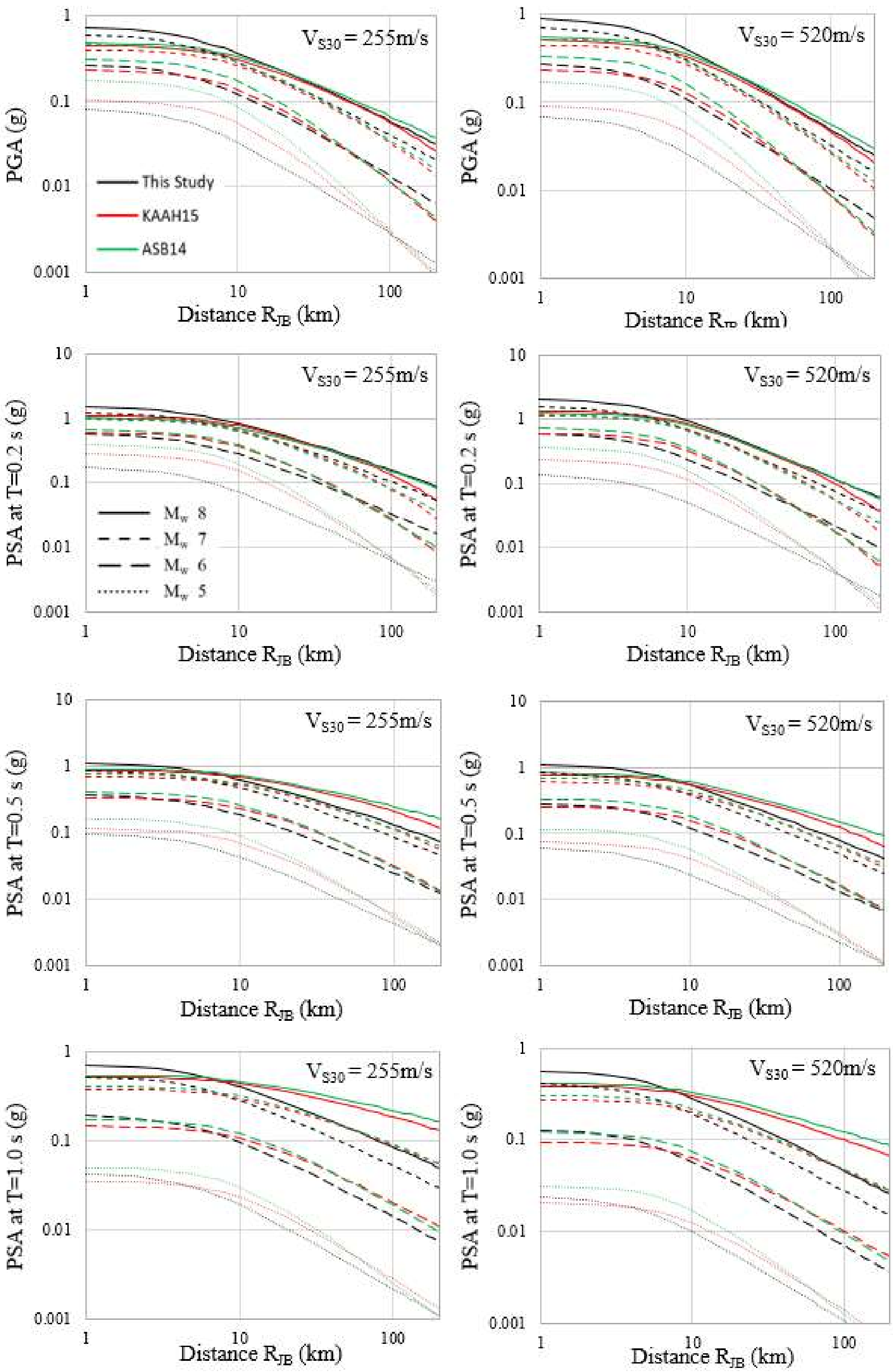

Figure B.1. Distance scaling comparisons between previous Turkish and European GMPEs and the proposed model at different spectral ordinates (PGA, PSA at T = 0.2s, 0.5s and 1s) for magnitudes M_w 5, 6, 7 and 8. The comparisons are done for sites with V_{S30} = 255 and 520 m/s.

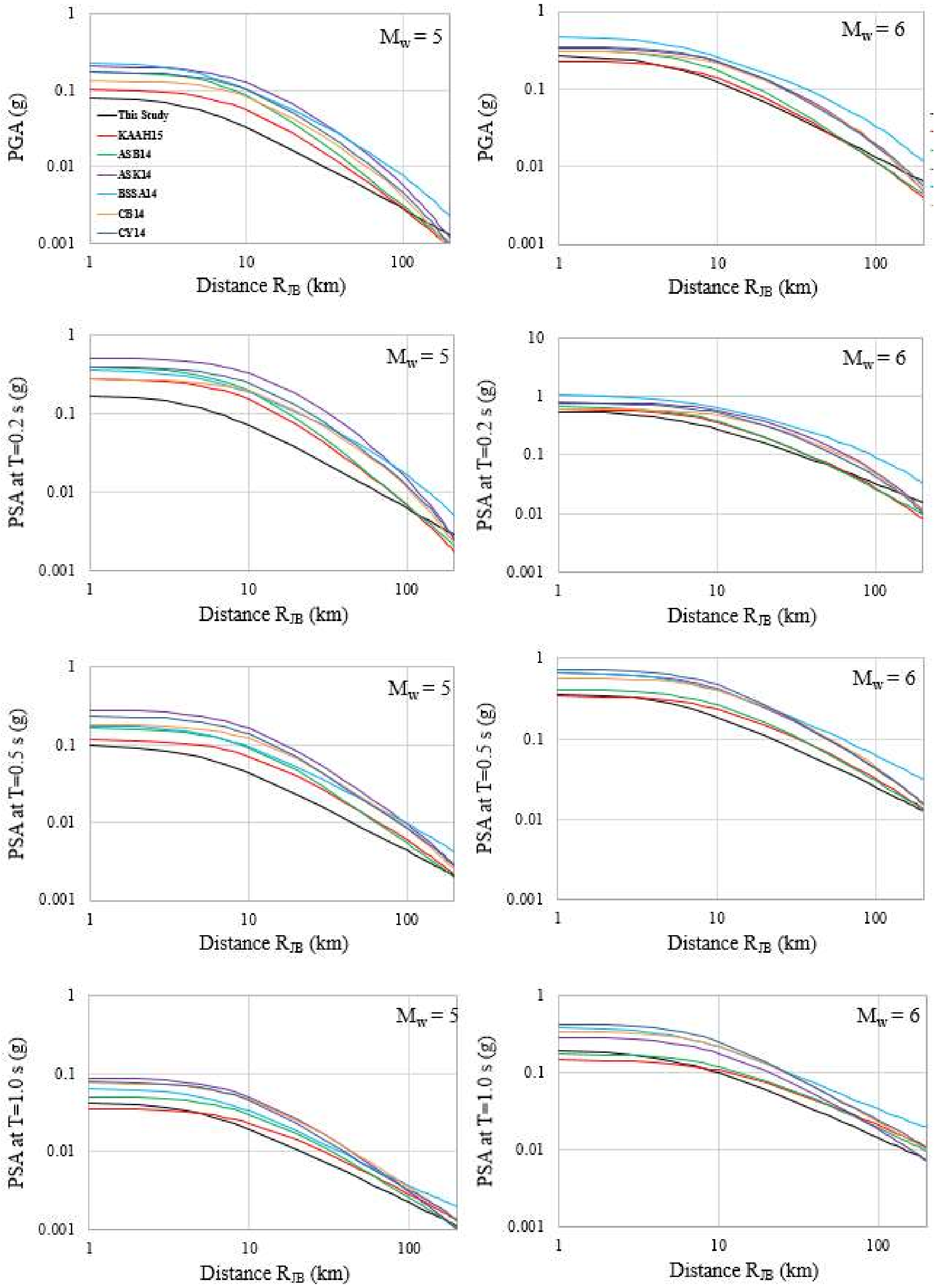

Figure B.2. Distance scaling comparisons between previous Turkish, European and NGA-West2 GMPEs and the proposed model at different spectral ordinates (PGA, PSA at T = 0.2s, 0.5s and 1s) for a soil site, V_{S30} = 255 m/s. The comparisons are done for M_w 5 and 6.

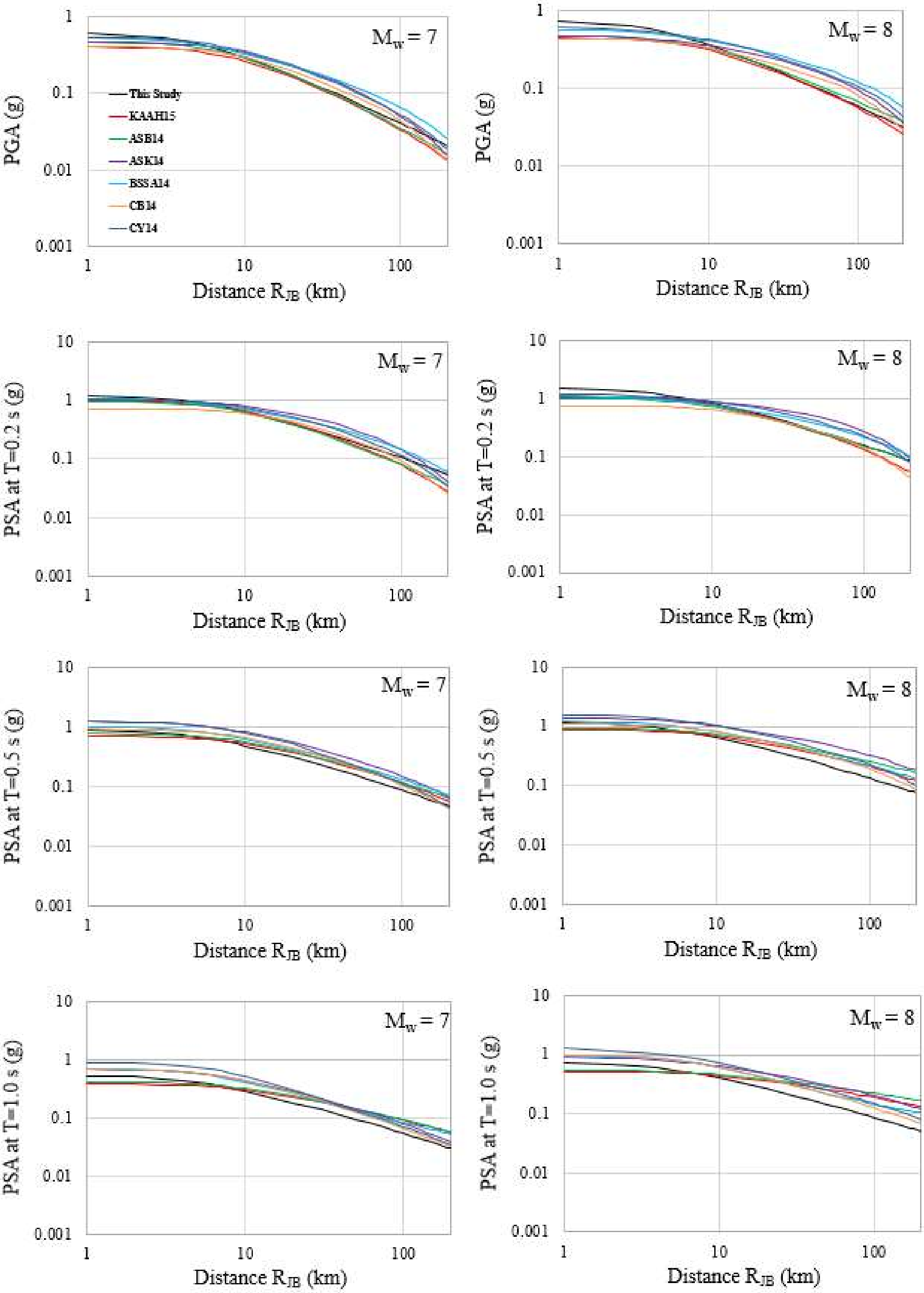

Figure B.3. Distance scaling comparisons between previous Turkish, European and NGA-West2 GMPEs and the proposed model at different spectral ordinates (PGA, PSA at T = 0.2s, 0.5s and 1s) for a soil site, V_{S30} = 255 m/s. The comparisons are done for M_w 7 and 8.

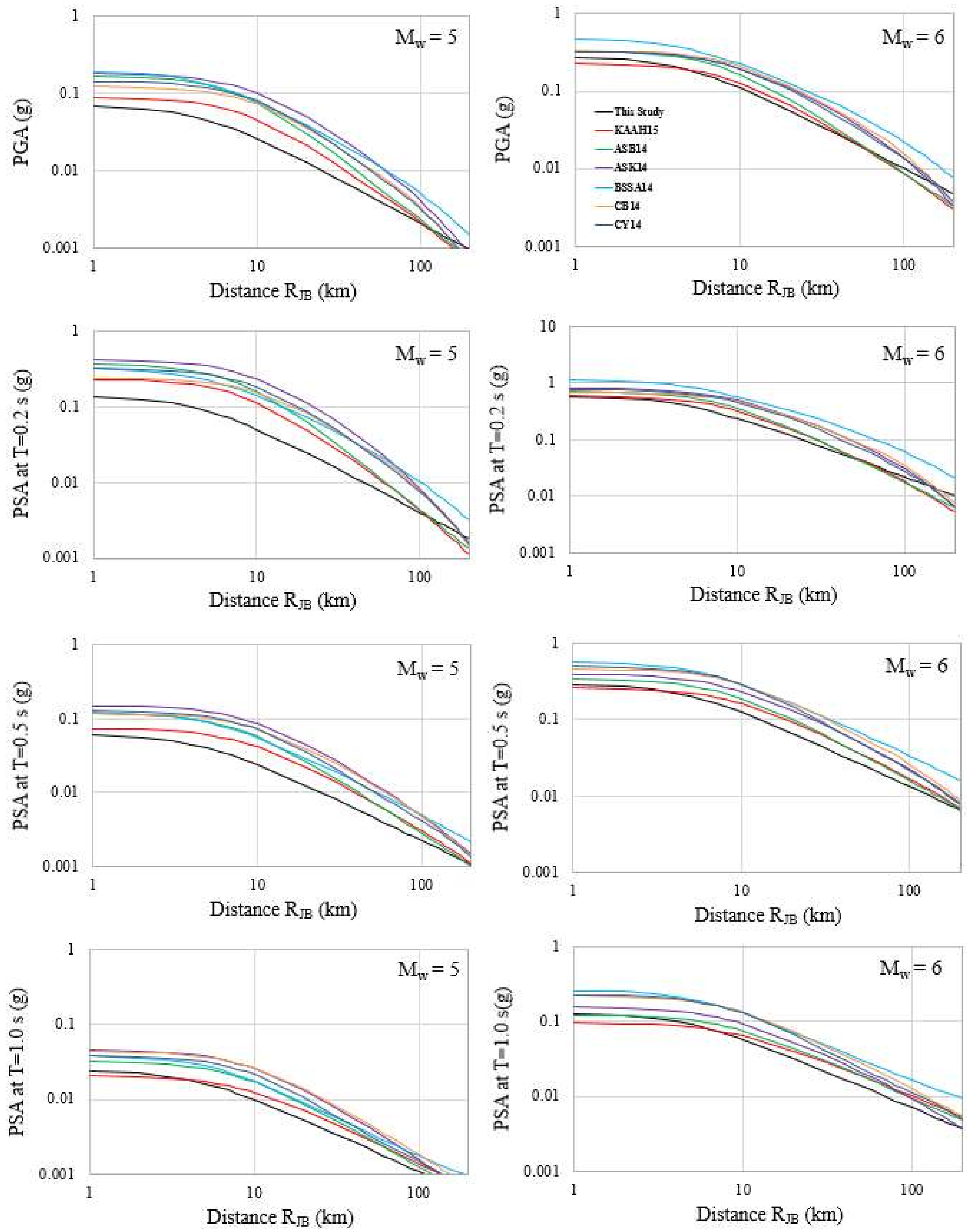

Figure B.4. Distance scaling comparisons between previous Turkish, European and NGA-West2 GMPEs and the proposed model at different spectral ordinates (PGA, PSA at T = 0.2s, 0.5s and 1s) for V_{S30} = 520 m/s. The comparisons are done for M_w 5 and 6.

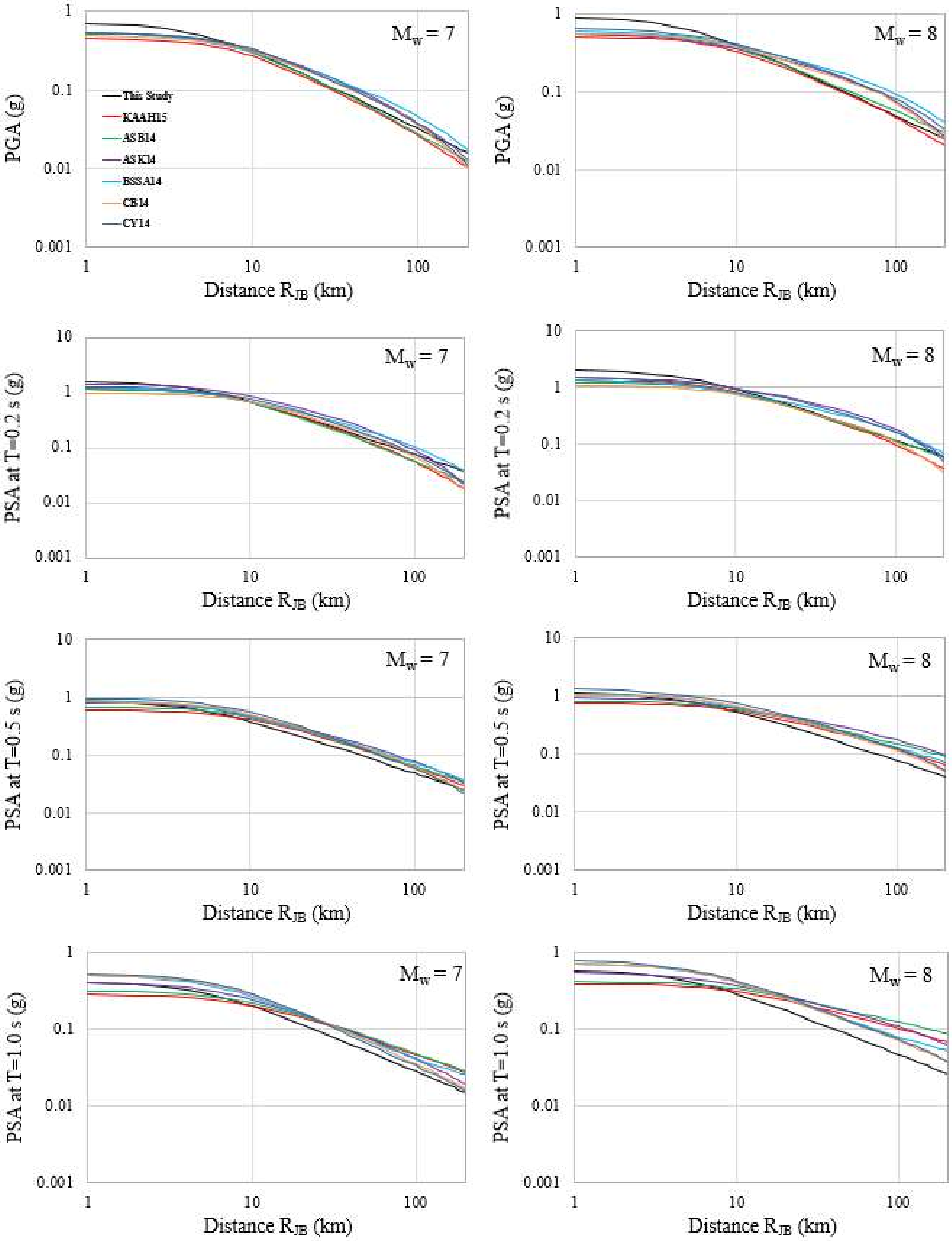

Figure B.5. Distance scaling comparisons between previous Turkish, European and NGA-West2 GMPEs and the proposed model at different spectral ordinates (PGA, PSA at T = 0.2s, 0.5s and 1s) for VS_{30} = 520 m/s. The comparisons are done for M_w 7 and 8.

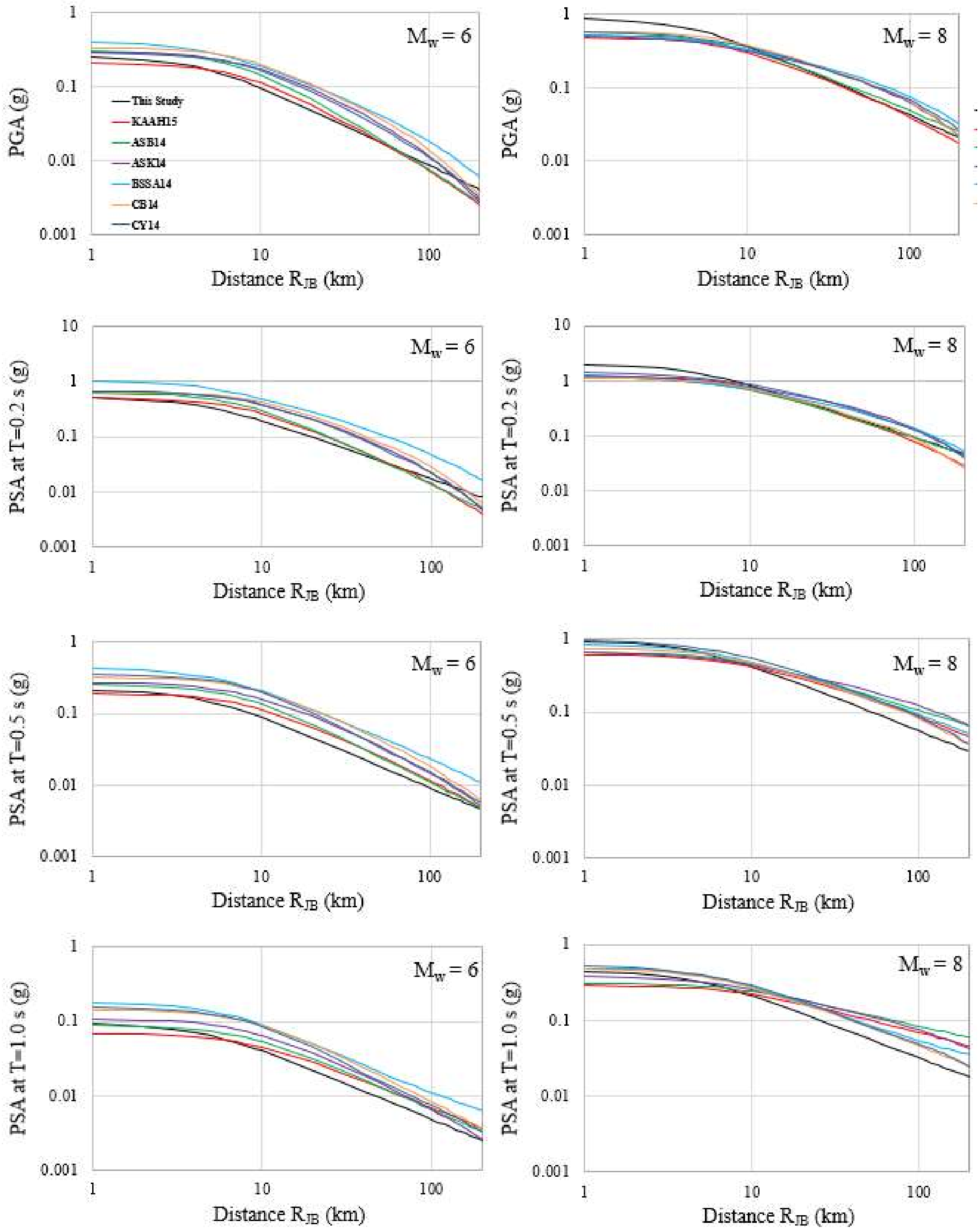

Figure B.6. Distance scaling comparisons between two previous Turkish, European and NGA-West2 GMPEs and the proposed model at different spectral ordinates (PGA, PSA at T = 0.2s, 0.5s and 1s) for V_{S30} = 760 m/s. The comparisons are done for M_w 6 and 8.

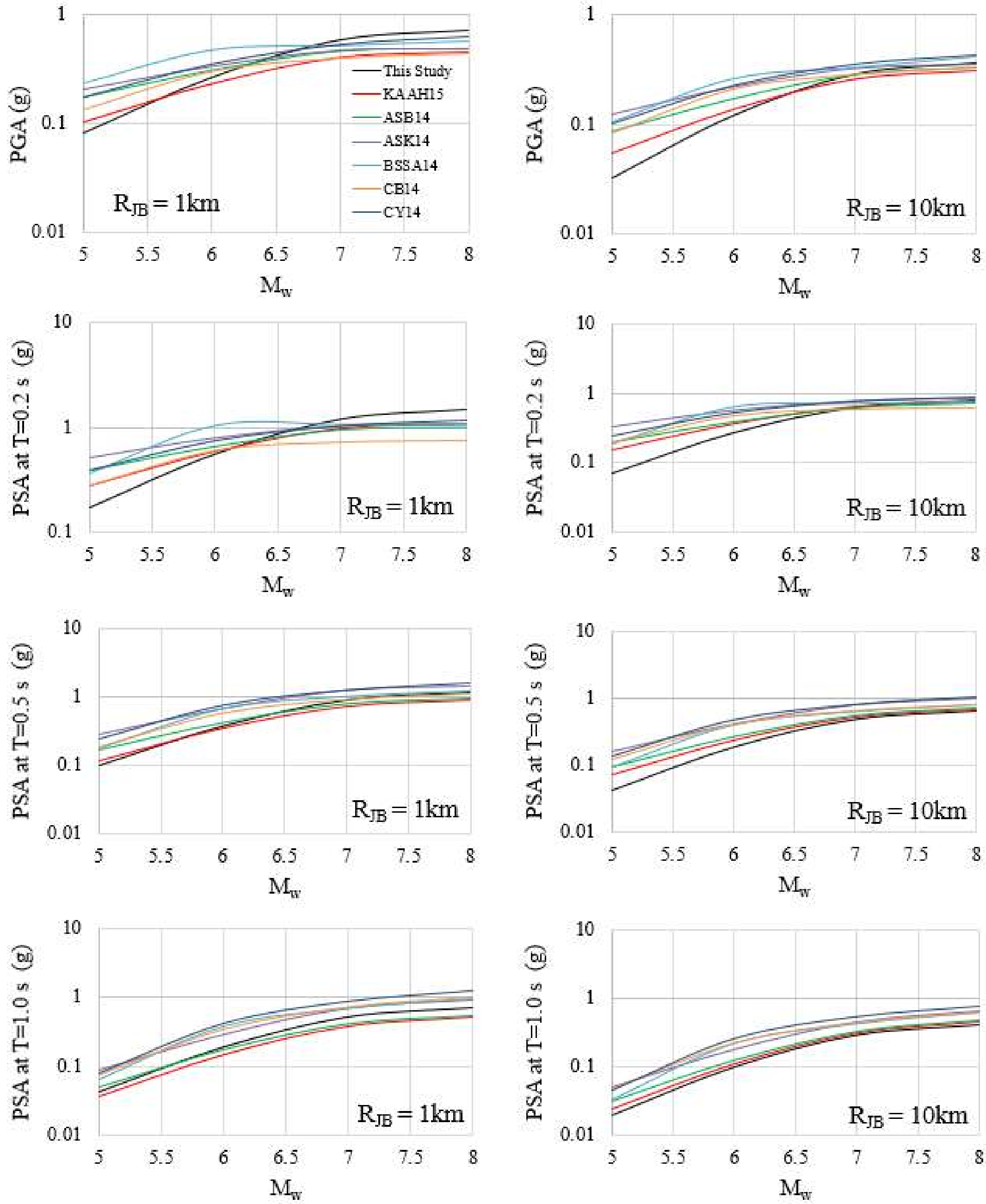

Figure B.7. Magnitude scaling comparisons of the proposed model with local, regional and global GMPEs at different spectral ordinates (PGA, PSA at T = 0.2s, 0.5s and 1s). The comparisons are done for a soil site, V_{S30} = 255 m/s at a distance of R_{JB} = 1 and 10 km from a strike slip fault.

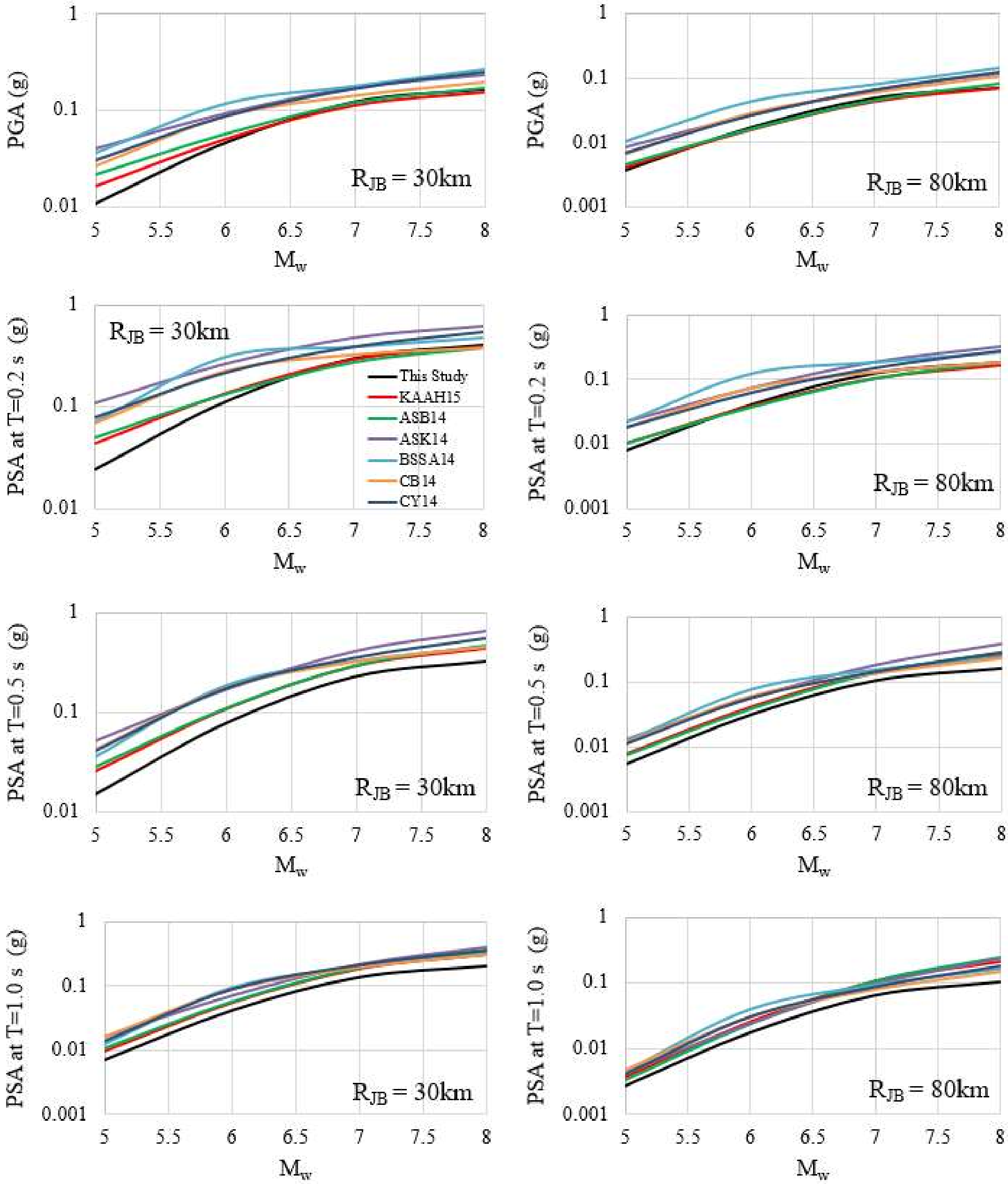

Figure B.8. Magnitude scaling comparisons of the proposed model with local, regional and global GMPEs at different spectral ordinates (PGA, PSA at T = 0.2s, 0.5s and 1s). The comparisons are done for a soil site, V_{S30} = 255 m/s at a distance of R_{JB} = 30 and 80 km from a strike slip fault.

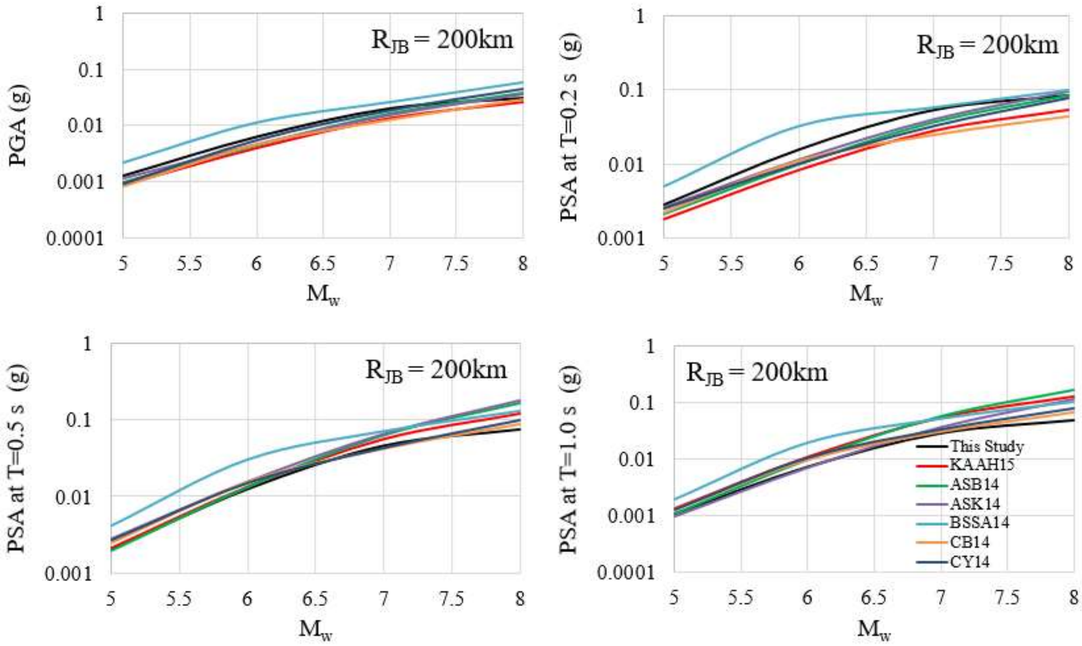

Figure B.9. Magnitude scaling comparisons of the proposed model with local, regional and global GMPEs at different spectral ordinates (PGA, PSA at T = 0.2s, 0.5s and 1s). The comparisons are done for a soil site, V_{S30} = 255 m/s at a distance of R_{JB} = 200 km from a strike slip fault.

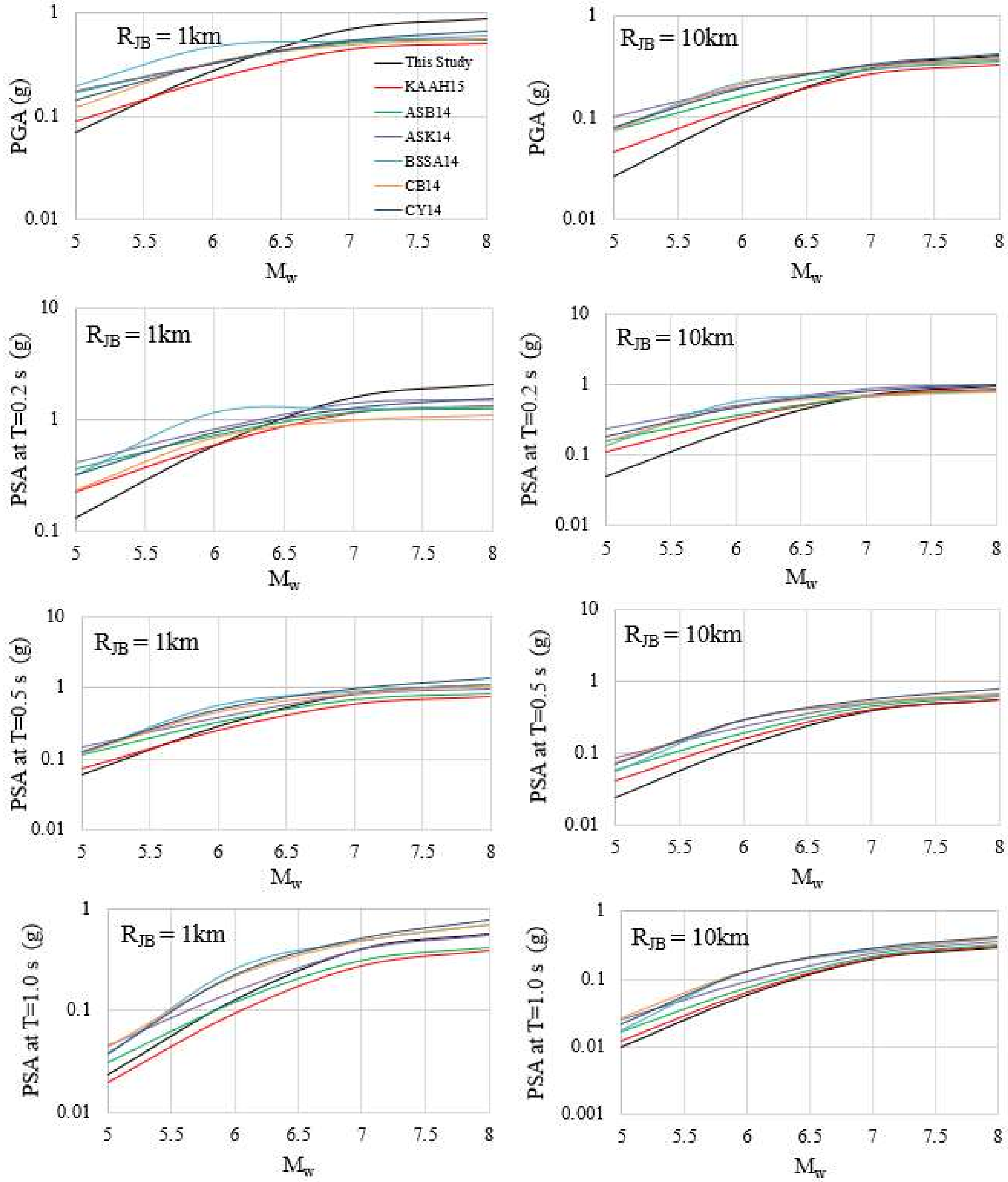

Figure B.10. Magnitude scaling comparisons of the proposed model with local, regional and global GMPEs at different spectral ordinates (PGA, PSA at T = 0.2s, 0.5s and 1s). The comparisons are done for V_{S30} = 520 m/s at a distance of R_{JB} = 1 and 10 km from a strike slip fault.

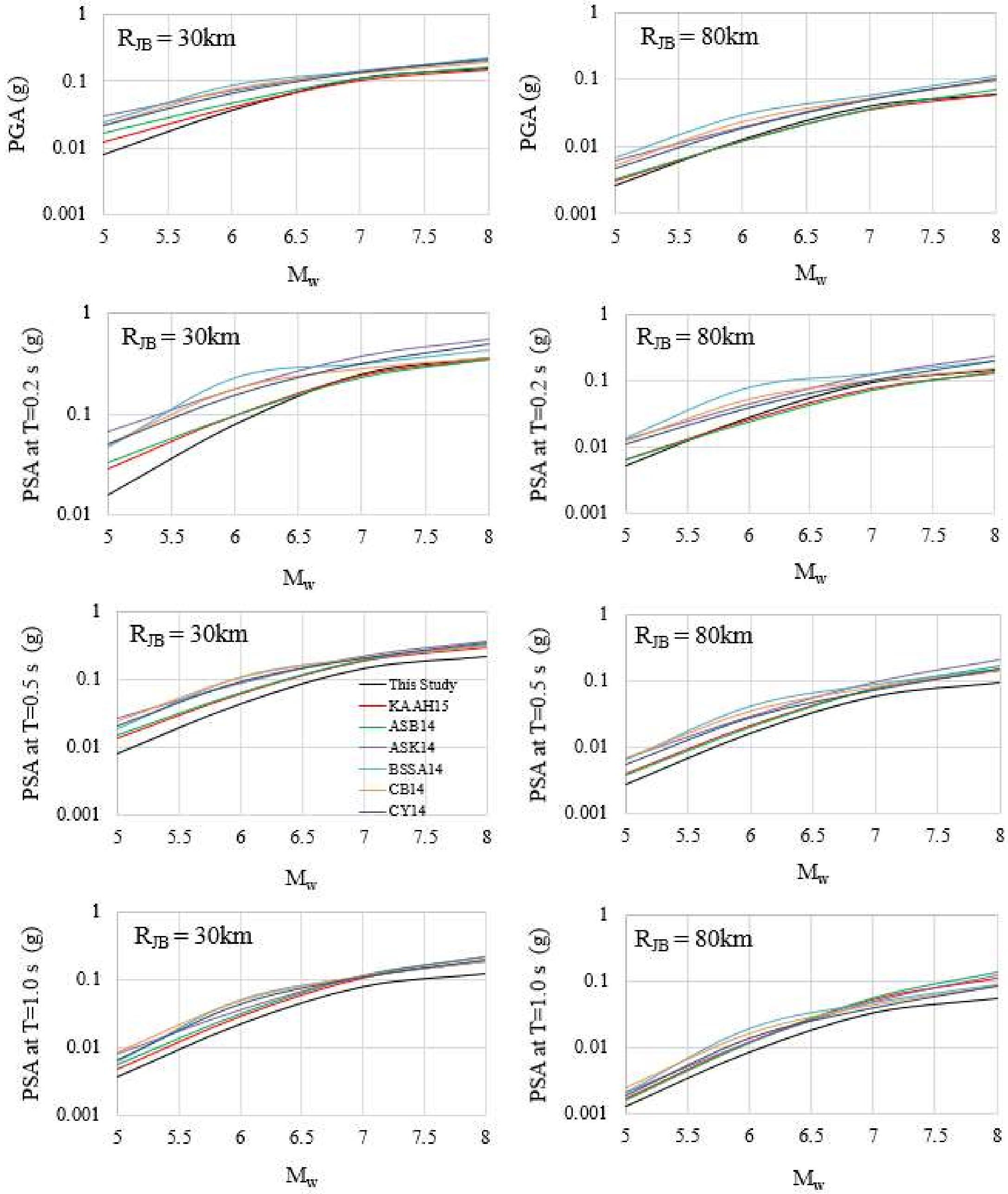

Figure B.11. Magnitude scaling comparisons of the proposed model with local, regional and global GMPEs at different spectral ordinates (PGA, PSA at T = 0.2s, 0.5s and 1s). The comparisons are done for V_{S30} = 520 m/s at a distance of R_{JB} = 30 and 80 km from a strike slip fault.

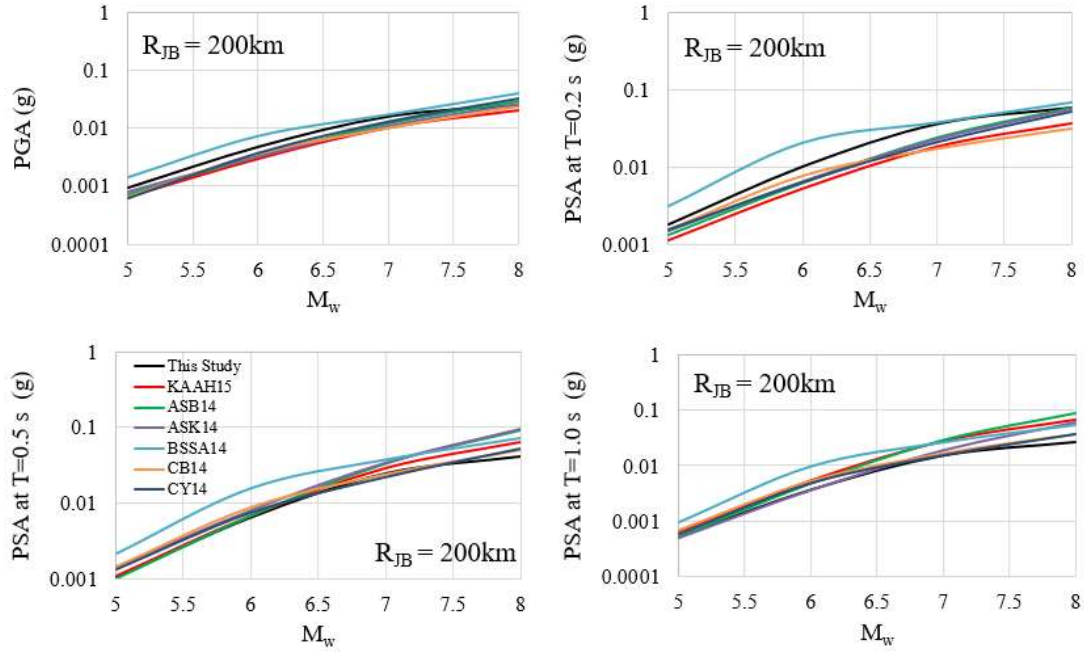

Figure B.12. Magnitude scaling comparisons of the proposed model with local, regional and global GMPEs at different spectral ordinates (PGA, PSA at T = 0.2s, 0.5s and 1s). The comparisons are done for V_{S30} = 520 m/s at a distance of R_{JB} = 200 km from a strike slip fault.

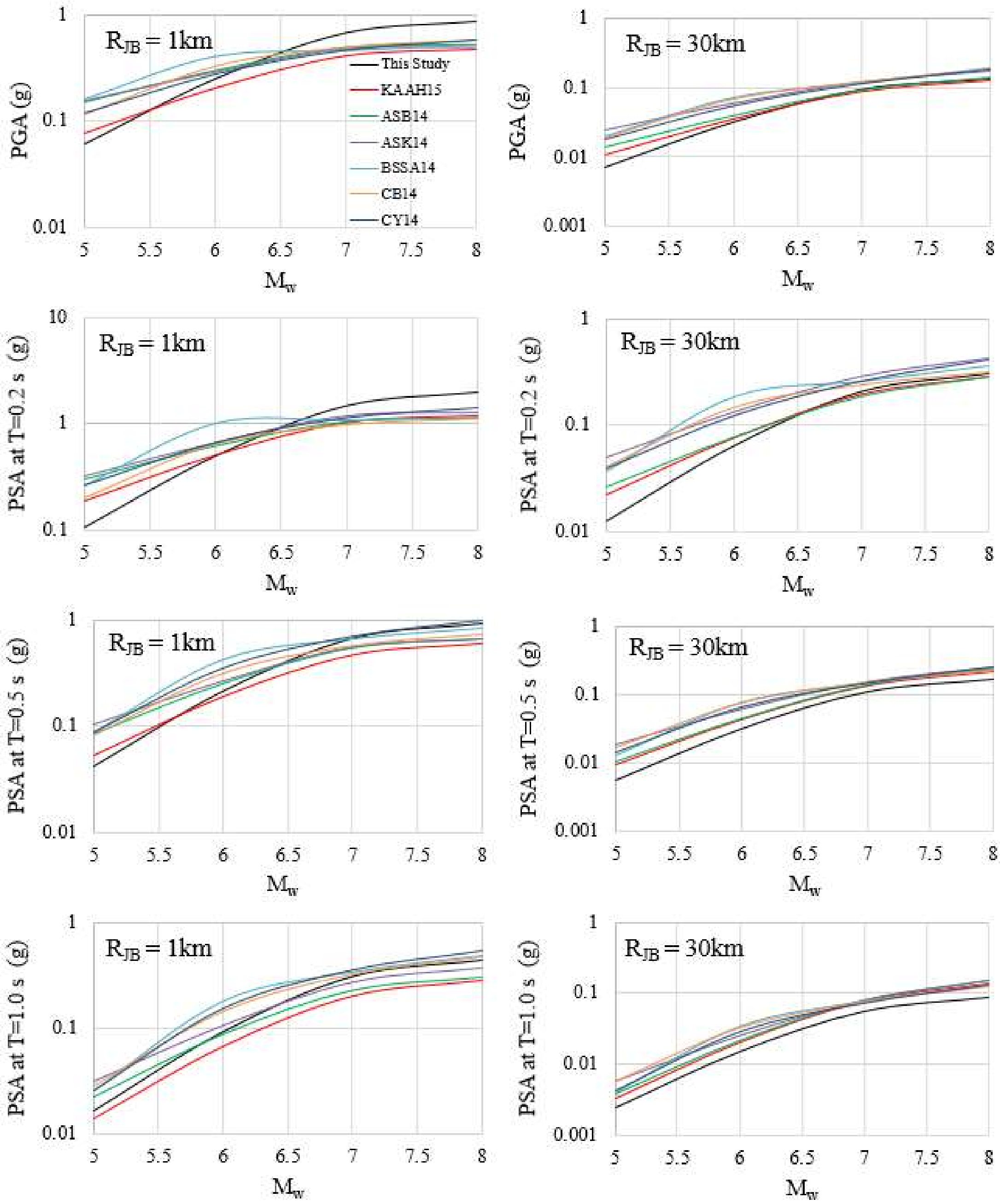

Figure B.13. Magnitude scaling comparisons of the proposed model with local, regional and global GMPEs at different spectral ordinates (PGA, PSA at T = 0.2s, 0.5s and 1s). The comparisons are done for V_{S30} = 760 m/s at a distance of R_{JB} = 1 and 30 km from a strike slip fault.

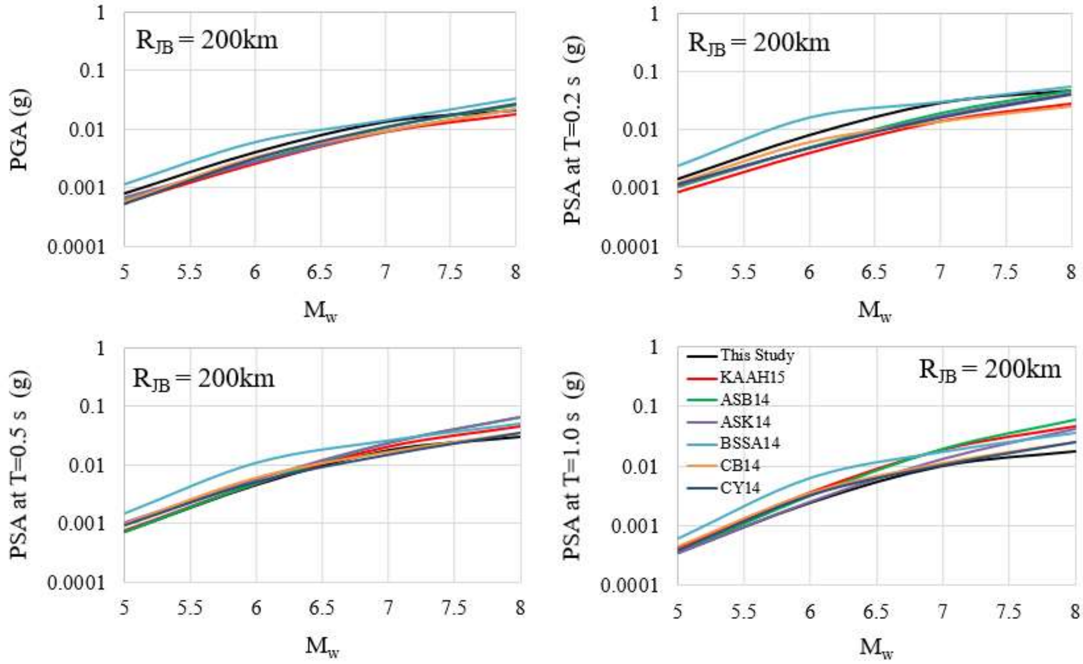

Figure B.14. Magnitude scaling comparisons of the proposed model with local, regional and global GMPEs at different spectral ordinates (PGA, PSA at T = 0.2s, 0.5s and 1s). The comparisons are done for V_{S30} = 760 m/s at a distance of R_{JB} = 200 km from a strike slip fault.

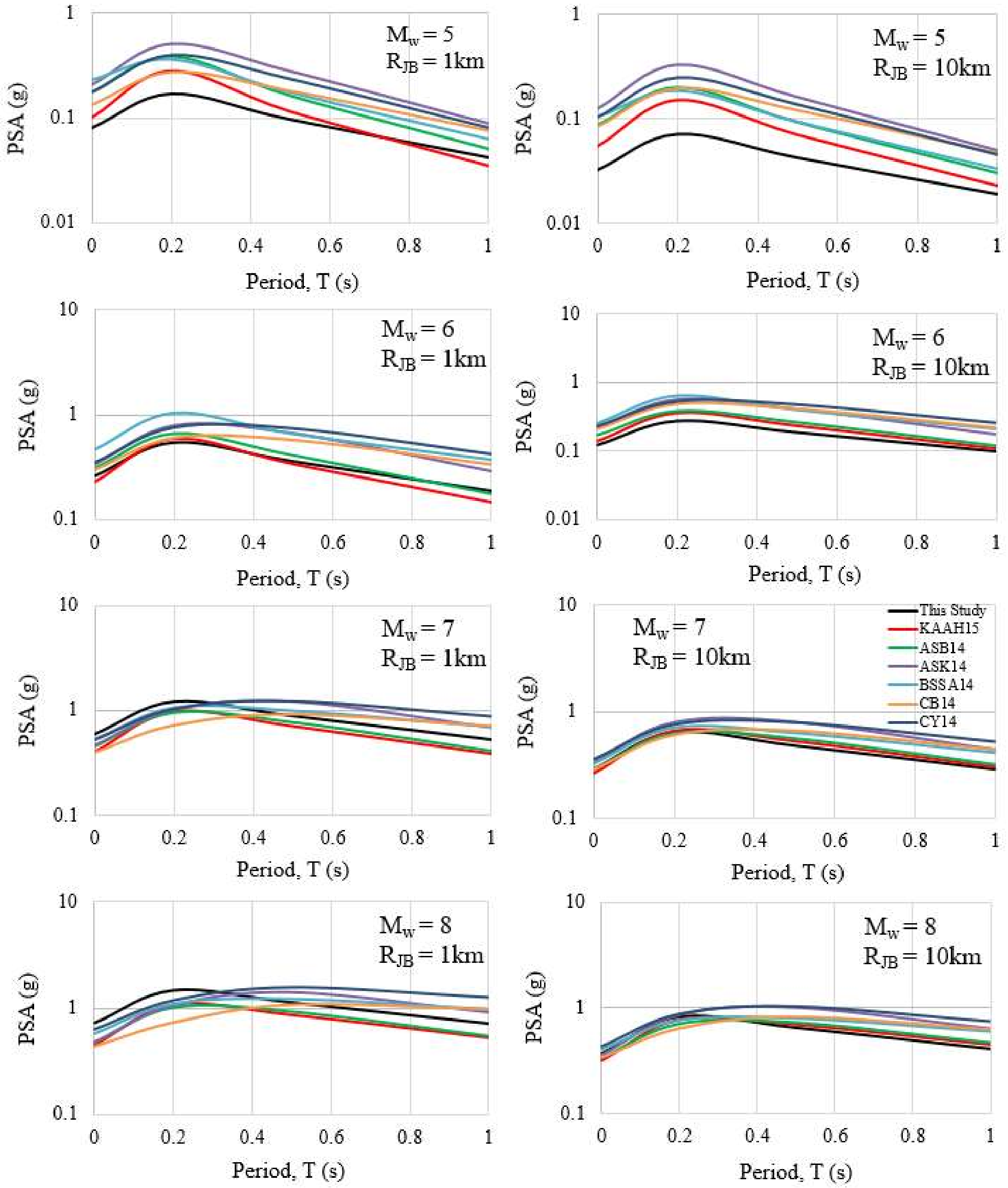

Figure B.15. Comparisons of spectral ordinates from the new model and local, regional and global GMPEs. The comparisons are done for a soil site, V_{S30} = 255 m/s at a distance of R_{JB} = 1 and 10 km from a strike slip fault for magnitudes M_w 5, 6, 7 and 8.

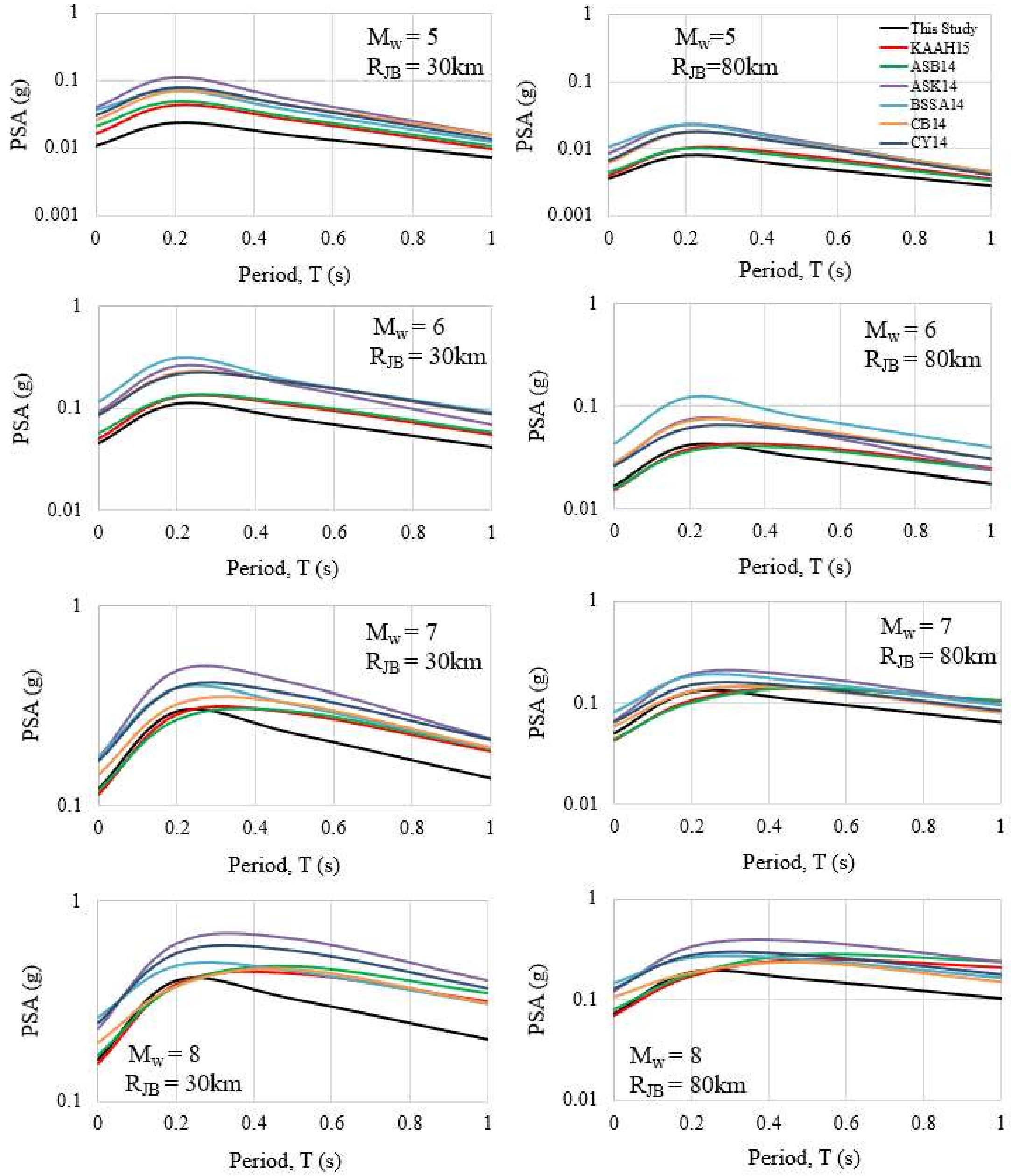

Figure B.16. Comparisons of spectral ordinates from the new model and local, regional and global GMPEs. The comparisons are done for a soil site, V_{S30} = 255 m/s at a distance of R_{JB} = 30 and 80 km from a strike slip fault for magnitudes M_w 5, 6, 7 and 8.

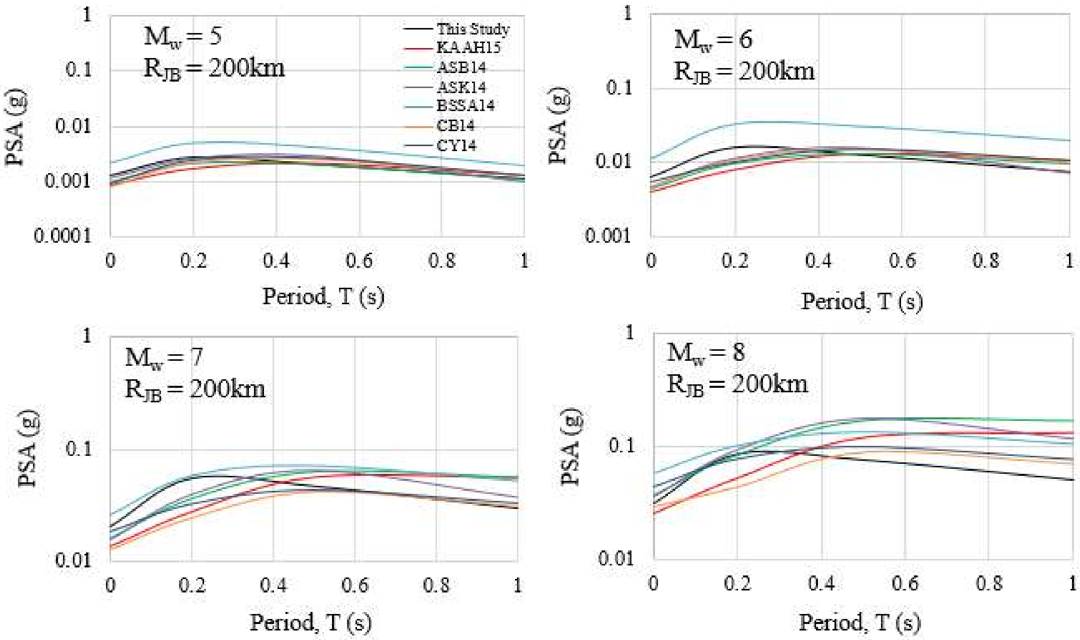

Figure B.17. Comparisons of spectral ordinates from the new model and local, regional and global GMPEs. The comparisons are done for a soil site, V_{S30} = 255 m/s at a distance of R_{JB} = 200 km from a strike slip fault for magnitudes M_w 5, 6, 7 and 8.

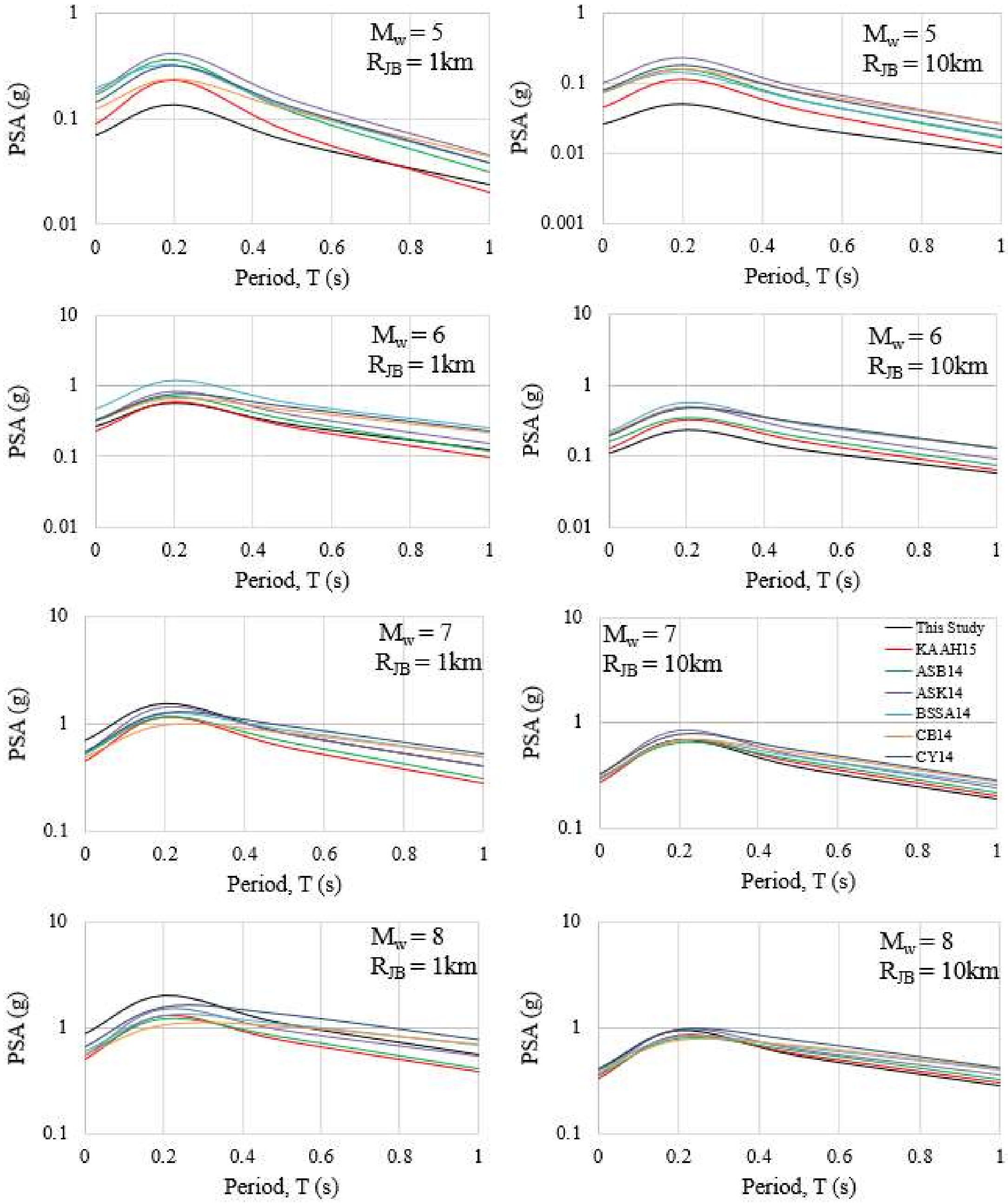

Figure B.18. Comparisons of spectral ordinates from the new model and local, regional and global GMPEs. The comparisons are done for V_{S30} = 520 m/s at a distance of R_{JB} = 1 and 10 km from a strike slip fault for magnitudes M_w 5, 6, 7 and 8.

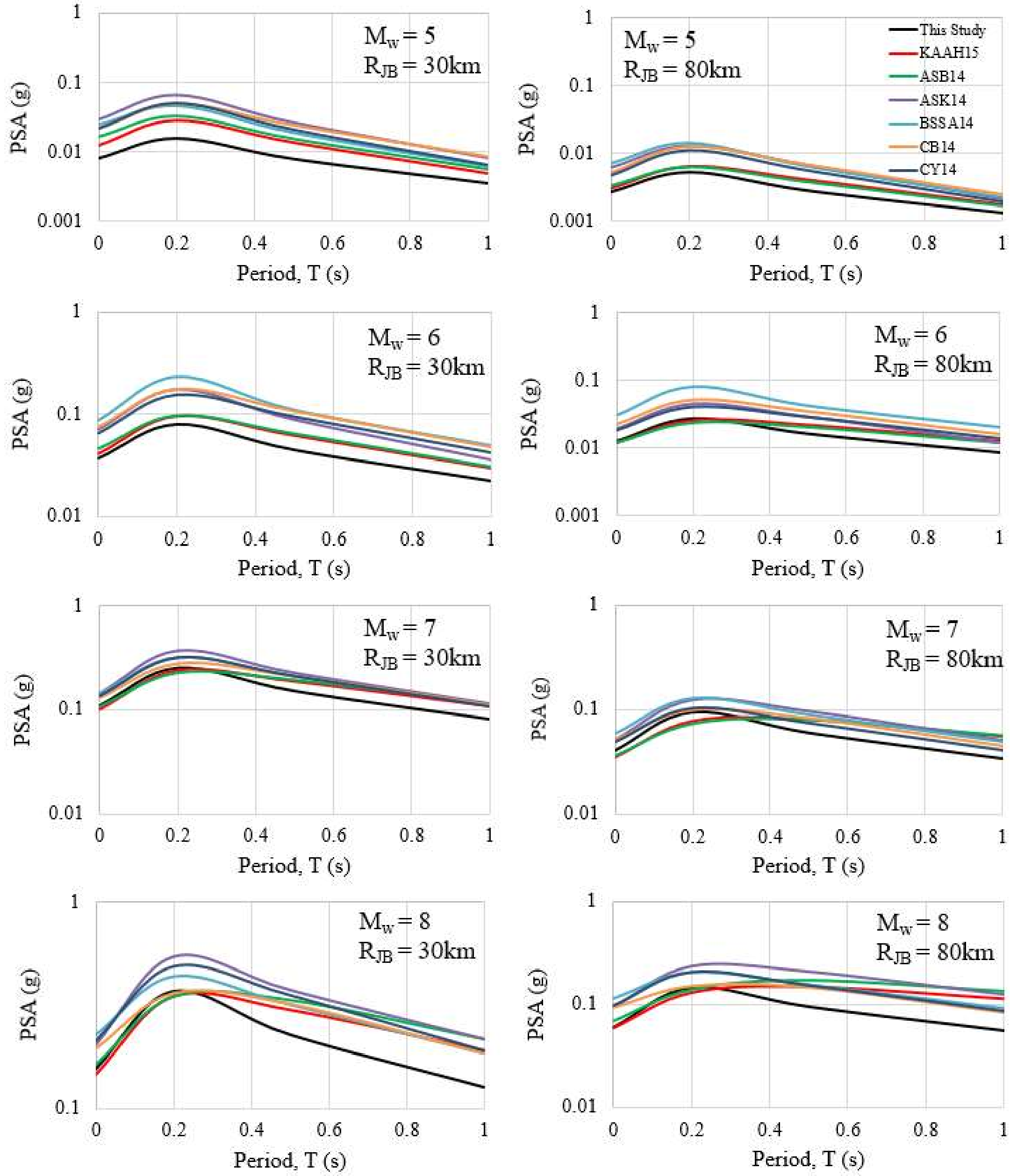

Figure B.19. Comparisons of spectral ordinates from the new model and local, regional and global GMPEs. The comparisons are done for V_{S30} = 520 m/s at a distance of R_{JB} = 30 and 80 km from a strike slip fault for magnitudes M_w 5, 6, 7 and 8.

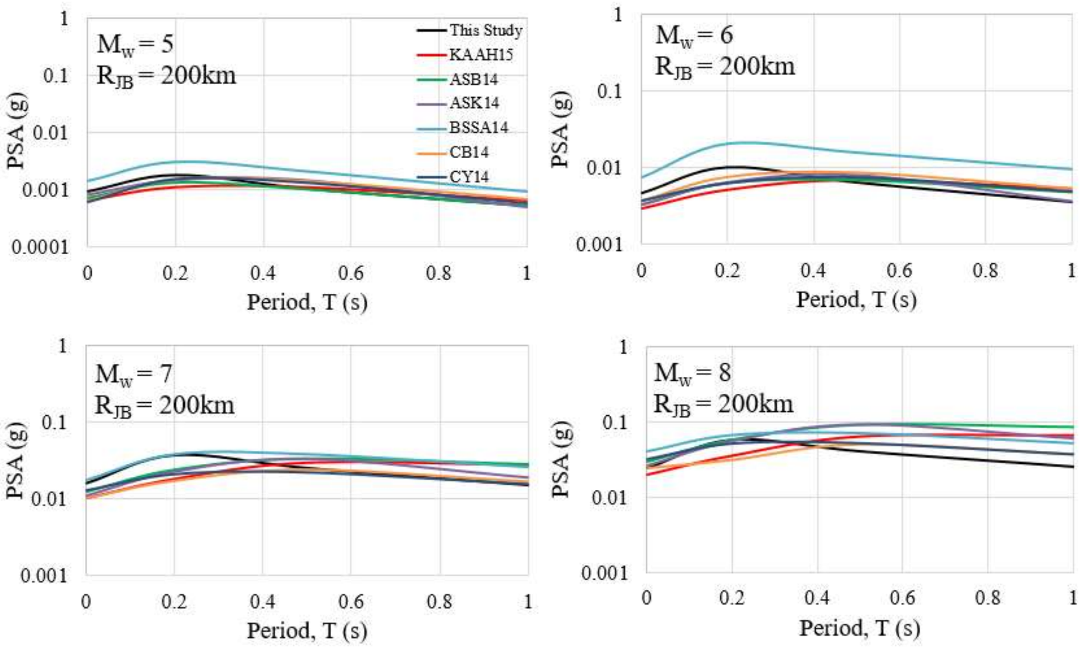

Figure B.20. Comparisons of spectral ordinates from the new model and local, regional and global GMPEs. The comparisons are done for V_{S30} = 520 m/s at a distance of R_{JB} = 200 km from a strike slip fault for magnitudes M_w 5, 6, 7 and 8.

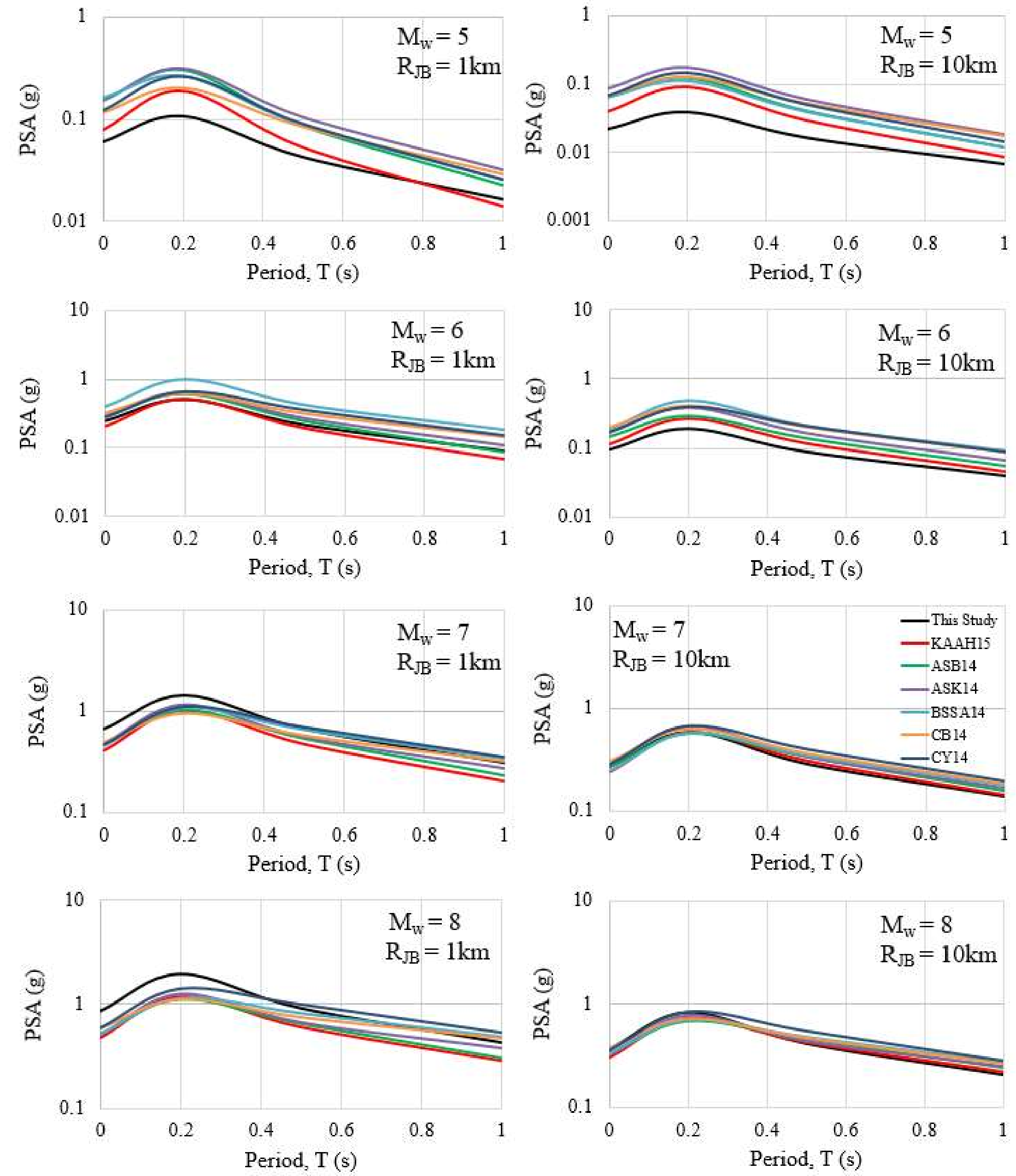

Figure B.21. Comparisons of spectral ordinates from the new model and local, regional and global GMPEs. The comparisons are done for V_{S30} = 760 m/s at a distance of R_{JB} = 1 and 10 km from a strike slip fault for magnitudes M_w 5, 6, 7 and 8.

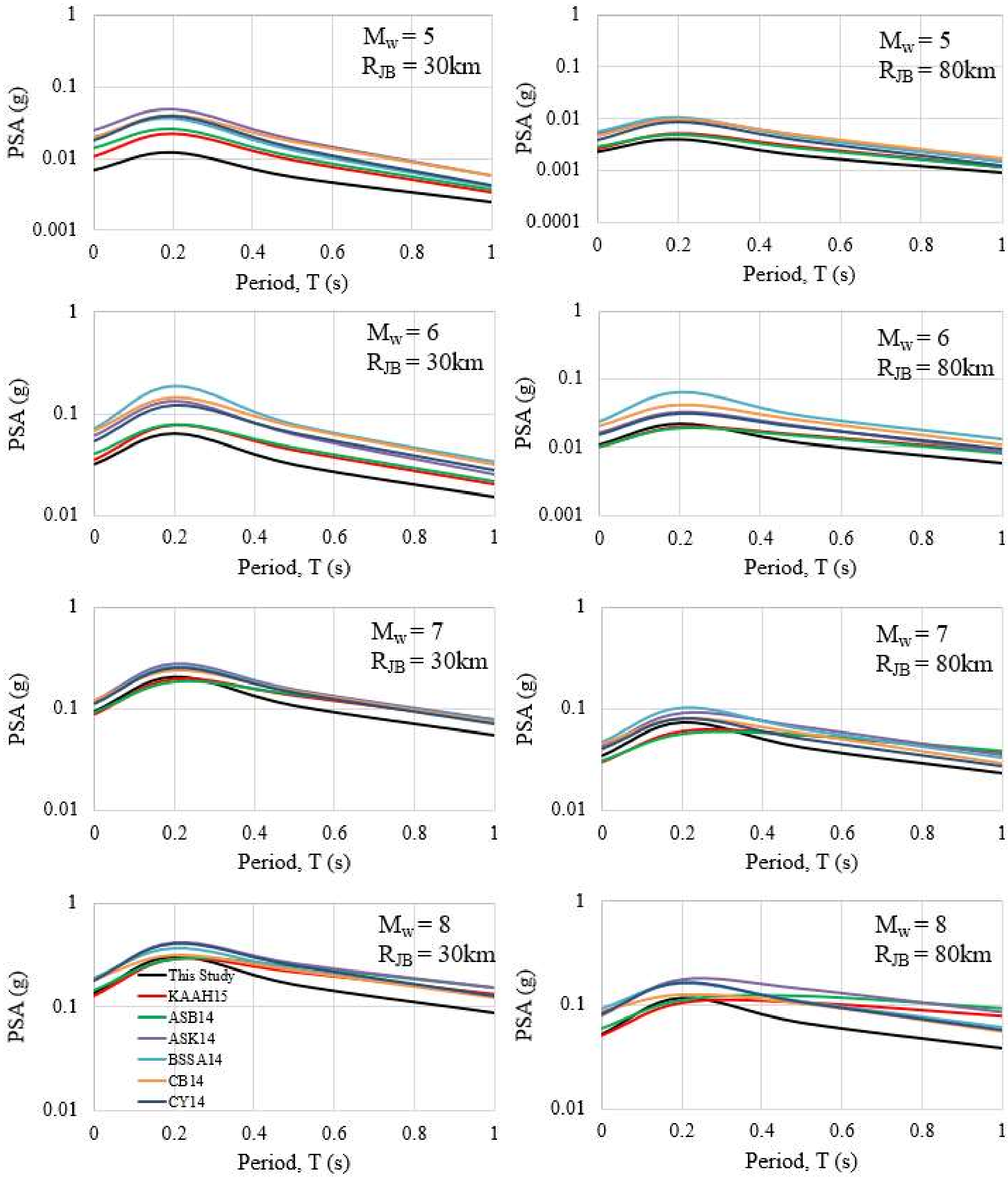

Figure B.22. Comparisons of spectral ordinates from the new model and local, regional and global GMPEs. The comparisons are done for V_{S30} = 760 m/s at a distance of R_{JB} = 30 and 80 km from a strike slip fault for magnitudes M_w 5, 6, 7 and 8.

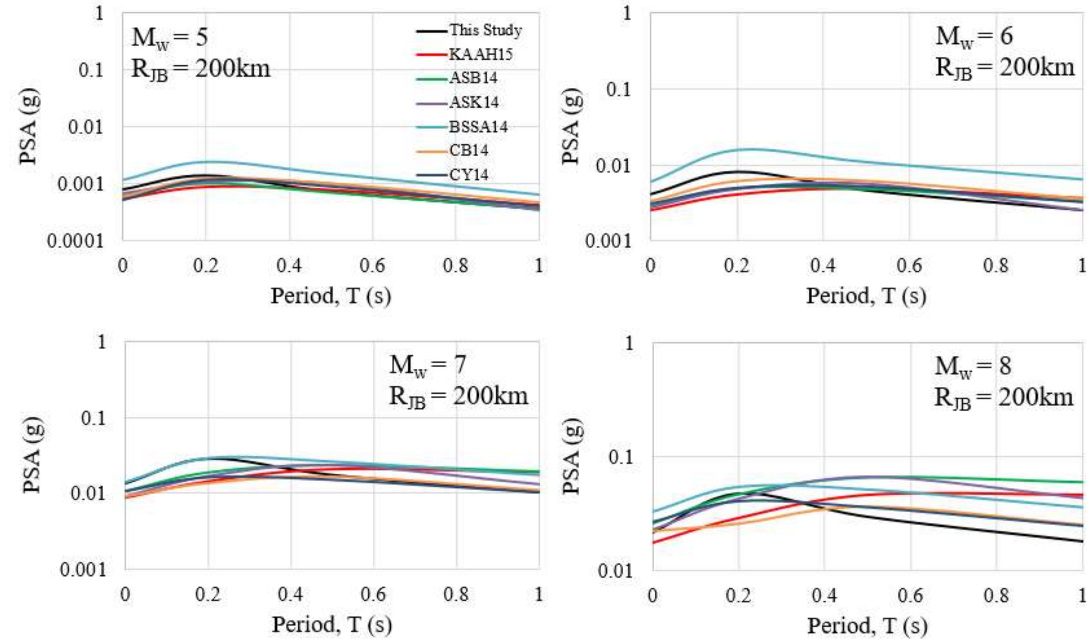

Figure B.23. Comparisons of spectral ordinates from the new model and local, regional and global GMPEs. The comparisons are done for V_{S30} = 760 m/s at a distance of R_{JB} = 200 km from a strike slip fault for magnitudes M_w 5, 6, 7 and 8.

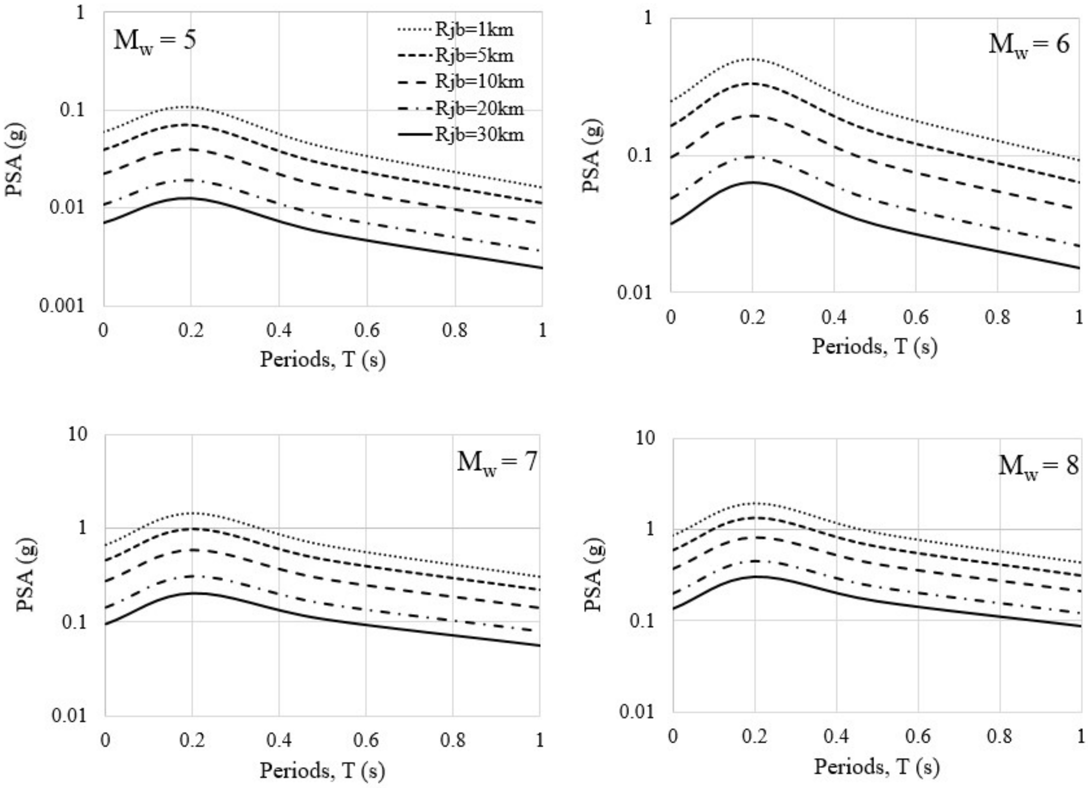

Figure B.24. Period scaling of the proposed GMPEs for distances ranging between 1 km ≤ R_{JB} ≤ 30 km. The comparisons are done for a reference rock site, V_{S30} = 760 m/s on a strike slip fault for magnitudes M_w 5, 6 7 and 8.